(2)

UNIVERSITY OF SOUTHERN CALIFORNIA

GEOPHYSICAL LABORATORY

TECHNICAL REPORT NUMBER 77-11

Short Title of Work: Crustal and Upper Mantle Velocity and Q Structures of Mainland China

Reported By: Ira Pines and Ta-liang Teng

Contractor: University of Southern California

Principal Investigator: Professor Ta-liang Teng (213) 741-6124

Contract Number: F49620 76-C-0010

Effective Date of Contract: 7/1/76

Contract Expiration Date: 9/30/77

Amount of Contract: $54,403

November, 1977

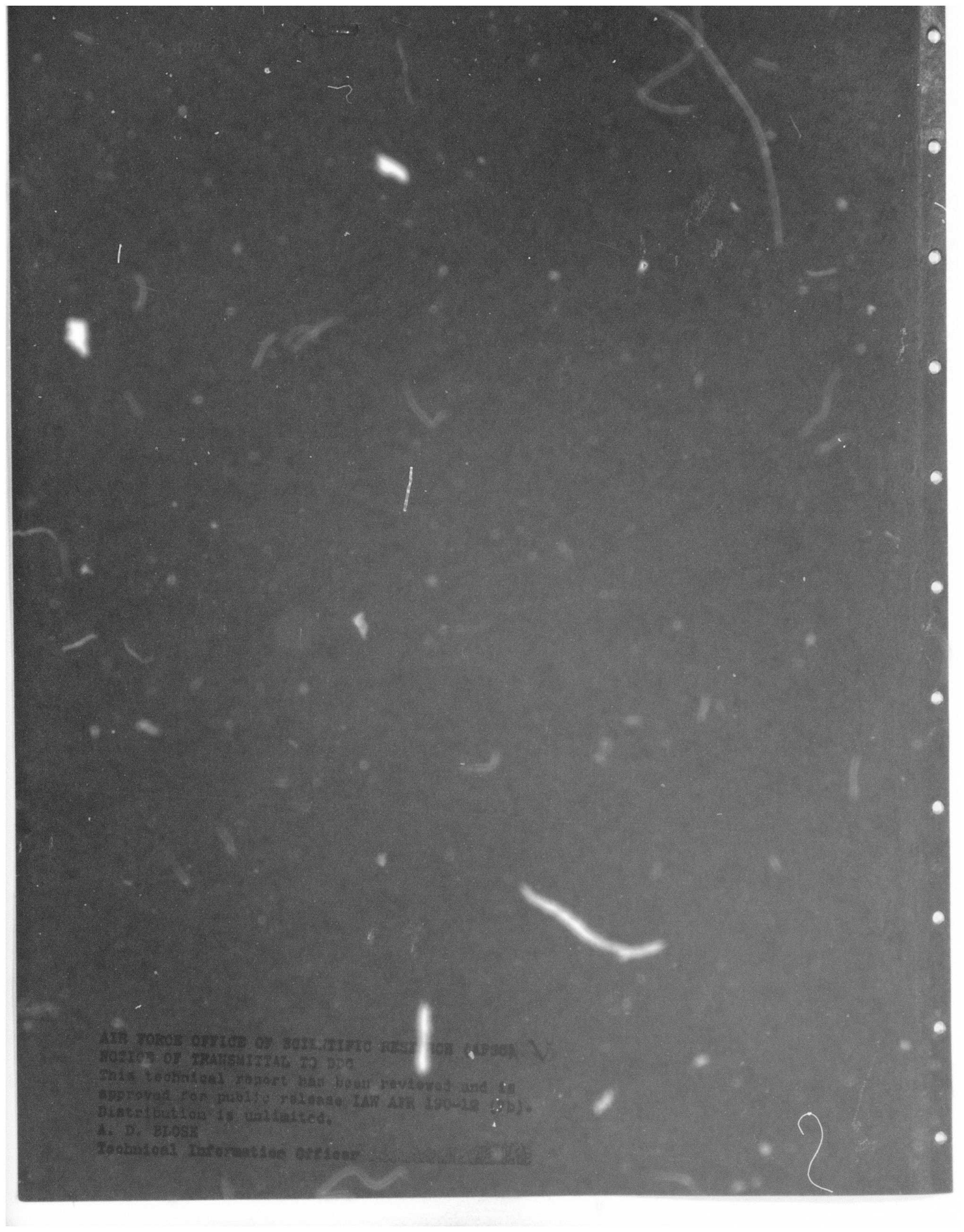

AIR FORCE OFFICE OF SCIENTIFIC RESEARCH (AFSC)
NOTICE OF TRANSMITTAL TO DDC
This technical report has been reviewed and is
approved for public release IAW AFR 190-12 (7b).
Distribution is unlimited.
A. D. BLOSE
Technical Information Officer

TABLE OF CONTENTS

LIST OF ILLUSTRATIONS AND TABLES

Figure

Tables

ABSTRACT

New data from the Seismological Research Observatory (SRO) is used in conjunction with a non-linear least squares technique to invert surface wave group velocity data for the shear wave velocity structure for paths crossing the Chinghai-Tibet, North China and South China subplates. A number of earthquakes are used over a single path in order to deduce a measure of the observational uncertainty. Group velocity standard deviations range from 0.04 km/sec to 0.20 km/sec for Rayleigh waves and 0.04 km/sec to 0.20 km/sec for Love waves over the period range 10-128 seconds.

The results of the inversion indicate a 4 layer total, 70 km thick crust is an adequate model for the Tibetan plateau. Group velocities obtained for the path crossing the Tibetan plateau are unusually low. Group velocities for the mixed path between Tangshan-Mashad, Iran are lower than the average continental dispersion. Results of the inversion indicate a 3 layer total, 45 km thick crust is an adequate model. Group velocities for the path between Tangshan-Taipei, Taiwan are closest of the three regions (at higher periods) to the average continental dispersion. Results of the inversion indicate that a 3 layer total, 30 km crust is an adequate model. Shear velocities derived from the inversion of group velocity data are presented for

the crust and upper mantle for each path.

INTRODUCTION

Preliminary studies of the Chinese Mainland by Tung (1974) and Sun and Teng (1977) have shown that China consists of a small number of subplates. Tung (1974) using Bouguer gravity distributions, physiography, and group velocity data divided mainland China into six subplates. Sun and Teng (1977) after an investigation of the surface geology, divided China into three subplates: (1) Chinghai-Tibet subplate; (2) North China subplate; and (3) South China subplate. The present study will focus attention on three distinct regions of mainland China: (1) the Tibetan plateau region of the Chinghai-Tibet subplate; (2) the North China subplate and Tien Shan fold belt, including the region between Tangshan and Mashad, Iran; and (3) the coastal region along the North China and South China subplates between Tangshan and Taipei, Taiwan.

Using a non-linear least squares inversion method, intermediate and long period group velocity data were inverted for a detailed shear wave velocity model of the crust and upper mantle. Two paths crossing the Tibetan Plateau of the Chinghai-Tibet subplate, recorded at the Seismological Research Observatory (SRO) station in Mashad, Iran are to be essentially pure paths, since they lie within one subplate. The first path across the Tibetan plateau

originates from a series of earthquakes occurring in the province of Szechwan on the eastern boundary of the Chinghai-Tibet subplate. The second path across the Tibetan plateau is based on a series of earthquakes located in Yunnan Province, approximately 650 km south of Szechwan. The other two surface wave paths studied are a consequence of the 1976 Tangshan earthquake and its aftershocks. The third surface wave path parallels the coast of China along the eastern boundary of the North China and South China subplates. The other path traverses the region between Tangshan and Mashad, Iran crossing the Tien Shan fold belt. Both these paths are mixed paths because they cross different subplates. Thus an average crustal thickness and shear wave velocity profile across the entire path will be presented.

It is well known that group velocity and phase velocity dispersion data contribute approximately the same information about a shear velocity model, although group velocity data tends to be more sensitive to the initial earth model and produce better resolution upon inversion (Block et al., 1969, Wiggins, 1972, Der and Landisman, 1972). The simultaneous combination of fundamental and higher mode dispersion data increases the accuracy and resolution of the inversion (Block et al., 1969, Wiggins, 1972, Der and Landisman, 1972). Previous studies (Wiggins, 1972, Der et al., 1970, Der and Landisman, 1972) have

shown that inversion for Rayleigh Waves contributes more information about an earth model than just inverting Love waves. Wiggins (1972) demonstates that simultaneous inversion of Love and Rayleigh waves permits one to obtain both a shear wave velocity and density structure. Complications often arise in using Love wave dispersion data owing to uncertainties resulting from interference of the fundamental and higher modes (Thatcher and Brune, 1969, Boore, 1969, James, 1971). The last statement is important because in order to invert simultaneously for both Rayleigh and Love waves correctly, the separate inversions for both Rayleigh and Love waves should approximately fit the same final velocity structures.

This study will obtain group velocity measurements from fundamental and higher mode Rayleigh and Love waves using a multiple filter analysis. A Gilbert-Backus (1967) type inversion is used to obtain a shear wave velocity structure for the crust and upper mantle for the regions traversed for each path.

GEOTECTONICS OF MAINLAND CHINA

Mainland China, between the Western Pacific and Alpine-Himalayan tectonic belts, presents a multitude of tectonic complexities of a vast range of topographic relief and geomorphologic features (Figure 1). The

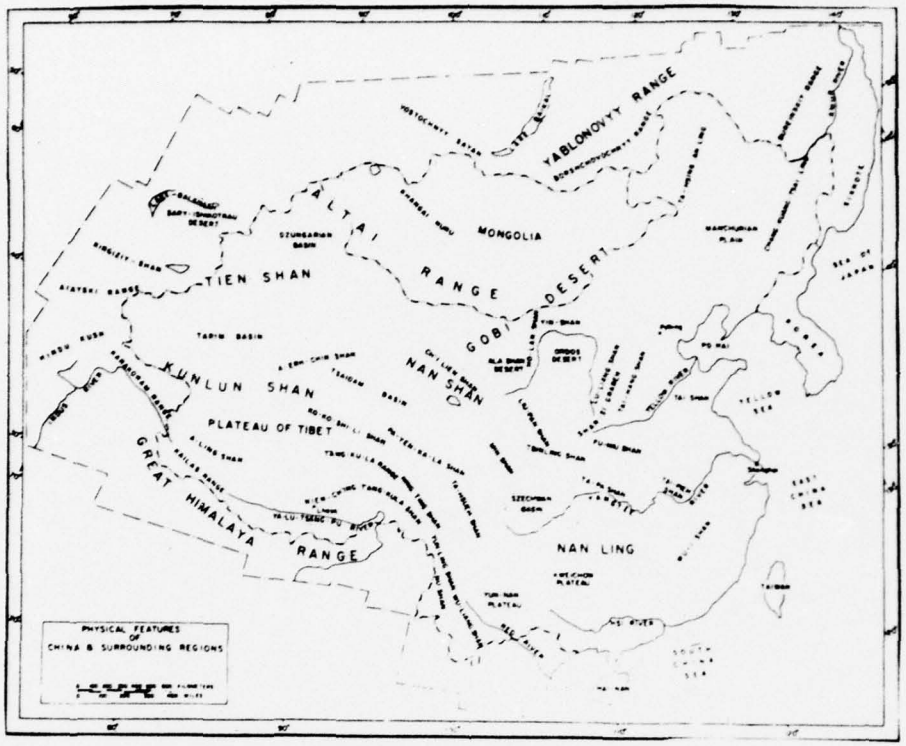

Physical features of China and surrounding regions.

FIGURE 1: Physiography of Mainland China (Cardwell and Isacks, 1976)

emergence of the theory of plate tectonics has permitted the combination of the results of geological and geophysical investigations into a coherent theory of the origin and evolution of many of the major tectonic features evident today on the Chinese Mainland.

Recent earthquakes, evident throughout China and most of Asia, are attributed to the consequences of the collision between the Indian and the Eurasian plates, (Figure 2), (Dewey and Bird, 1968, Dewey and Burke, 1973, Molnar, et al., 1973). This is evident in Mainland China from the pattern of the trend of the major fault zones (Figure 3). In western China the major fault zones strike in an east-west direction, whereas in eastern China the zones strike north-northeasterly. Along the major fault zones important changes in both the Bouguer gravity distribution (Figure 4) and crustal thickness (Figure 5) occur.

Reconstruction of the history of the collision of the Indian and Eurasian plates suggest initial contact in Late Cretaceous, and infer a decrease in the rate of collision by one-half since the Eocene (Dewey and Bird, 1968, Dewey and Burke, 1973, Molnar et al., 1973). As a result of this collision, as much as 1500 km of crustal shortening since the Eocene has occured as Molnar and Tapponier suggest (1975) from observation of the Earth Resources Technology Satellite (ERTS) photographs, and

The locations of tectonic plates associated with China.

Direction of plate motion.

Plate boundaries drawn from seismicity of the world (USGS, 1967; Molnar et al., 1973).

Convergent plate motion.

FIGURE 2

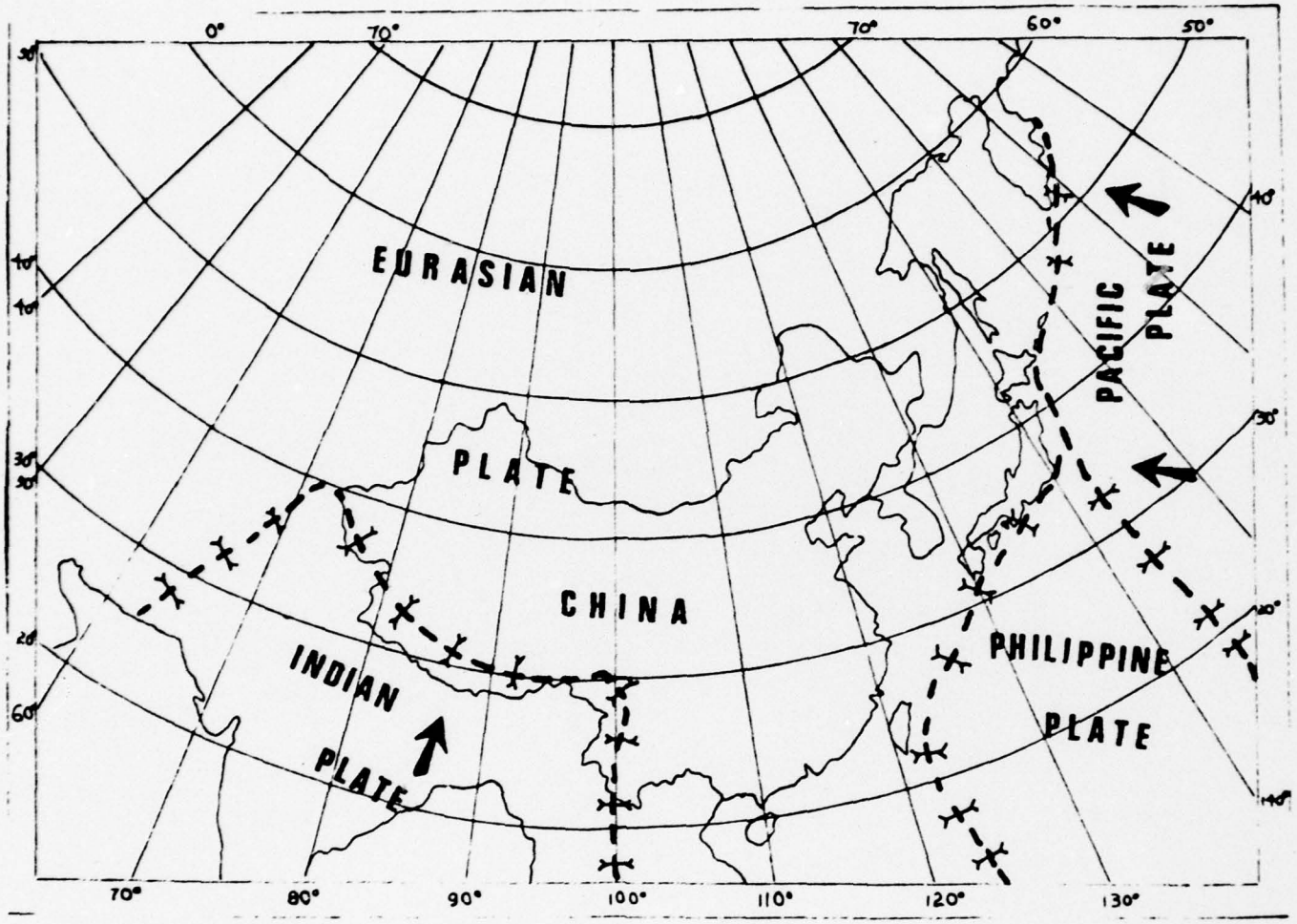
EURASIAN
PLATE
CHINA
INDIAN
PLATE
PACIFIC
PLATE
PHILIPPINE
PLATE
0°
70°
70°
60°
50°
40°
30°
20°
10°
70°
80°
90°
100°
110°
120°
130°
140°

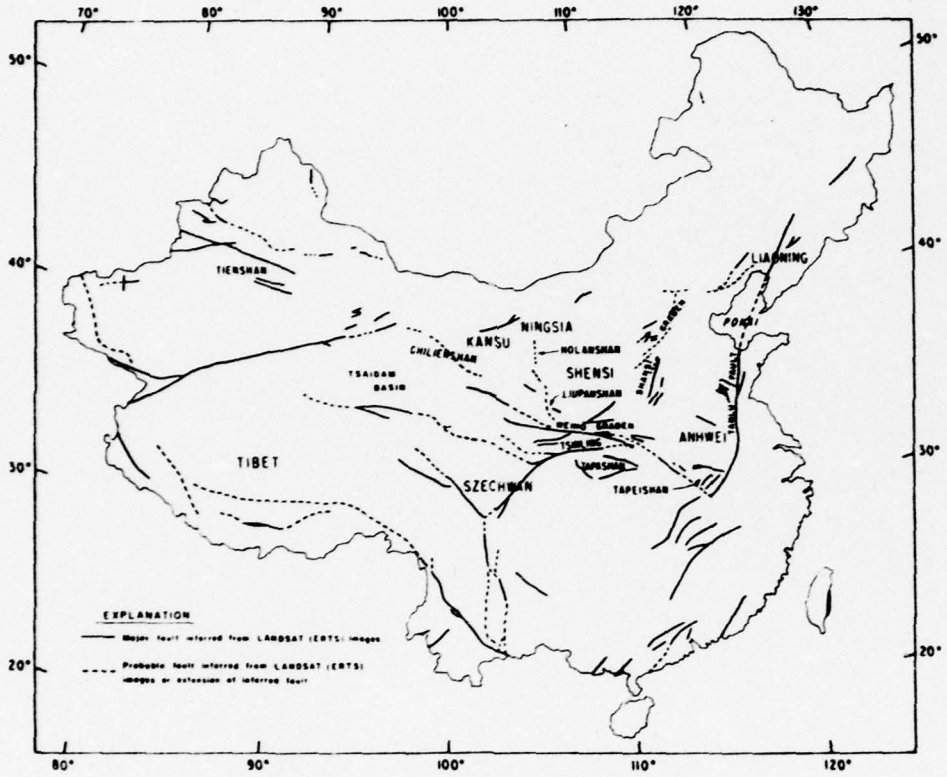

Simplified fault map of China based on LANDSAT (ERTS) images using Albers equal-area projection. Since not all faults can be identified by this method, this fault map is not complete.

FIGURE 3: Fault distribution in China

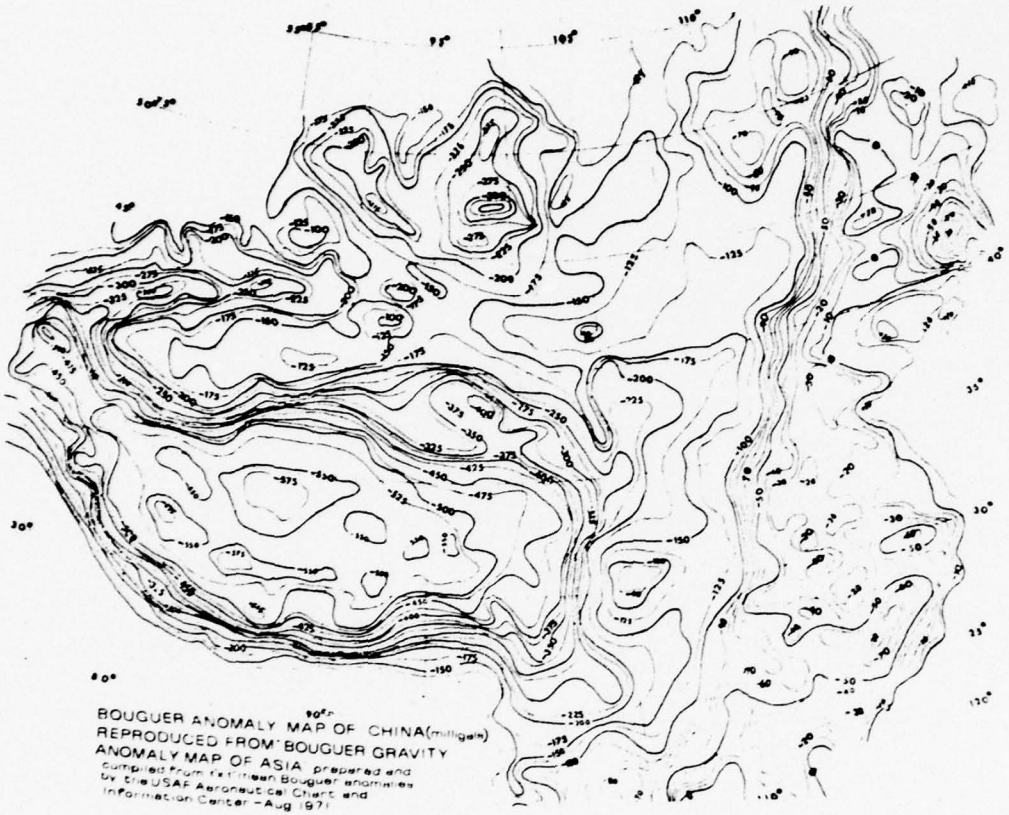

FIGURE 4: Bouguer anomaly map of China (U.S. Air Force, 1971)

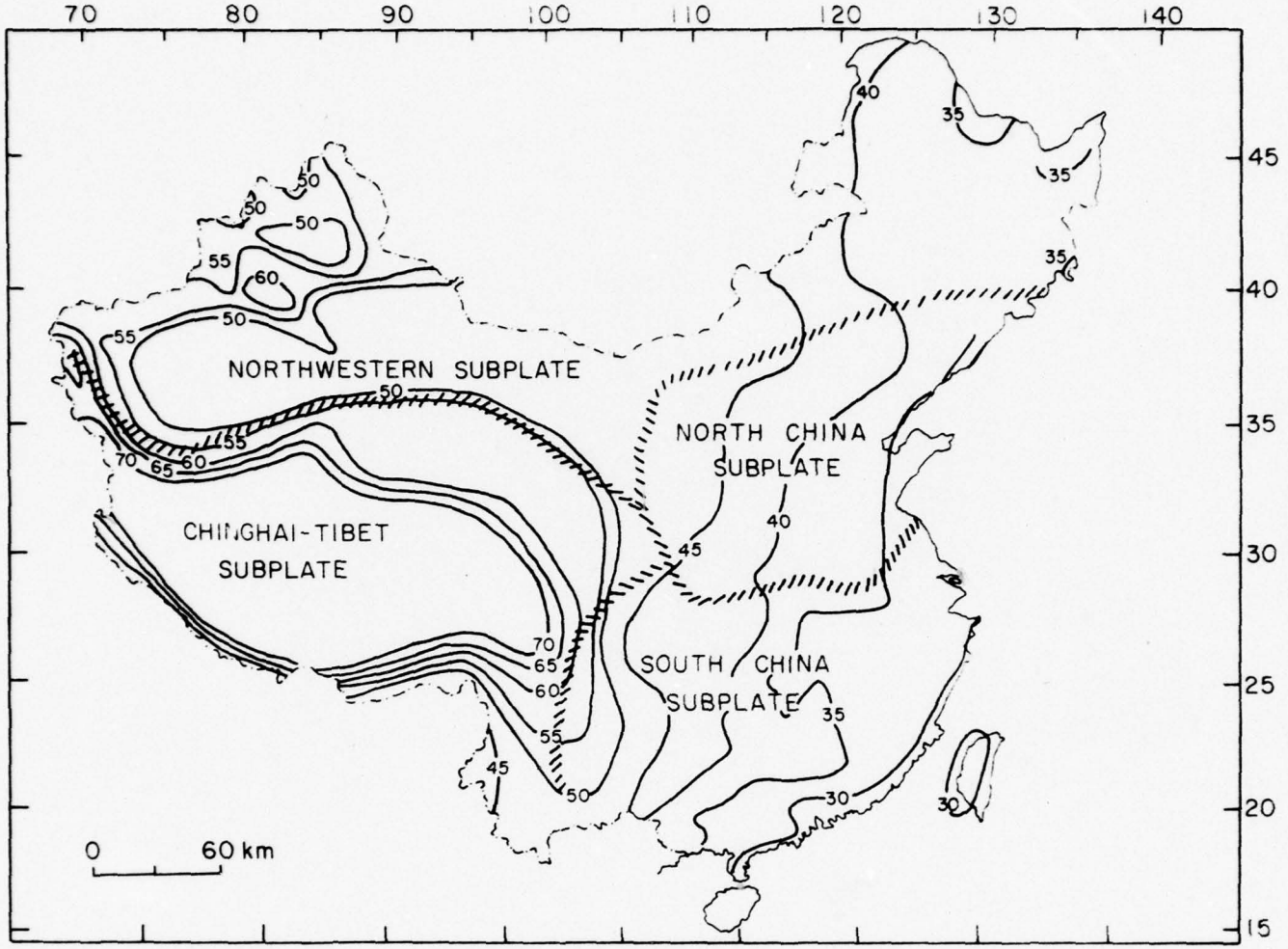

FIGURE 5: Crustal thickness map of China (Chinese Academy of Science, 1974)

that deformation in response to the collision extends as much as 3000 km northeast of the Himalayas.

Crustal shortening resulting from the underthrusting of the Indian Plate below the Himalayas and Tibet, accounts for 300 to 700 km of crust, while another 200 to 400 km of crust may be attributed to thrusting and crustal thickening in the Pamirs, Tien Shan, Altai, Nan Shan and other mountain belts (Figure 1) (Molnar and Tapponier, 1975). Rastogi, et al. (1973) using P wave first motions from earthquakes in both the Assam-Burma region and the Himalayas concluded that the major tectonic activity was thrust faulting and uplift in Tibet. Based on ophiolites found in western China and Mongolia, Zonenshain (1973) reported the existence of ancient oceans which were associated with this region. Shi, et al. (1973) reported earthquakes deeper than 200 km in the Tien-Shan region, which are often associated with zones of plate subduction. Chang and Zeng (1973) observed that belts of acidic and ultrabasic intrusions together with marine deposits are associated with mountain ranges to the north of the Himalayas, which they (1973) attributed to successive stages of subduction (Figure 6). In each stage of subduction, the southern plate was thrust below the Eurasion Plate resulting in crustal thickening.

The crustal thickening explains at, at the most, 60 percent of total crustal shortening. Molnar, et al.

FIGURE 6: Subduction of plates in the Tibetan platform

(Chang and Zeng, 1973)

ALTKUN SHEN TUNKULA SHEN HIMALAYA SHEN

KUNLUN SHEN GUNDIS SHEN

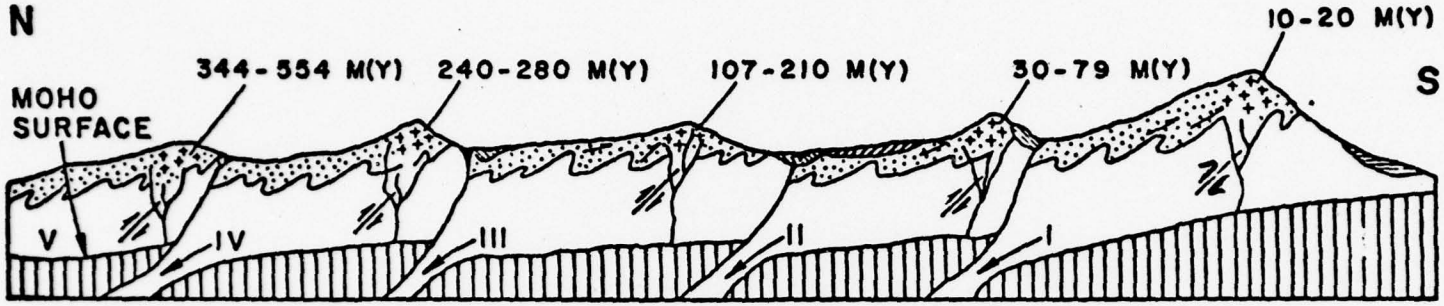

SEDIMENTARY LAYERS
INTERMEDIATE IGNEOUS ROCKS
MOLASSE
CONTINENTAL CRUST
LITHOSPHERE
SERPENTINITE
GRANITE
FLYSCH

I INDIAN PLATE
II SOUTH SI-SANG PLATE
III NORTH SI-SANG PLATE
IV CHIEN TUN PLATE
V TSAIDAM PLATE

(1973) and Molnar and Tapponier (1975) attributed the other major fraction of the crustal shortening to major strike-slip faults in China and Mongolia. The strike-slip faulting associated with earthquakes indicates Asia is being squeezed in a direction lying between north-south and northeast-southwest, compatible with India's northern motion. The squeezing causes the crust to thicken in places. The strike-slip faults in this region trend in an east-west direction which is approximately perpendicular to the Bouguer gravity contours (Figure 4). From a correlation of crustal thickness and Bouguer gravity anomalies, Tung (1974) concludes that the structural changes occur in a northeast-southwest direction similar to the direction of maximum compressive stress associated with strike-slip faulting (Molnar et al., 1973). Molnar and Tapponier (1975), from the ERTS photographs, observed several major left-lateral strike slip faults, trending roughly east-west. Also evident were long linear valleys and adjacent ridges. These features are characteristic of strike-slip faulting. In eastern China, especially in the northeast, Shi, et al. (1973) have discussed the existence of deep fault zones which have been considered inactive. Recent seismic activity at Tangshan, in northeast China, as discussed by Molnar and Tapponier (1977) indicate that the earthquakes are a result of complex tectonic movements resulting from an underthrusting

of the Indian plate below the Eurasian plate.

The mainland of China is subdivided into three subplates (Figure 5). The division of China into major subplates is not new, but has been discussed by McElhinny (1973) using paleomagnetic data, Whittington and Hughes (1972) and Jell (1973) using paleontological data, and Dewey and Bird (1970), Hamilton (1970) and Burret (1974) from geological studies. From study of the surface geology, Sun and Teng (1977) divided the Chinese Mainland into three subplates: (1) the Chinghai-Tibet subplate; (2) the North China subplate; and (3) the South China subplate (Figure 5). They are separated by the North-South and East-West Tectonic Zones (Sun and Teng, 1977). Each subplate differs in its geomorphologic features, gravity anomalies and crustal thickness as discussed by both Tung (1974) and Sun and Teng (1977). The major seismic events on the Chinese Mainland occur on the boundaries between the subplates and can be related to the tectonic mechanisms discussed by Molnar and Tapponier (1975, 1977).

The North China subplate is bounded on the north by the Siberian platform (Hamilton, 1970) and to the south by the Tsinling Shan (Figure 1). In the west the North China plate is bounded by the Shansi graben and the Ordos desert. The Shansi graben consists of a series of northeast striking faults. The Shansi graben

system extends to the north into the Ordos platform and is one of the largest graben regions in the world. These features have been observed by LANDSAT-1 imagery as discussed by Cardwell and Isacks (1976). The major part of the North China subplate consists of the North China plain. The North China plain has an average elevation of less than 100 m and is a sediment filled basin surrounded by uplifted areas of more than 1 km. Although the North China subplate is considered an "intraplate" area, it has a long history of seismic activity (Lee et al., 1976).

The Tsinling Shan is a sharp paleontological and physical boundary between the North and South China subplates. The Tsinling Shan consists of a series of faults striking northwesterly into the Nanshan fold belt. Kobayashi (1967) extended the Tsinling Shan as far north as Korea.

The Chinghai-Tibet subplate consists of the area north of the Himalayas including the Kun Lun mountain range. The Tanim basin and the Tien Shan fold belt, to the north of the Chinghai-Tibet subplate, are considered separate tectonic units, although this area has had a homogenous fauna since the Paleozoic (Burrett, 1974).

The South China subplate is to the south of the Tsinling Shan and to the west of the Tibetan and Tsaidam plateaus. The South China subplate consists of the Yangtze fault block in the northwest and the South China fold

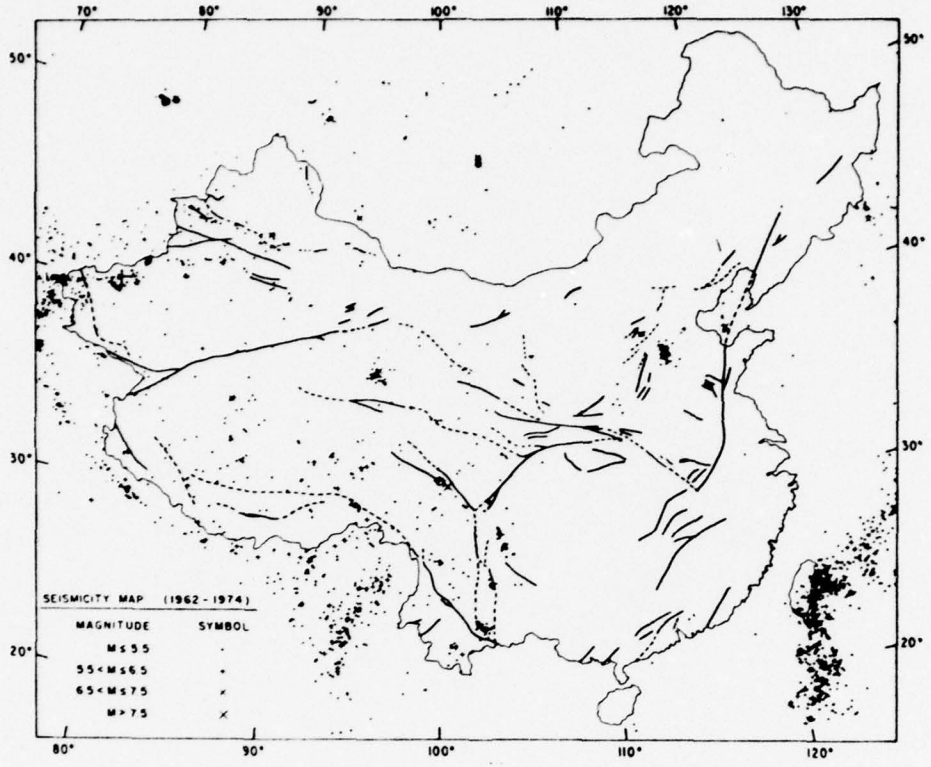

Map showing distribution of epicenters of recent earthquakes in China (1962–1974) using Albers equal-area projection.

FIGURE 7: Seismic map of China (Lee, et al., 1976)

block in the southeast (Sun and Teng, 1977). The eastern boundary of the South China subplate runs parallel to the southeast coast of China, and is coincident with the subduction of the Pacific plate below the Eurasian plate. The presence of a mélange in the East Coast mountain range of Taiwan, glaucophane schist in the Central mountain range of Taiwan, (Sun and Teng, 1977) and considerable seismic activity in northeast Taiwan (Katsumata and Sykes, 1969) has been used as evidence that this region is an active subduction zone.

The division of China into three major subplates is helpful from the standpoint of surface wave dispersion studies. The concept of regionalization, first proposed by Toksoz and Anderson (1966) consists of dividing a surface wave path into oceanic, shield, and mountain tectonic segments. Each segment has a different effect upon the average group velocity. Toksoz and Anderson (1966) noted that shield areas raise the average group velocity. In contrast, active tectonic and mountainous regions have the effect of lowering the average group velocity. As a result, surface wave paths crossing different tectonic regions will have different velocity dispersion curves. Tung (1974) studied the relationship between the concept of regionalization as applied to Mainland China and its tectonic implications and concluded that Mainland China could be divided into several major subplates

PREVIOUS GEOPHYSICAL STUDIES

Previous geophysical studies of the crustal and upper mantle structure of mainland China have made use of seismic refraction and reflection profiling, surface wave dispersion and Bouguer gravity. In the absense of data from explosion seismology and due to the lack of a sufficient number of seismological observatories, the study of the dispersion of surface waves remains the only method presently available to study the crust and upper mantle in many of these regions.

Tibetan Plateau

Knowledge of crustal thickness velocity structure under the Himalayas and the Tibetan plateau from other surface wave dispersion studies is limited. The earliest surface wave dispersion studies in this region were performed by Stonely (1955), Tandon and Chaudhury (1963) and Saha (1965). These studies concluded that crustal thickness beneath the Himalayas and the Tibetan plateau was greater than for an average continental region; however, these studies failed to provide either a velocity profile or an estimate of crustal thickness. Tandon and Chaudhury (1963) established an average crustal thickness of 45 km between Novaya Zemlya and New Delhi by studying dispersion of Rayleigh waves generated from a high yield Soviet nuclear explosion. A similar average crustal thickness was reported by Saha (1965) using the same path but a

different nuclear event.

Gupta and Nasrain, (1967) using an earthquake north of the Soviet Union, recorded in Seoul, Hong Kong, New Dehli and Shillong, calculated an average crustal thickness of 45 km for those paths that pass through the Tibetan Plateau. Comparing the observed dispersion curves with a theoretical dispersion curve for a three layer earth, Gupta and Nasrain (1967) arrived at a crustal thickness below the Himalayas and the Tibetan plateau of 65 to 70 km.

Negi and Singh, (1973) using the same event as Gupta and Nasrain (1967) but investigating the Love wave dispersion characteristics by ray-theory techniques, calculated a crustal thickness of 50 km for a laterally inhomogeneous crust. Negi and Singh (1973) reported an average shear velocity in the crust of 3.55 km/sec and an average shear velocity of 4.61 km/sec in the upper mantle.

Tseng, et al. (1963) using two earthquakes with epicenters in the New Britain Islands, recorded at stations throughout China, evaluated phase velocities along these paths by applying the tripartite method. They estimated a crustal thickness beneath the Tibetan plateau of 72-76 km (Figure 8).

Tung (1974), using events occurring on the eastern boundary of the Tibetan plateau performed surface wave inversion for four distinct pure paths located within the Tibetan Plateau. The method used by Tung (1974) as with

FIGURE 8: Location of recording stations and the resulting crustal thickness (Tseng and Sung, 1963)

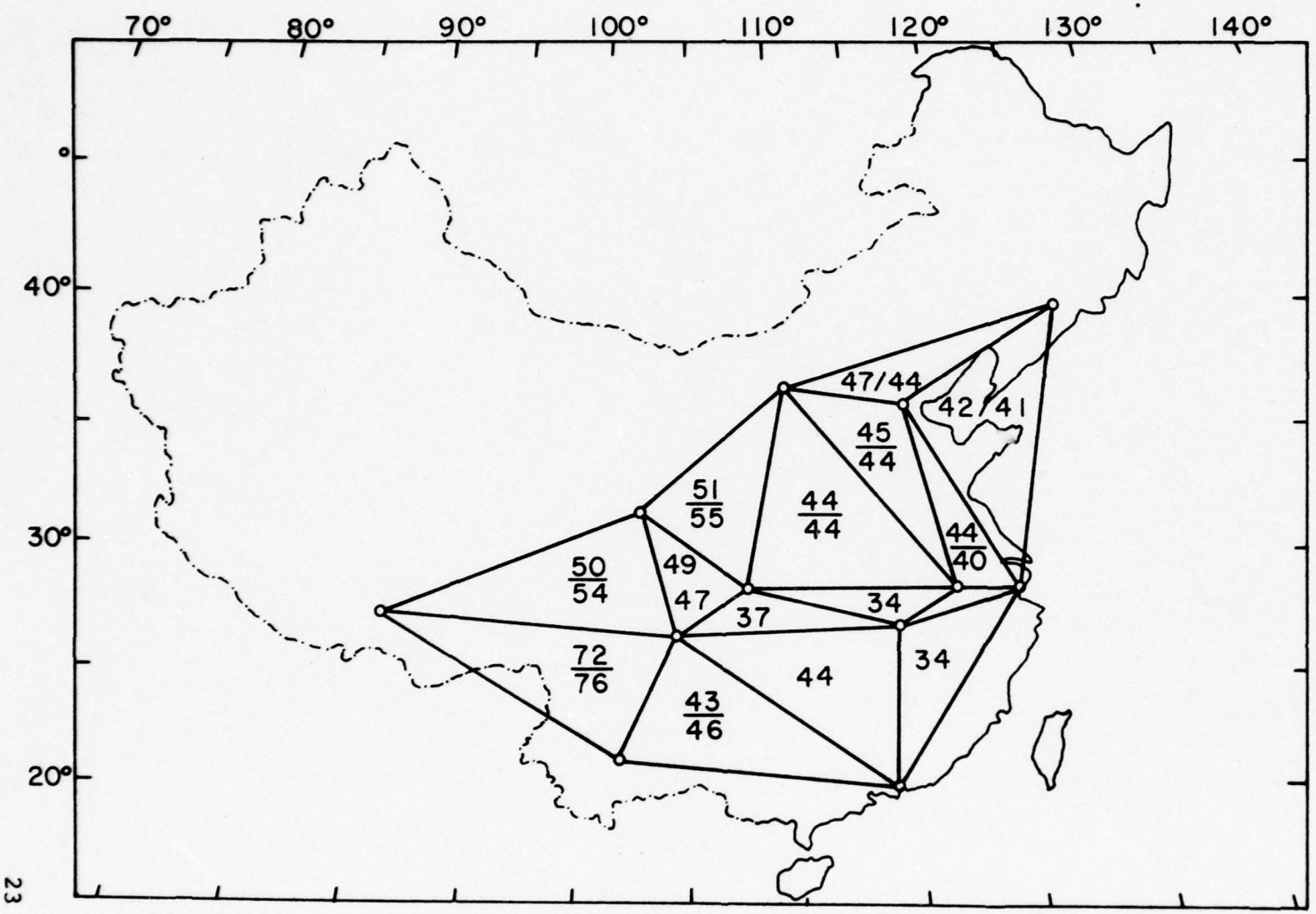
70°
80°
90°
100°
110°
120°
130°
140°
40°
30°
20°
47/44
42/41
45/44
51/55
44/44
44/40
50/54
49
47
37
34
72/76
44
34
43/46

previous investigators who performed surface wave inversions is a trial-and-error technique and does not provide a measure on the resolution or standard deviation for the resulting velocity structure. Tung (1974) reported group velocities substantially lower than the average continental dispersion (Ewing et al., 1957). The differences in group velocities extend to periods of 120 seconds, which infer abnormal structure in the upper mantle under the Tibetan plateau. Tung (1974) fitted the observed Rayleigh wave data to a theoretical model with four layers in the crust. The first layer with an average shear velocity of 2.80 km/sec corresponds to a sedimentary layer. The second and third layers have average shear velocities of 3.2 and 3.6 km/sec respectively, corresponding to granitic and basaltic rocks. The fourth layer has an average shear velocity of 3.8 to 4.0 km/sec. This velocity corresponds to basaltic rocks under 20 kilobars of pressure at depths of 50 to 70 kms. Tung (1974) cited a crustal thickness of 78 km. At the top of the upper mantle the shear wave velocity range is 4.35 to 4.55 km/sec. The low velocity zone was estimated to be at a depth of approximately 90 km with shear wave velocities as low as 4.10 km/sec indicating a high percentage of partial melting, Tung (1974).

Bird and Toksoz (1966) performed Rayleigh wave attenuation studies using data recorded at Kabul, Nilore,

New Dehli, Shillong, and Hong Kong for six earthquakes with paths crossing the Tibetan plateau. Based on an earth model compatible with their observation, they found the best fitting attenuation layer, centered at a depth of 70 km. The structural model they presented for the Tibetan plateau was a 70 km thick crust with the lower most part of the crust having a shear velocity of approximately 3.8 km/sec.

Chun and Yoshii (1977), using Rayleigh and Love waves recorded at WWNSS stations surrounding Tibet in the period range of 5 to 100 seconds were able to fit a crustal thickness of 70 km to their data and observed a low velocity zone at intermediate depths. A detailed analysis of the short period data (5-15 seconds) showed that the Tibetan plateau is devoid of thick low velocity sediments. They attribute the strong dispersion of short period surface waves to a low velocity uppermost crust of the Himalayas and the Gangetic basin, for events recorded at New Dehli.

Other geophysical studies of importance to the crustal structure of the Tibetan plateau are Bouguer gravity surveys and seismic reflection and refraction studies. The Bouguer gravity distribution (Figure 4) compiled by the United States Air Force (1971) shows a Bouguer gravity anomaly of -575 milligals centered on the Tibetan Plateau, with a belt of rapid decrease relative to adjacent areas

from -200 to -550 milligals around the periphery. Masaru (1974), as part of the Japanese Mount Everest Expedition of 1970, performed gravity measurements in East Nepal and the lower and higher Himalayas. He calculated a crustal thickness in these regions between 63.4 and 74.5 km in accordance with the gravity data. The tectonic map (Figure 5) of the Institute of Geology of the Chinese Academy of Sciences (1974), composed of the results of seismic reflection and refraction and gravity surveys shows the 60-70 km isopath coinciding with the borders of Tibet.

Northern and Northwestern China

The early geophysical studies of northwestern China include results of explosion seismology, surface wave dispersion, and body wave travel time studies performed by Tandon (1954), Nagmune (1956), Riznichendo (1958), Kovach (1959), Saverensky and Sheckov (1961), Zverev (1962), Sheckov (1964) and Arkhangel'skaya (1964). Riznichendo (1958) proposed that the roots of the Tien Shan Hercynian belt are due to a thick basaltic layer (approximately 20 km of granite over 30 km of basalt) which corresponds to a 50 km crust. Kosminakaya, et al. (1958), using deep seismic soundings in the Tien Shan and Pamir mountain ranges arrived at a crustal thickness of 65 km. Using a theoretical model proposed by Dorman (1959) for Love wave dispersion (case 201), Schechkov (1961, 1964)

and Saverensky and Schechkov (1961) were able to fit surface wave dispersion data to a theoretical model for a three layer earth with a crustal thickness of 50 km, for paths across Northwestern China.

Tseng, et al. (1963), using phase velocities, determined crustal thicknesses of 50 to 55 km for Northwestern China, 44 to 47 km for North Central China, and 40 to 42 km for Northeastern China.

From Rayleigh and Love wave dispersion data for paths which crossed Northwestern, Central and Northeastern China, Tung (1974) arrived at the following conclusions:

(1) Northeastern China has crust approximately 30 km thick with an upper mantle structure similar to Southeastern China.

(2) Central China has a crust approximately 40 km thick with a low velocity zone more prominent than Northeastern China.

(3) Northwestern China has a crustal thickness of approximately 45 km with crustal thickening towards the Tien Shan mountain range. The upper mantle structure of Northwestern China is similar to that of Tibet.

The Air Force Bouguer gravity map (1971) for Northwestern China shows the -400 milligal Bouguer anomaly contour running east-west, parallel to the Kun Lun and Tien Shan mountain ranges, with a gravity high of -100 milligals in the middle of the Tarim basin. In North

Central China the Bouguer gravity anomalies range from approximately -175 milligals in the west to -70 milligals in the east. Finally, in Northeastern China the Bouguer gravity anomalies range between -70 milligals in the western region to 0 milligals along the coastal regions (Figure 4).

The tectonic map of China compiled by the Institute of Geology of the Chinese Academy of Sciences (1974) (Figure 5) shows isopaths in the Kun Lun Mountain range and eastern most segment of the Tien Shan. To the east of the north-south tectonic zone the isopaths run roughly parallel in the direction of north, north-east from 45 km in the west to 30 km in the east.

Coastal Region Between Tangshan to Taipei

Previous geophysical studies in the region between Tangshan (near Peking) and Taipei have been of a seismic reflection or seismic refraction nature and have been compiled in the form of a map (Figure 5) presented by the Institute of Geology of the Chinese Academy of Sciences (1974). Tangshan lies just off the 40 km isopath. The path from Tangshan to Taipei crosses the 35 km isopath, and parallels the 30 km isopath. From the U.S. Air Force Bouguer gravity map (1971) the region between Tangshan and Taipei has gravity anomalies ranging between -20 to +20 milligals (Figure 4).

SURFACE WAVE ANALYSIS

Data

Earthquakes used in this study (Table 1) were chosen such that a major portion of their wave paths would fall within the three subplates of which the Chinese Mainland consists. Wave paths across the Chinghai-Tibet, North, and South China subplates are shown in Figure 9. A number of earthquakes are used for each path in order to obtain data repeatability and observational uncertainties. The path lengths range from approximately 1700 km to over 5000 km. For the path length that was less than 2000 km (Tangshan to Taipei) the accuracy of surface wave data of periods greater than 64 seconds was limited.

All events were recorded at two Seismological Research Observatory (SRO) stations in Mashad, Iran (MAIO), and Taipei, Taiwan (TATO). The SRO stations at Mashad and Taipei were chosen because they fulfilled the geographic requirement that a major portion of the path be within the subplate to be studied.

Data obtained for an SRO station is digitized, multiplexed and stored on tape. Three long period channels (vertical, east-west, and north-south) are sampled continuously at a rate of once per second. Short period data is sampled only when an event is detected (Rosenthal and Teng, 1977). Peterson (1976) has described the structure of the information on the SRO data tapes.

TABLE 1

Earthquakes and Recording Stations

Used in this Study

Location	Origin Time	Recording Station	Magnitude
39.8° N 118.6° E N.E. China	July 28, 1976 15 hr 35 min 55.3 sec	MAIO	5.4
40.1° N 118.3° E N.E. China	July 28, 1976 16 hr 24 min 04.7 sec	MAIO	4.2
39.9° N 118.0° E N.E. China	July 29, 1976 1 hr. 01 min 04.1 sec	MAIO	5.1
39.8° N 117.8° E N.E. China	July 30, 1976 21 hr 23 min 13.8 sec	MAIO	5.4
39.6° N 117.9° E N.E. China	Aug 2, 1976 9 hr 16 min 00.5 sec	MAIO	4.4
39.7° N 118.5° E N.E. China	Aug 8, 1976 1 hr 0.9 min 12.4 sec	MAIO	4.9
40.2° N 118.9° E N.E. China	Aug 8, 1976 22 hr 41 min 34.3 sec	MAIO	5.1
39.6° N 118.5° E N.E. China	Aug 14, 1976 16 hr 02 min 44.5 sec	MAIO	4.7
32.753° N 104.157° E Szechwan	Aug 16, 1976 14 hr 6 min 45.9 sec	MAIO	6.1
32.893° N 104.189° E Szechwan	Aug 19, 1976 12 hr 49 min 47.7 sec	MAIO	5.4
32.571° N 104.152° E Szechwan	Aug 21, 1976 21 hr 49 min 54.2 sec	MAIO	6.1

TABLE 1 (Continued)

Location	Origin Time	Recording Station	Magnitude
32.492° N 104.181° E Szechwan	Aug 23, 1976 3 hr 30 min 7.6 sec	MAIO	6.2
32.460° N 104.152° E Szechwan	Sept 1, 1976 1 hr 6 min 51.8 sec	MAIO	5.1
24.343° N 98.642° E Yunnan	May 31, 1976 5 hr 8 min 28.5 sec	MAIO	5.5
24.191° N 98.676° E Yunnan	July 3, 1976 16 hr 33 min 23.1 sec	MAIO	5.3
39.8° E 118.6° E N.E. China	July 28, 1976 15 hr 35 min 55.3 sec	TATO	5.4
39.9° N 118.8° E N.E. China	July 29, 1976 1 hr 01 min 04.1 sec	TATO	5.1
39.8° N 118.9° E N.E. China	July 30, 1976	TATO	5.4
39.6° N 117.8° E N.E. China	Aug 1, 1976 20 hr 53 min 53.6 sec	TATO	4.6
39.9° N 118.8° E N.E. China	Sept 6, 1976 17 hr 02 min 01.5 sec	TATO	4.8

MAIO: Mashad, Iran 36.30° N 59.49° E

TATO: Tapei, Taiwan 24.976° N 121.489° E

FIGURE 9: Location and wavepaths for Mainland China

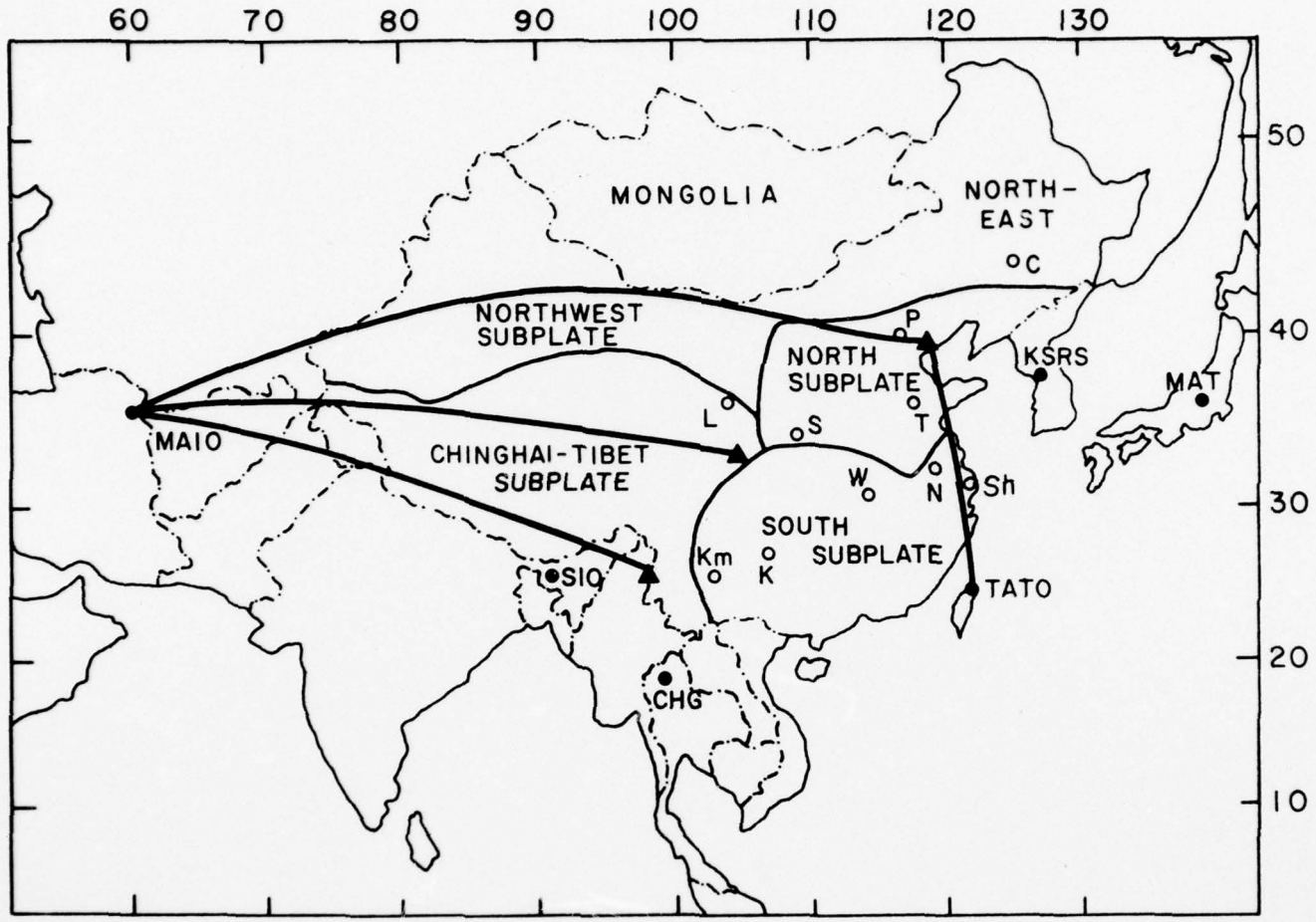
60
70
80
90
100
110
120
130
50
40
30
20
10
MONGOLIA
NORTH-
EAST
C
NORTHWEST
SUBPLATE
P
NORTH
SUBPLATE
KSRS
MAT
L
S
T
MAIO
CHINGHAI-TIBET
SUBPLATE
W
N
Sh
SOUTH
SUBPLATE
Km
K
SIO
TATO
CHG

Each SRO data tape consists of 1000 words (2000 bytes). The first ten words are header information, while the next 990 words are long period data (approximately 5 minutes, 30 seconds).

Rosenthal and Teng (1977) calculated the amplitude and phase response for the long period instrument which is given in Table 2. The numerical fit to a transfer function was also obtained and has the form (Figure 10):

$$T = \sum_{i=o}^{3} \frac{a_i Z^i}{b_i Z^i}$$

where Z is a complex number.

$a_0 = 1.7442 \times 10^{-4}$ $\quad b_0 = 3.531 \times 10^{-3}$

$a_1 = 3.1635 \times 10^{-3}$ $\quad b_1 = 3.3316 \times 10^{-2}$

$a_2 = 0.21163$ $\quad b_2 = 0.12378$

$a_3 = 0.14127$ $\quad b_3 = 1.0$

Each seismic event must be decoded and plotted from the data tapes. The radial Rayleigh component and Love component are obtained by an appropriate rotation of the data coordinates. Figures (11) and (12) show the unrotated and rotated seismograms for an event for the path from Tangshan to Mashad. Representative seismograms for the other three paths (unrotated and rotated) are

TABLE 2

Frequency	Relative Amplitude	Phase Angle (Radians)
.0667	.460	-1.33
.05556	.672	-1.00
.04546	.912	-0.63
.04	1.00	-0.42
.0333	1.01	-0.13
.02778	.9	0.10
.02326	.724	0.30
.02	.550	0.47
.01667	.400	0.63
.0125	.200	0.92
.01	.108	1.10
.00667	.031	1.34
.005	.0104	1.51
.0025	.00084	1.84
.00167	.000184	2.00

FIGURE 10: Numerical fit of the response of long period SRO data (Rosenthal and Teng, 1977)

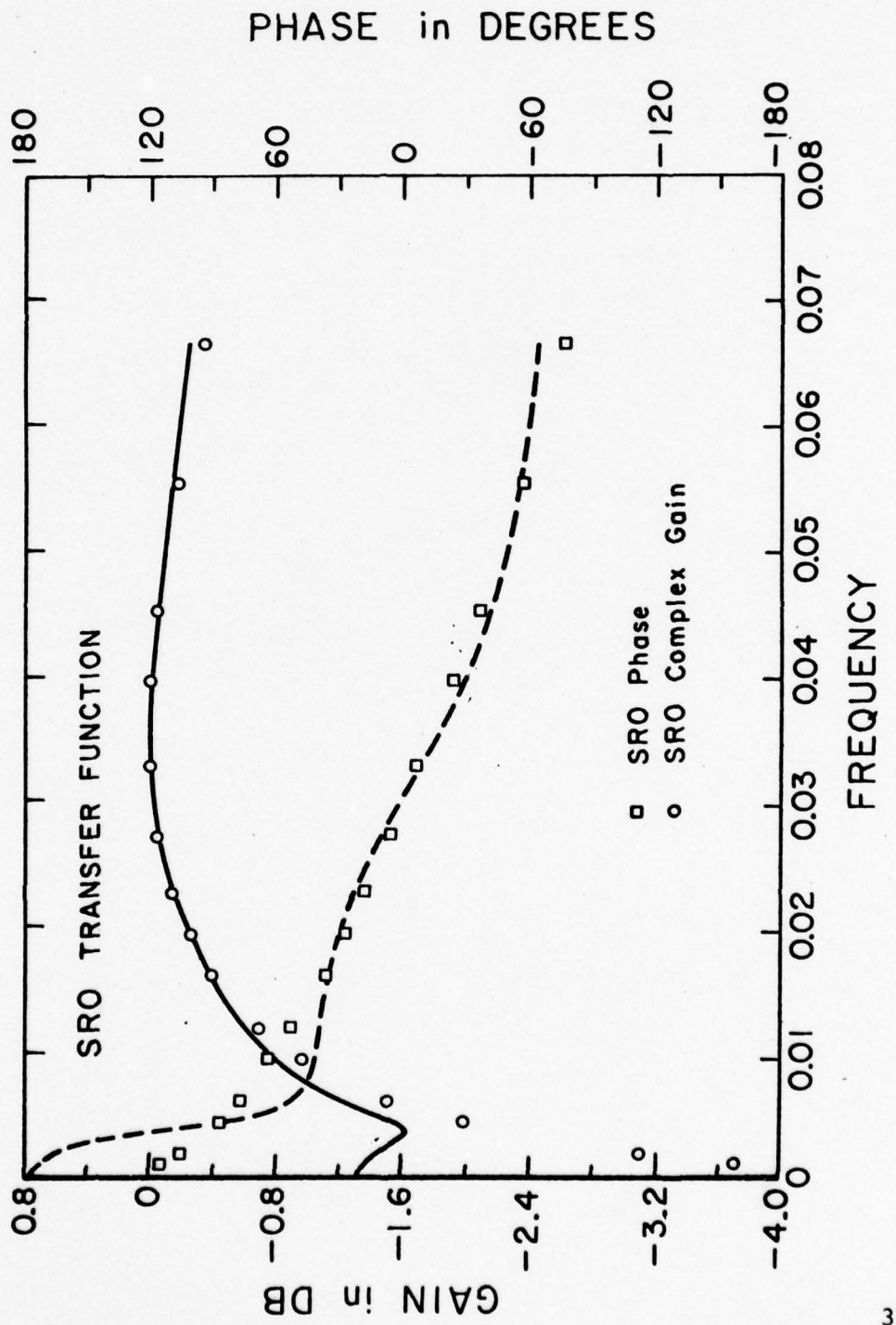
PHASE in DEGREES
180
120
60
0
-60
-120
-180
0.08
0.07
0.06
0.05
0.04
0.03
0.02
0.01
0
FREQUENCY
SRO TRANSFER FUNCTION
SRO Phase
SRO Complex Gain
0.8
0
-0.8
-1.6
-2.4
-3.2
-4.0
GAIN in DB

FIGURE 11: Unrotated seismogram for the path Tangshan-Mashad, August 8, 1976

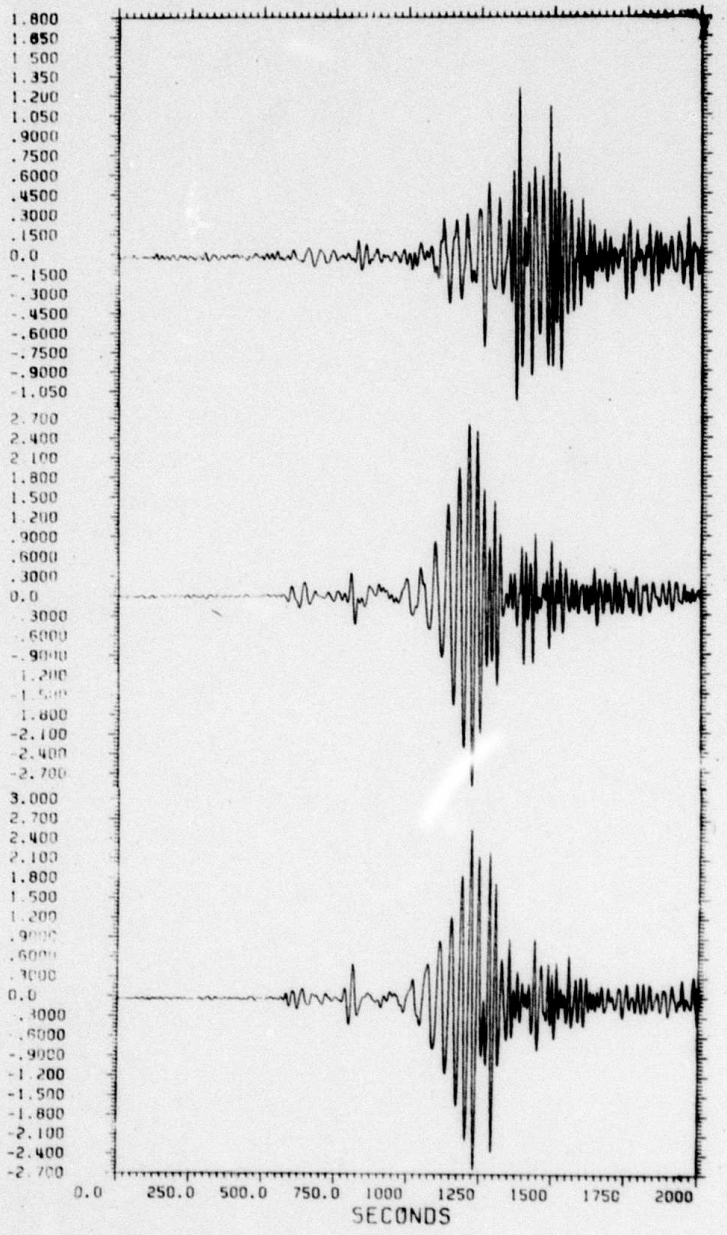
1.800
1.650
1.500
1.350
1.200
1.050
.9000
.7500
.6000
.4500
.3000
.1500
0.0
-.1500
-.3000
-.4500
-.6000
-.7500
-.9000
-1.050
2.700
2.400
2.100
1.800
1.500
1.200
.9000
.6000
.3000
0.0
-.3000
-.6000
-.9000
-1.200
-1.500
-1.800
-2.100
-2.400
-2.700
3.000
2.700
2.400
2.100
1.800
1.500
1.200
.9000
.6000
.3000
0.0
-.3000
-.6000
-.9000
-1.200
-1.500
-1.800
-2.100
-2.400
-2.700
0.0
250.0
500.0
750.0
1000
1250
1500
1750
2000
SECONDS

FIGURE 12: Rotated seismogram for the path Tangshan-Mashad, August 8, 1976

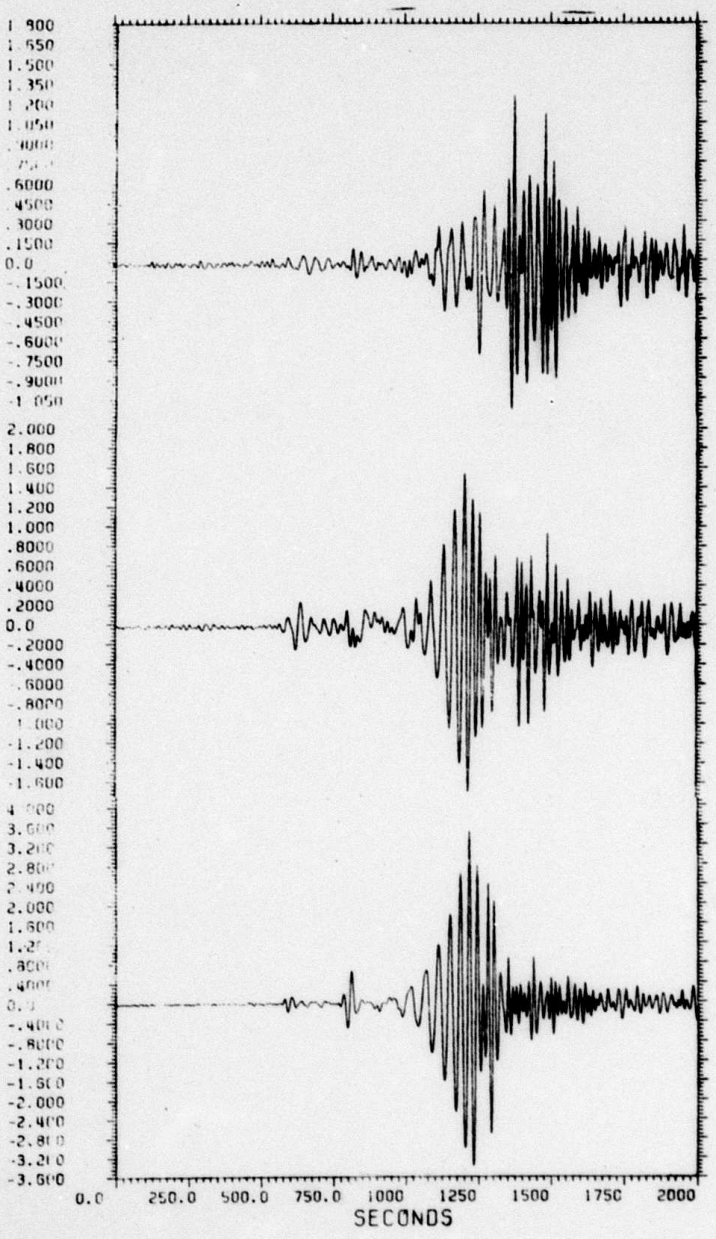
1.800
1.650
1.500
1.350
1.200
1.050
.6000
.4500
.3000
.1500
0.0
-.1500
-.3000
-.4500
-.6000
-.7500
-.9000
-1.050
2.000
1.800
1.600
1.400
1.200
1.000
.8000
.6000
.4000
.2000
0.0
-.2000
-.4000
-.6000
-.8000
-1.000
-1.200
-1.400
-1.600
-2.000
-2.400
-2.800
-3.200
-3.600
0.0
250.0
500.0
750.0
1000
1250
1500
1750
2000
SECONDS

presented in Appendix 1.

Method and Theory

Analysis of the data was performed by using computer programs adaped for the IBM 370/150 at the University of Southern California. The first portion of the data analysis requires the use of a multiple filtering program (Dziewonski and Hales, 1970) which reads the distance, time lapse between earthquake and start of digitization, and the digitized Seismogram. Transformation from the time domain to the frequency domain is carried out by a Fast Fourier Transform (Cooley and Tukey, 1965). A Gaussian filter is used as extensively described by Hermann (1973) and Tung (1974) to be of the form:

$$H(\omega-\omega_0) = \exp\left[-\alpha\left(\frac{\omega-\omega_0}{\omega_0}\right)^2\right]$$

where α is chosen to control the bandwidth of the filter. The value of ω_0 ranges from periods of 11 to 128 seconds.

After the transformation to the frequency domain was performed, the instrument corrections were made. For each value the spectral amplitude was normalized representing the group velocity arrival for that period. Figures (13), (14), and (15) give the energy plot of group arrivals for the Rayleigh, radial Rayleigh and Love components for a representative event over the Tangshan to Taipei path after multifilter analysis is performed.

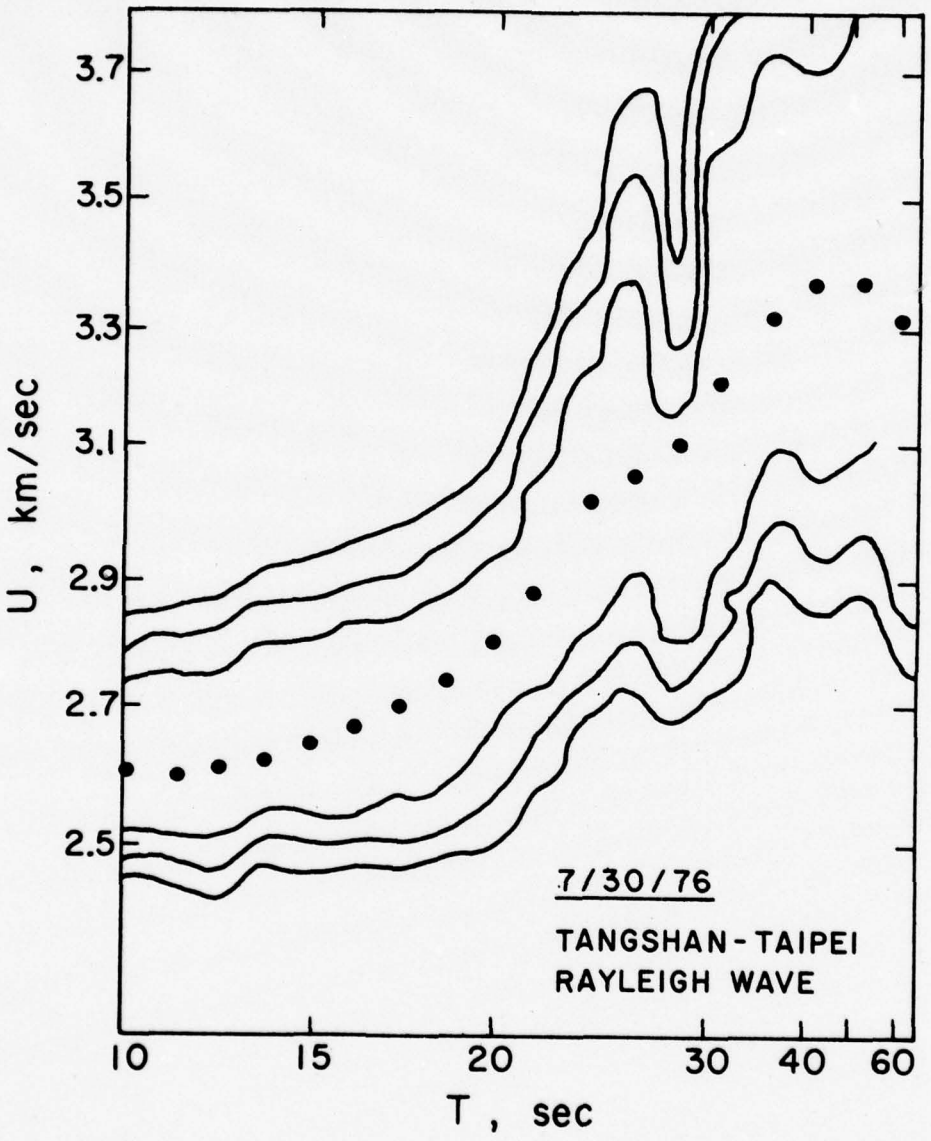

FIGURE 13: Results of multiple filtering of Rayleigh component, Tangshan-Taipei, July 30, 1976

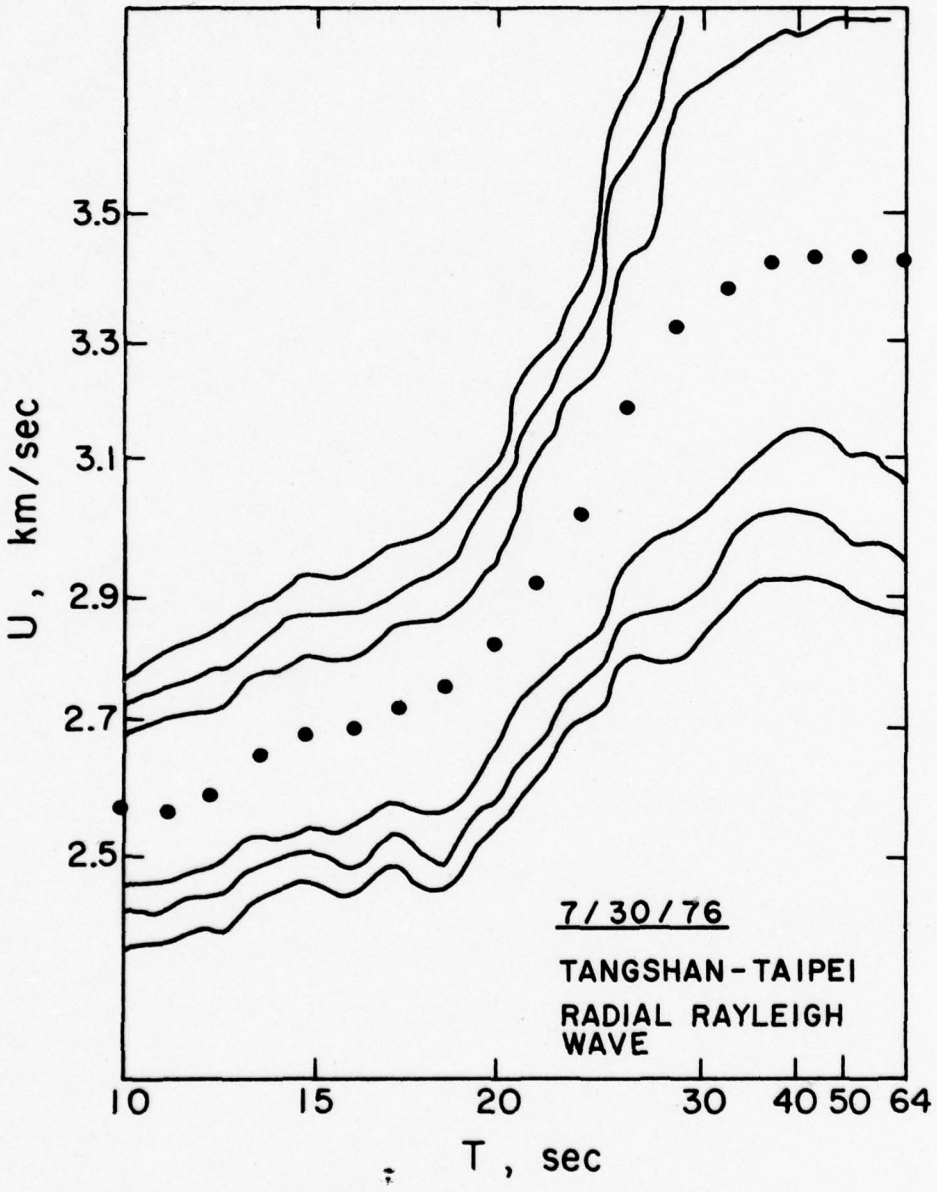

FIGURE 14: Results of multiple filtering of radial Rayleigh component, Tangshan-Taipei, July 30, 1976

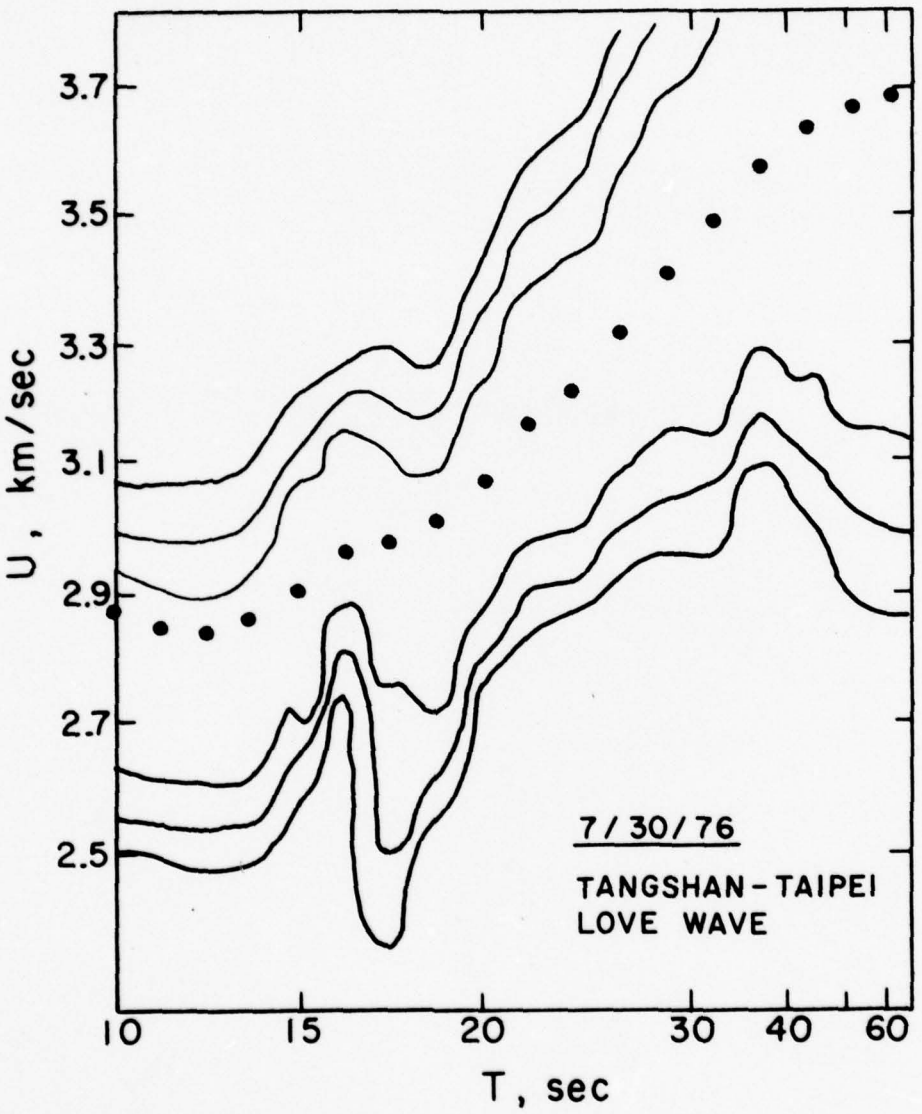

FIGURE 15: Results of multiple filtering of Love component, Tangshan-Taipei, July 30, 1976

Representative multifilter analysis for the other paths are presented in Appendix 2. The contours drawn represent the relative amplitude of wave energy arrivals and the dispersion curve is derived by connecting the maximum amplitude points. Often at the low period end (below 20 seconds) ambiguity arises in drawing contours resulting from interference by S waves. The contour lines give several local maxima and will not allow a clear-cut determination of group velocity values.

The dispersion curves for Rayleigh and Love waves are plotted for all events of each path in Figures (16-23). Included are higher mode data when observable from the multifilter analysis. Statistical properties of the observations for each path are shown in Tables (3) - (6).

The program used for the inversion of the surface wave dispersion data is based upon a Backus-Gilbert inversion method (1967, 1968, 1970) as applied to intermediate and long period group velocity data. Lucid descriptions of the Backus-Gilbert method in a matrix formulation have been presented by Jackson (1972), Wiggins (1972), Crossen (1976) and Rosenthal and Teng (1977). A brief outline of the method is presented below.

The fundamental equation for the generalized least squares linear inverse problem is:

$$Y = AX \qquad (1)$$

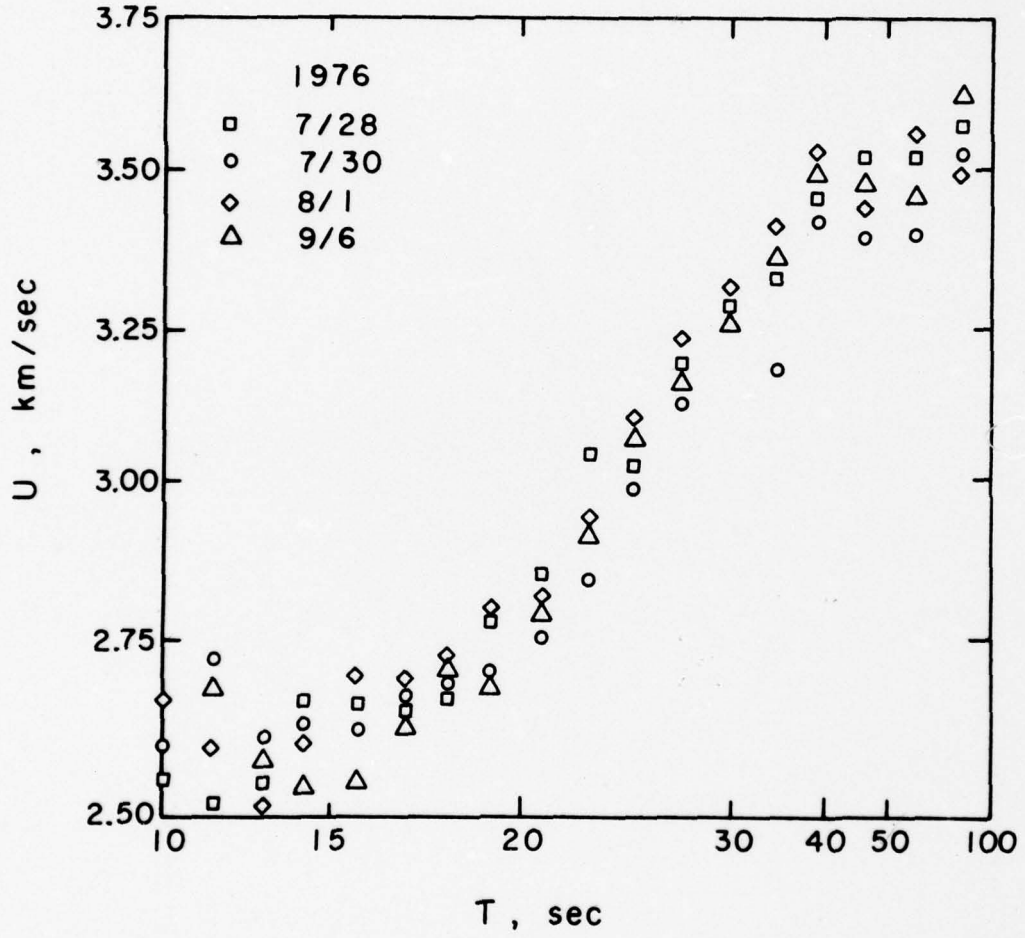

FIGURE 16: Group velocities of the Rayleigh component for all events of the path Tangshan-Taipei

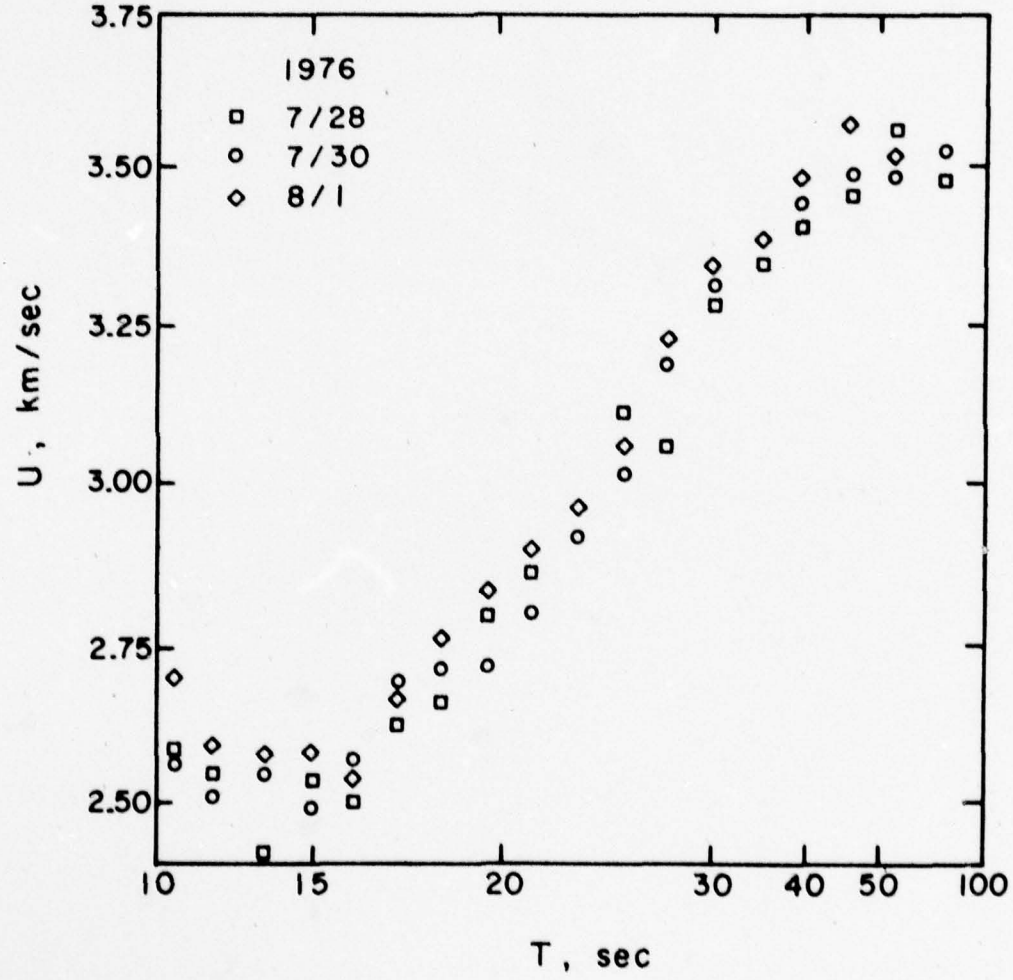

FIGURE 17: Group velocities of the radial Rayleigh component for all events of the path Tangshan-Taipei

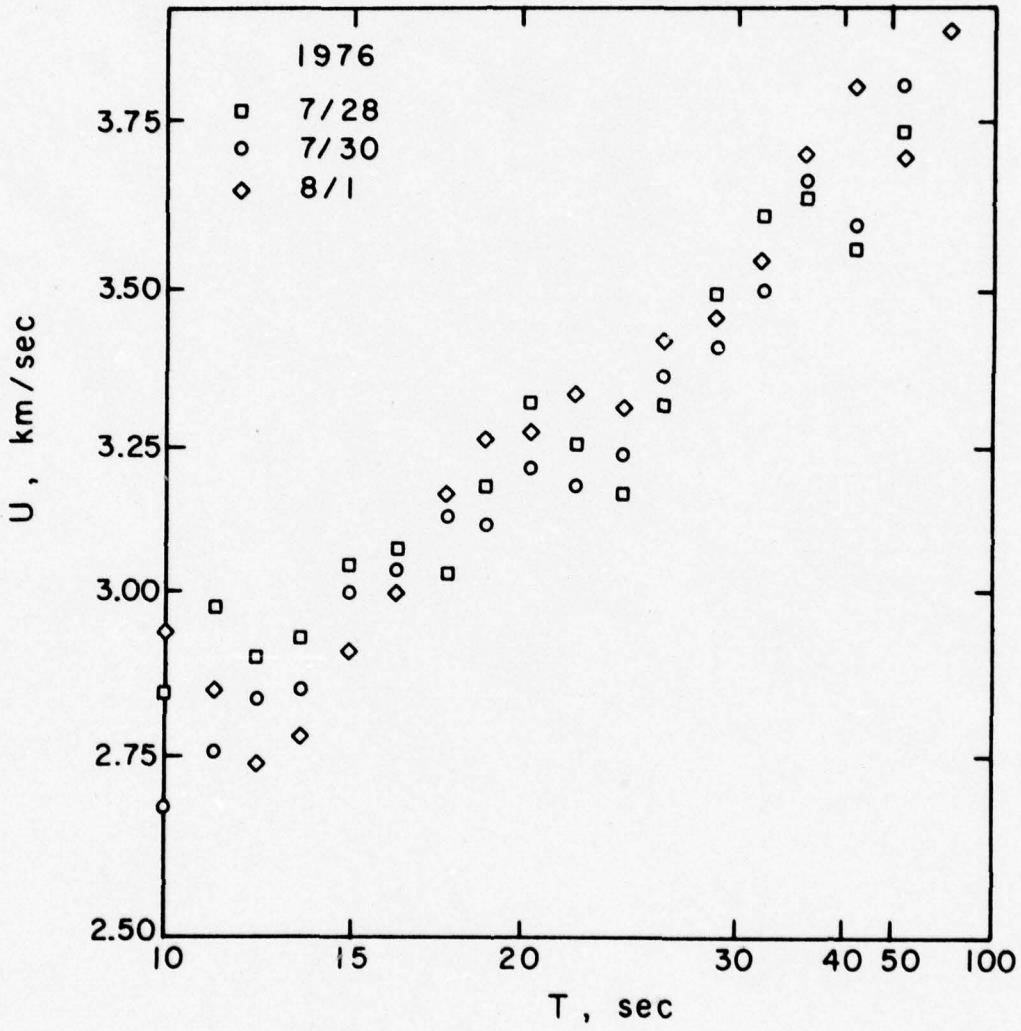

FIGURE 18: Group velocities of the Love component for all events of the path Tangshan-Taipei

FIGURE 19: Group velocities of the Rayleigh component for all events of the path Tangshan-Mashad

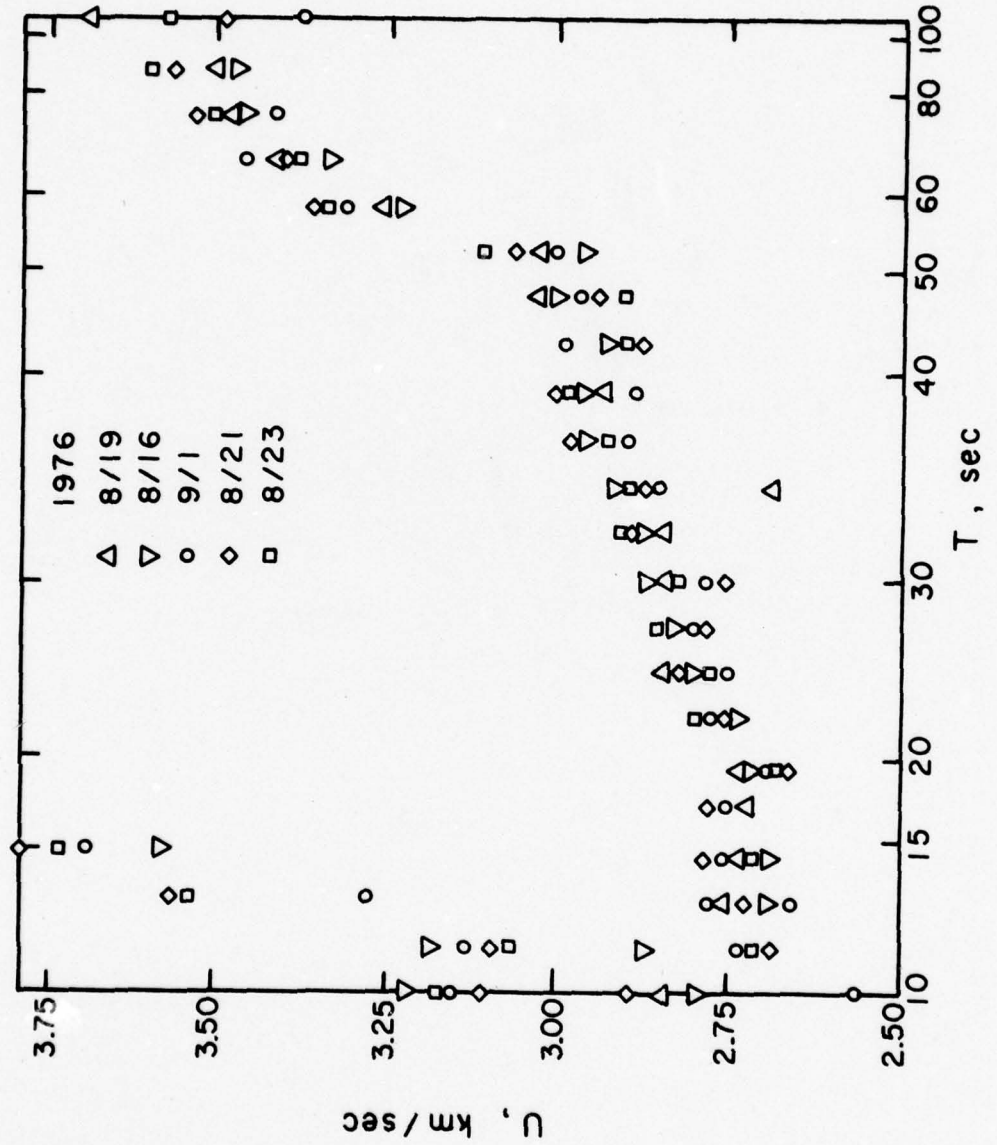
1976
8/19
8/16
9/1
8/21
8/23
T, sec
10
15
20
30
40
50
60
80
100
2.50
2.75
3.00
3.25
3.50
3.75
U, km/sec

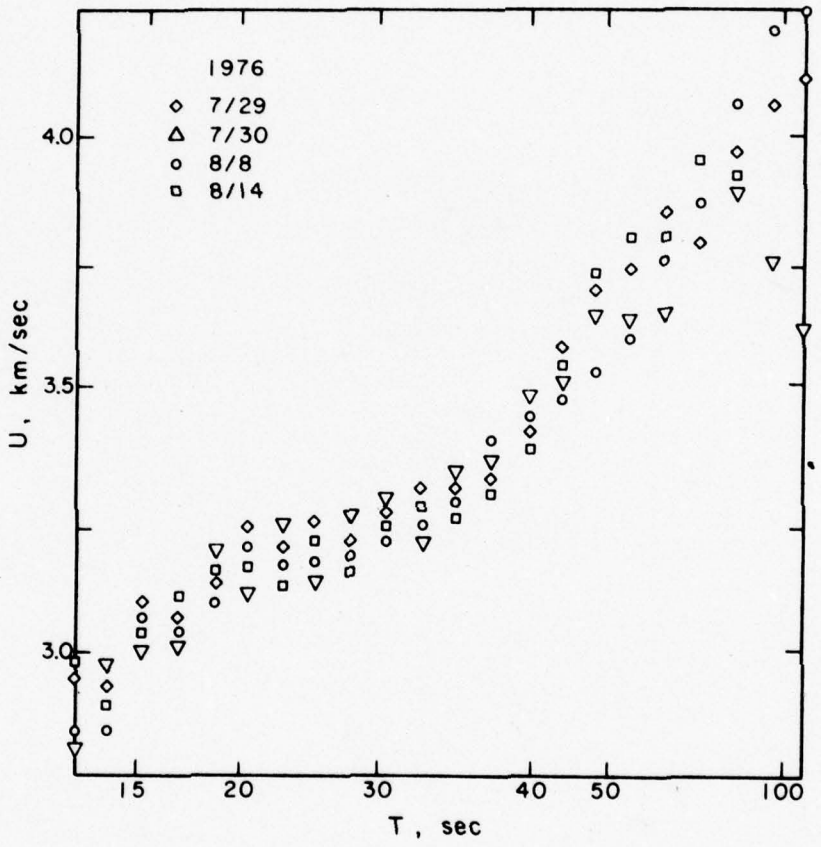

FIGURE 20: Group velocities for all events of the path Tangshan-Mashad

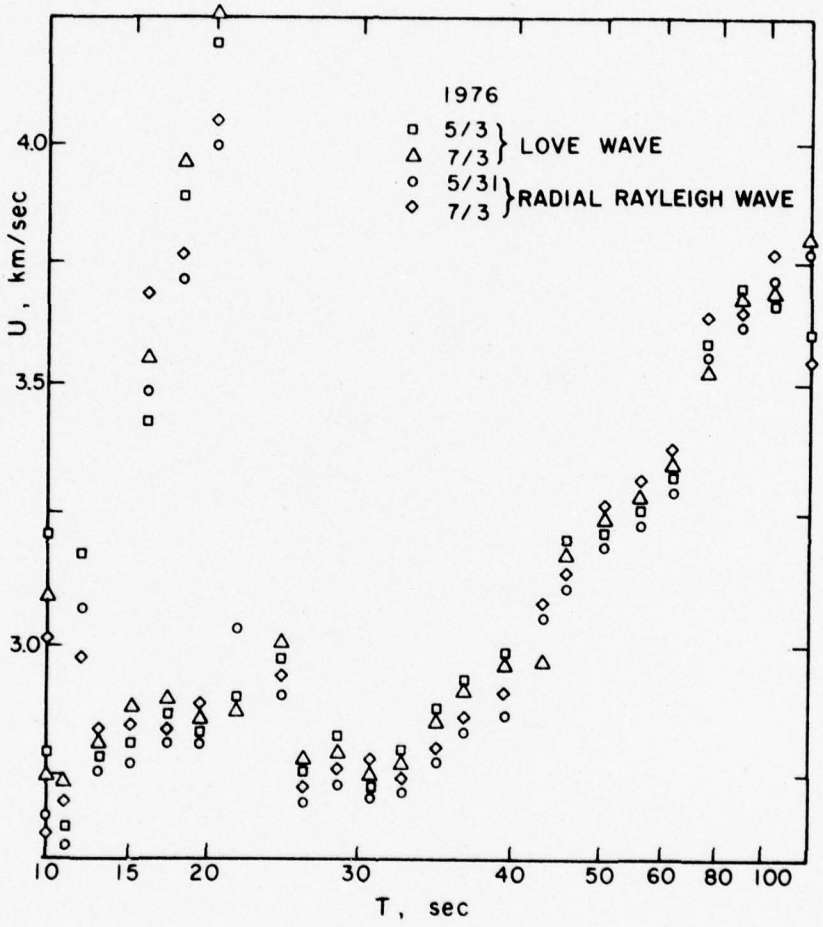

FIGURE 21: Group velocities of the Rayleigh and radial Rayleigh component for all events of the path Yunnan-Mashad

FIGURE 22: Group velocities of the Rayleigh component for all events of the path Szechwan-Mashad

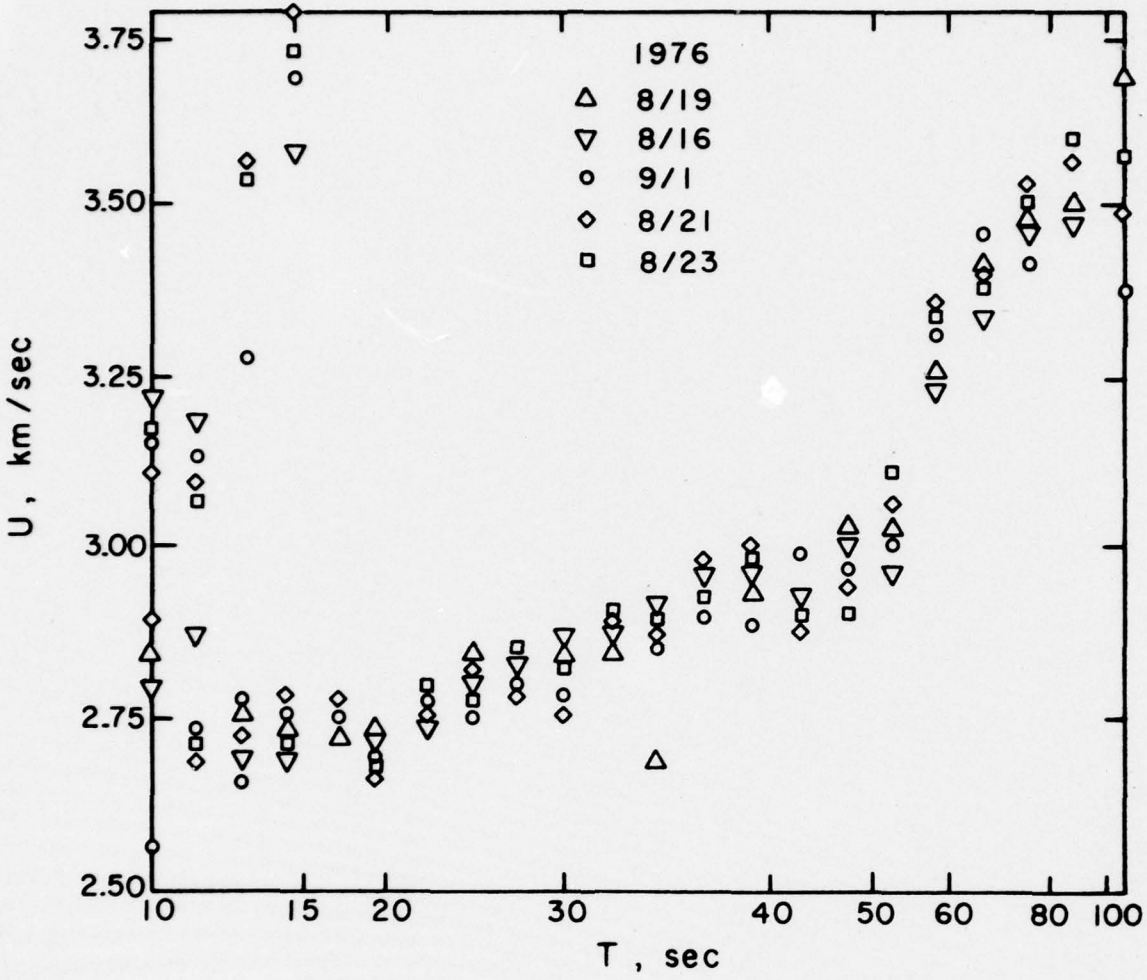
1976
8/19
8/16
9/1
8/21
8/23
3.75
3.50
3.25
3.00
2.75
2.50
U, km/sec
10
15
20
30
40
50
60
80
100
T, sec

FIGURE 23: Group velocities of the radial Rayleigh component for all events of the path Szechwan-Mashad

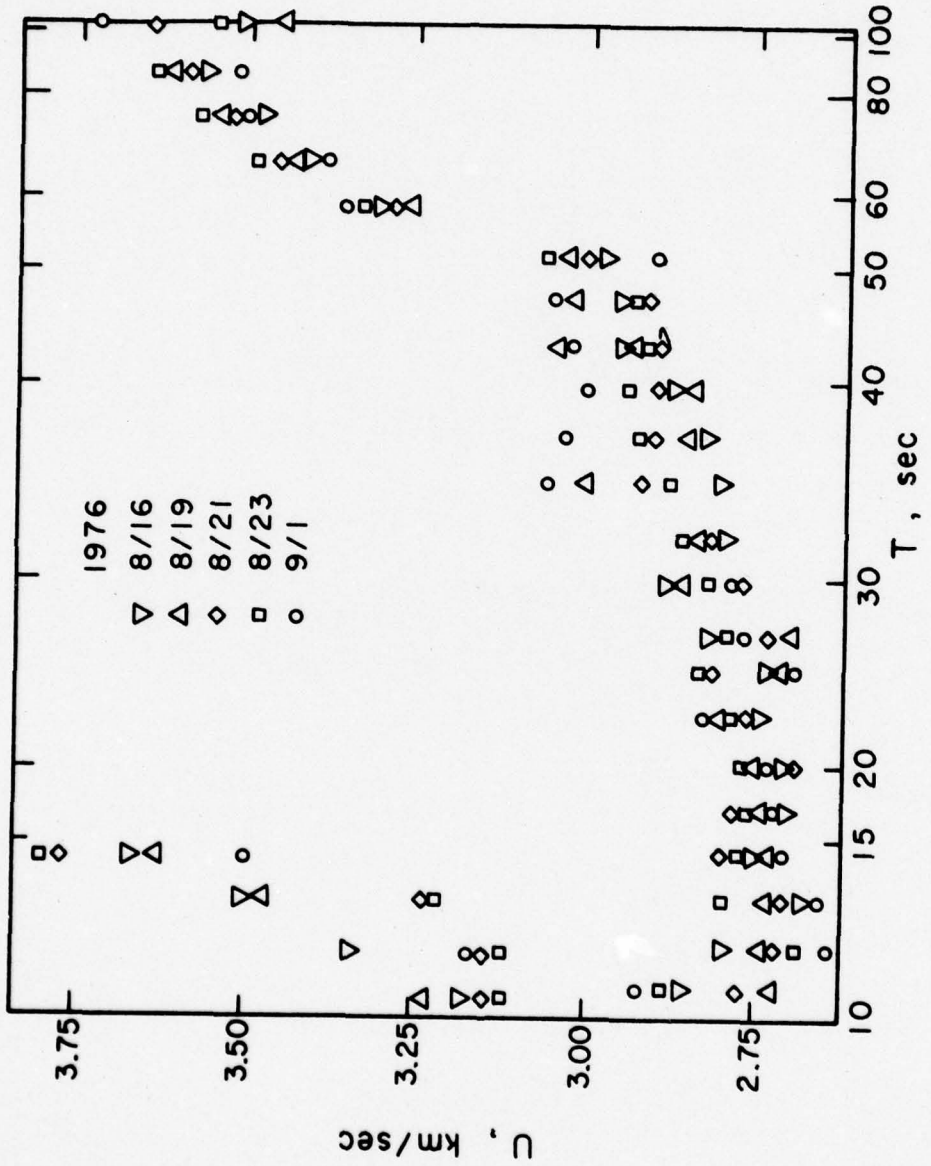
1976
8/16
8/19
8/21
8/23
9/1
C , km/sec
3.75
3.50
3.25
3.00
2.75
10
15
20
30
40
50
60
80
100
T , sec

TABLE 3

Tangshan-Taipei Observed Dispersion Data

Period (sec)	Rayleigh Wave (km/sec)	Love Wave (km/sec)
64.0	3.49 ± .06	3.85 ± .15
51.2	3.48 ± .09	3.71 ± .10
42.7	3.46 ± .11	3.69 ± .06
36.6	3.48 ± .11	3.59 ± .05
32.0	3.30 ± .09	3.52 ± .08
28.4	3.29 ± .05	3.37 ± .05
25.6	3.15 ± .08	3.31 ± .05
23.3	3.04 ± .05	3.19 ± .05
21.3	3.00 ± .06	3.19 ± .05
19.7	2.84 ± .06	3.12 ± .09
18.3	2.76 ± .09	3.12 ± .07
17.1	2.72 ± .06	3.04 ± .09
16.0	2.67 ± .05	3.02 ± .04
15.1	2.63 ± .10	2.93 ± .05
13.5	2.58 ± .13	2.89 ± .10
12.2	2.52 ± .10	2.85 ± .15
11.1	2.59 ± .18	2.90 ± .07
10.2	2.64 ± .17	2.91 ± .15

TABLE 4

Tangshan-Mashad Observed Dispersion Data

Period (sec)	Rayleigh Wave (km/sec)	Love Wave (km/sec)
102.4	3.73 ± .20	4.00 ± .20
85.3	3.65 ± .18	3.91 ± .13
73.1	3.69 ± .10	3.91 ± .10
64.0	3.57 ± .10	3.85 ± .05
56.9	3.65 ± .18	3.74 ± .06
51.2	3.54 ± .05	3.70 ± .11
46.5	3.47 ± .05	3.66 ± .10
42.6	3.43 ± .05	3.56 ± .06
39.4	3.35 ± .05	3.46 ± .05
36.6	3.22 ± .05	3.38 ± .05
34.1	3.14 ± .04	3.36 ± .05
32.0	3.10 ± .05	3.31 ± .05
30.1	3.01 ± .06	3.29 ± .06
26.9	2.93 ± .06	3.21 ± .05
24.4	2.91 ± .08	3.18 ± .05
22.3	2.85 ± .10	3.16 ± .07
20.5	2.74 ± .06	3.17 ± .05
18.9	2.78 ± .10	3.14 ± .05
16.0	2.82 ± .18	3.06 ± .06
13.8	2.75 ± .07	3.01 ± .06
12.2	2.79 ± .08	2.95 ± .10
10.9	2.69 ± .08	2.89 ± .15

TABLE 5

Yunnan-Mashad Observed Dispersion Data

Period(sec)	Rayleigh Wave(km/sec) Fundamental	First Higher Mode
102.4	3.52 ± .15	
85.3	3.49 ± .15	
73.1	3.41 ± .10	
64.0	3.25 ± .15	
56.9	3.12 ± .10	
51.2	3.05 ± .10	
46.5	3.00 ± .10	
42.7	2.95 ± .10	
39.4	2.87 ± .07	
36.6	2.79 ± .07	
34.1	2.73 ± .07	
32.0	2.71 ± .07	
30.1	2.73 ± .15	
27.0	2.67 ± .15	
24.4	2.85 ± .15	
22.3	2.79 ± .05	
20.5	2.79 ± .05	4.09 ± .15
18.9	2.77 ± .05	3.80 ± .17
16.0	2.77 ± .06	3.48 ± .10
13.8	2.77 ± .06	
12.2	2.64 ± .15	3.17 ± .08
10.9	2.71 ± .10	3.15 ± .07

TABLE 6

Szechwan-Mashad Observed Dispersion Data

Period (sec)	Rayleigh Wave (km/sec) Fundamental	First Higher Mode
102.4	3.54 ± .17	
85.3	3.56 ± .09	
73.1	3.49 ± .06	
64.0	3.41 ± .07	
56.9	3.28 ± .06	
51.2	2.96 ± .15	
46.5	2.96 ± .15	
42.7	2.95 ± .07	
39.4	2.87 ± .06	
36.7	2.87 ± .08	
34.1	2.87 ± .09	
32.0	2.79 ± .10	
30.1	2.76 ± .09	
26.9	2.75 ± .06	
24.4	2.74 ± .07	
22.3	2.76 ± .04	
20.5	2.69 ± .05	
18.9	2.71 ± .04	
16.0	2.73 ± .04	3.71 ± .20
13.8	2.70 ± .07	3.45 ± .15
12.2	2.73 ± .13	3.35 ± .15
10.8		3.16 ± .10

where Y represents the observations which are related to the parameters of the model X by the matrix A. The problem is assumed to be linear or to have been linearized, in which case Y is the difference between the observations and the theoretical data determined for an initial model X_0. X is a vector which consists of parameter changes which are to be determined and which must be added to X_0, the initial parameter model, to cause Y to be minimized. A is a matrix of partial derivatives which are first order Taylor Series expansions of the non-linear function about the initial model X_0.

$$\Delta Y = A\Delta X \tag{2}$$

In our case, the observations are group velocities of Rayleigh and Love waves, the model parameters are the compressional velocities, shear velocities, and densities for a horizontally layered earth, and the partial derivatives of matrix A are generated numerically by the method described by Rodi, et al. (1974)

The matrix A by means of a single value decomposition described by Lanczos (1964) may be written as

$$A = U\Lambda V^T \tag{3}$$

where the columns of U are the eigenvectors associated

with the columns of A, the rows of V are associated with the rows of A, and Λ is a diagonal matrix of non-zero eigenvalues of matrix A.

$$\Lambda = A^T A = \begin{matrix} \lambda_1 & & & \\ & \ddots & & \\ & & \ddots & \\ & & & \lambda_n \end{matrix} \tag{4}$$

Following the development described by Jackson (1972) we let:

$$H = (A^T A)^{-1} A^T \tag{5}$$

$$HA\Delta X = H\Delta Y \tag{6}$$

$$\Delta\hat{X} + HA\Delta X = H\Delta Y \tag{7}$$

Substituting equation (3) into equation (7):

$$\Delta\hat{X} = (\Lambda V^{-1} U^T)\Delta Y \tag{8}$$

where

$$H = \Lambda V^{-1} U^T \tag{9}$$

The product $A^T A$ of equation (4) is often near singular causing: (1) the solution vector to become too large

which will cause the problem to leave the region of linearity; or (2) the solution vector to oscillate with each iteration. The cause of the instability is when H, the pseudo inverse of equation (2):

$$H = V\Lambda^{-1}U^T \tag{10}$$

where

$$\Lambda^{-1} = \begin{matrix} \lambda_1 & 0 & . & . & . & . & -1 \\ 0 & \lambda_2 & 0 & . & . & . & \\ . & . & . & . & . & . & \\ 0 & . & . & . & . & \lambda_n & \end{matrix}$$

has eigenvalues, λ_i, which approach zero. This will result in a large change in $\Delta\hat{X}$ for a very small eigenvalue λ_i. Both Franklin (1970) and Marquardt (Crossen, 1976) developed methods to overcome this instability in the inversion due to small eigenvalues.

The method developed by Franklin (1970) is known as the stochatic inverse method. The parameter changes, X, are determined in the presence of noise and equation (2) becomes:

$$A\Delta X + N = \Delta Y \tag{11}$$

where N is observational noise. The solution is represented as:

$$\Delta X = WA^T(AWA^T + ED)^{-1}\Delta X \tag{12}$$

where W is the covariance matrix of the parameters and ED is the covariance matrix of the observations (Rosenthal and Teng, 1977).

In the Marquardt method (Crossen, 1976) equation (12) is written:

$$\Delta X = (A^TA + \delta^2 I)A^T\Delta Y \tag{13}$$

where δ^2 is known as the trade-off parameter. Substituting equation (3) into equation (13):

$$\Delta X = V|(\Lambda^2 + \delta^2 I)^{-1}\Lambda|U^T\Delta Y \tag{14}$$

Following the development by Crossen (1976) and Rosenthal and Teng (1977) the elements in the brackets are:

$$|(\Lambda^2 + \delta^2 I)^{-1}\Lambda_i| = \lambda_i/(\lambda_i^2 + \delta^2)$$

The instability is eliminated by tapering the eigenvalue spectrum. As λ_i approaches zero, ΔX_i approaches zero. The resolution matrix now may be written as either:

$$R = HA = (A^TA + \delta^2 I)A^TA = V|(\Lambda + \delta^2 I)^{-1}\Lambda^2|V^T \qquad (15)$$

using the Marquardt method or:

$$R = |(\Lambda^2 + \delta^2 I)^{-1}\Lambda^2|VV^T \qquad (16)$$

using the stochastic inverse method. The parameter is adjusted in both methods until a suitable trade-off σ^2 between standard deviation and resolution is achieved.

Either the Marquardt method or the stochastic inverse method are applied in the inversion depending on the number of parameters and observations. If the number of observations exceeds the number of parameters the Marquardt method is used. If the number of parameters exceeds the number of observations the stochastic inverse method is used.

Two other elements used in the inversion process are the apriore (SDX_o) and postpriori (SDX) standard deviations of the inversion parameters.

$$SDX_o = D^T(\delta W_p^{-1})D \qquad (17)$$

$$SDX = (D^TA^TED^{-1}A + \delta W_p^{-1})^{-1}D^{\frac{1}{2}} \qquad (18)$$

where D is a row vector of delta matrix, (0, 0, . . . 1

. . . 0). By comparing the magnitude of SDX to SDX_0 one can determine how much new information is coming from the data. For example, if the value of SDX and SDX_o are approximately equal then little new information is being obtained from the data.

RESULTS AND DISCUSSIONS

From topography, Bouguer gravity, and surface wave dispersion information, Mainland China may be divided into three subplates. When a pure path configuration is possible, like in the Tibetan plateau, the interpretation of the shear wave velocity profile in the crust and upper mantle is straightforward. Where a path crosses two or more subplates only an average shear wave velocity profile will be presented.

Initial models for the inversion were based upon the results of a previous surface wave study of Mainland China by Tung (1974). Inversions were performed for compressional wave velocity, shear wave velocity, and density. As discussed by Wiggins (1972), Der, et al. (1973), and Jackson (1976) the partial derivatives for shear wave velocity are larger than those for compressional wave velocity or density. Therefore the resolution for shear wave velocity is considerably better than for the two other parameters and only the resolution matrix for the partial derivatives with respect to shear wave velocity

shall be presented.

When group velocities are inverted for an earth structure in the model fitting process, they are within 0.2 km/sec of the observed group velocity for both pure and mixed paths.

Tibetan Plateau

Two separate paths across the Tibetan plateau were used (Figure 9). Both paths originate from earthquakes on the eastern boundary of the Tibetan plateau. The first group occurred in Szechwan Province and the second group of earthquakes occurred in Yunnan Province, south of Szechwan Province. A list of the surface wave trains used across the Tibetan plateau is given in Tables (7) and (8).

For each path across the Tibetan plateau, inversions were performed using the fundamental and first higher mode Rayleigh waves. The fit of the theoretical model to the observed group velocities are presented in Figures (24-26). A comparison of the average continental dispersion for Rayleigh waves (Ewing et al., 1957) to Rayleigh waves of the four paths across China is presented in Figure (2). The group velocities across the Tibetan plateau are less than the group velocities for the average continental structure. The difference extends to periods of 120 seconds which infers an abnormal upper mantle structure.

TABLE 7

Seismogram Components Used for the

Path Szechwan to Mashad

Earthquake	Recording Station	Component	Wave Type	Distance(km)
Aug 16, 1976	MAIO	Vertical	Rayleigh	4080
Aug 16, 1976	MAIO	Radial	Rayleigh	4080
Aug 19, 1976	MAIO	Vertical	Rayleigh	4078
Aug 19, 1976	MAIO	Radial	Rayleigh	4078
Aug 21, 1976	MAIO	Vertical	Rayleigh	4095
Aug 21, 1976	MAIO	Radial	Rayleigh	4095
Aug 23, 1976	MAIO	Vertical	Rayleigh	4088
Aug 23, 1976	MAIO	Radial	Rayleigh	4088
Sept 1, 1976	MAIO	Vertical	Rayleigh	4090
Sept 1, 1976	MAIO	Radial	Rayleigh	4090

TABLE 8

Seismogram Components Used for the

Path Yunnan-Mashad

Earthquake	Recording Station	Component	Wave Type	Distance(km)
May 31, 1976	MAIO	Vertical	Rayleigh	3956
May 31, 1976	MAIO	Radial	Rayleigh	3956
July 3, 1976	MAIO	Vertical	Rayleigh	3967
July 3, 1976	MAIO	Radial	Rayleigh	3967

FIGURE 24: Theoretical and observed group velocities for SMI

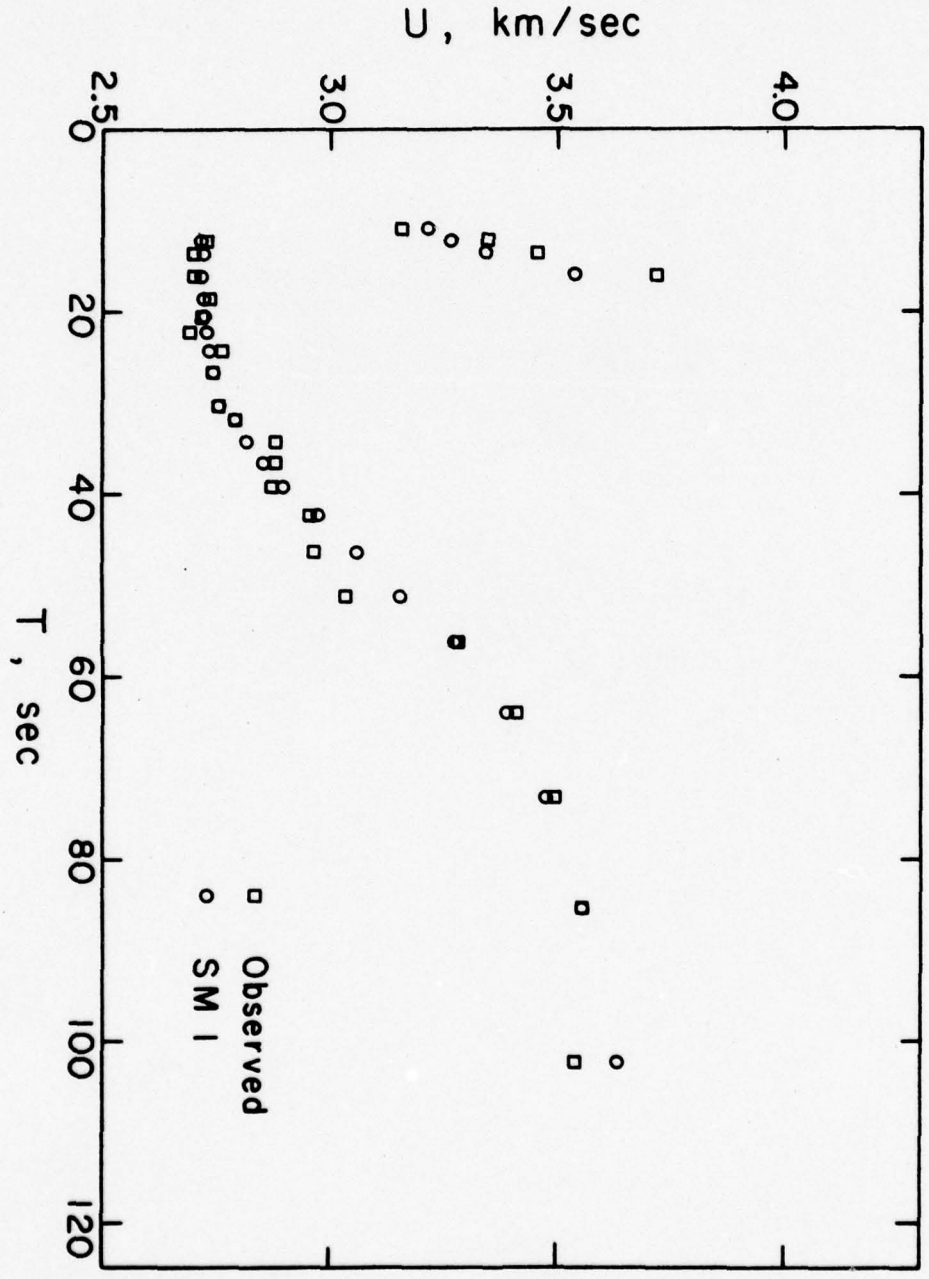
U, km/sec
2.5
3.0
3.5
4.0
T, sec
20
40
60
80
100
120
Observed
SM I

FIGURE 25: Theoretical and observed group velocities for model SM2

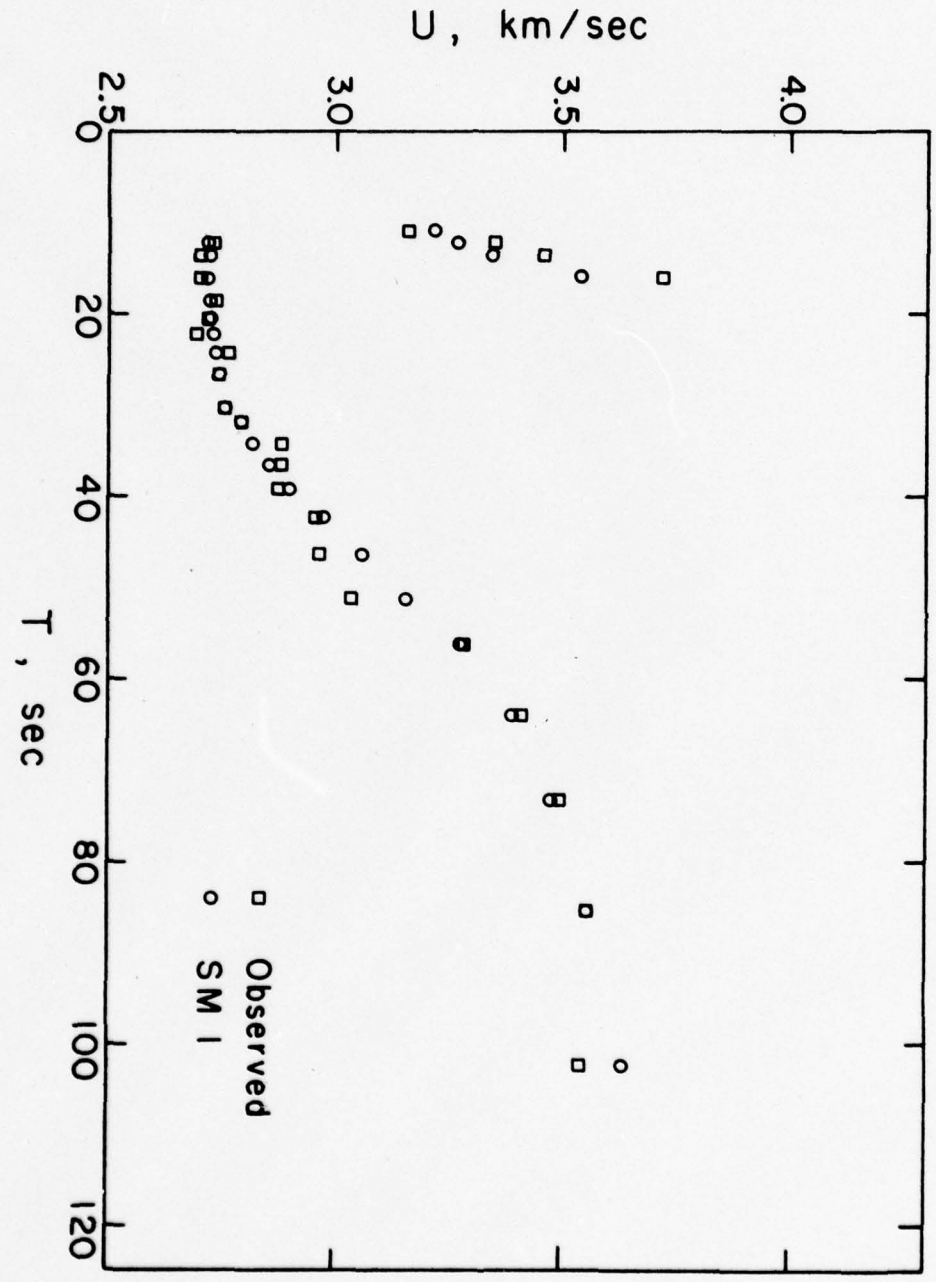
U, km/sec
2.5
3.0
3.5
4.0
T, sec
20
40
60
80
100
120
Observed
SM I

FIGURE 26: Theoretical and observed group velocities for YM1

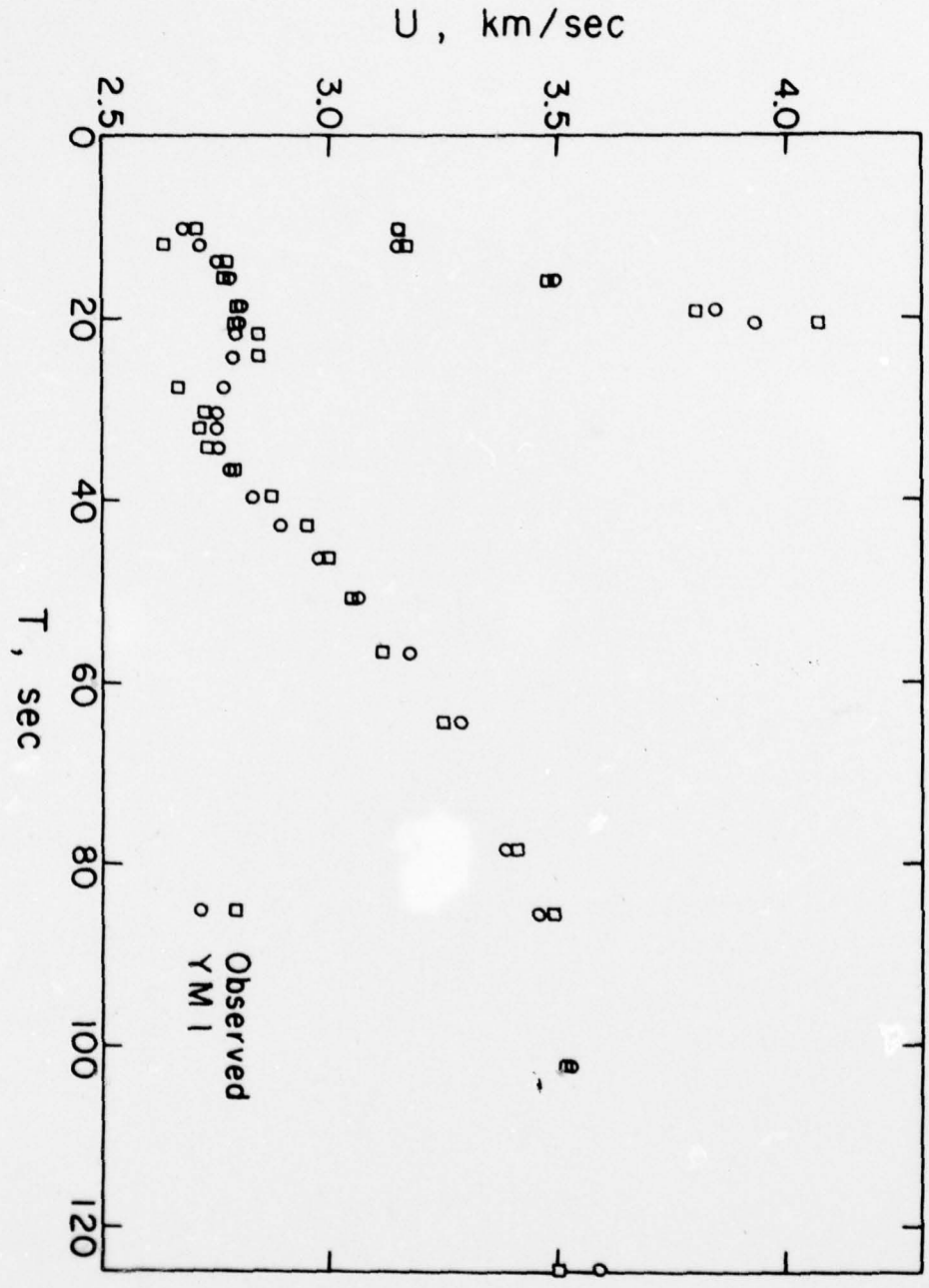
U , km/sec
2.5
3.0
3.5
4.0
0
20
40
60
80
100
120
T , sec
Observed
YM I

FIGURE 27: Comparison of Rayleigh wave group velocities from all the paths across China with the average continental dispersion (Ewing et al., 1957)

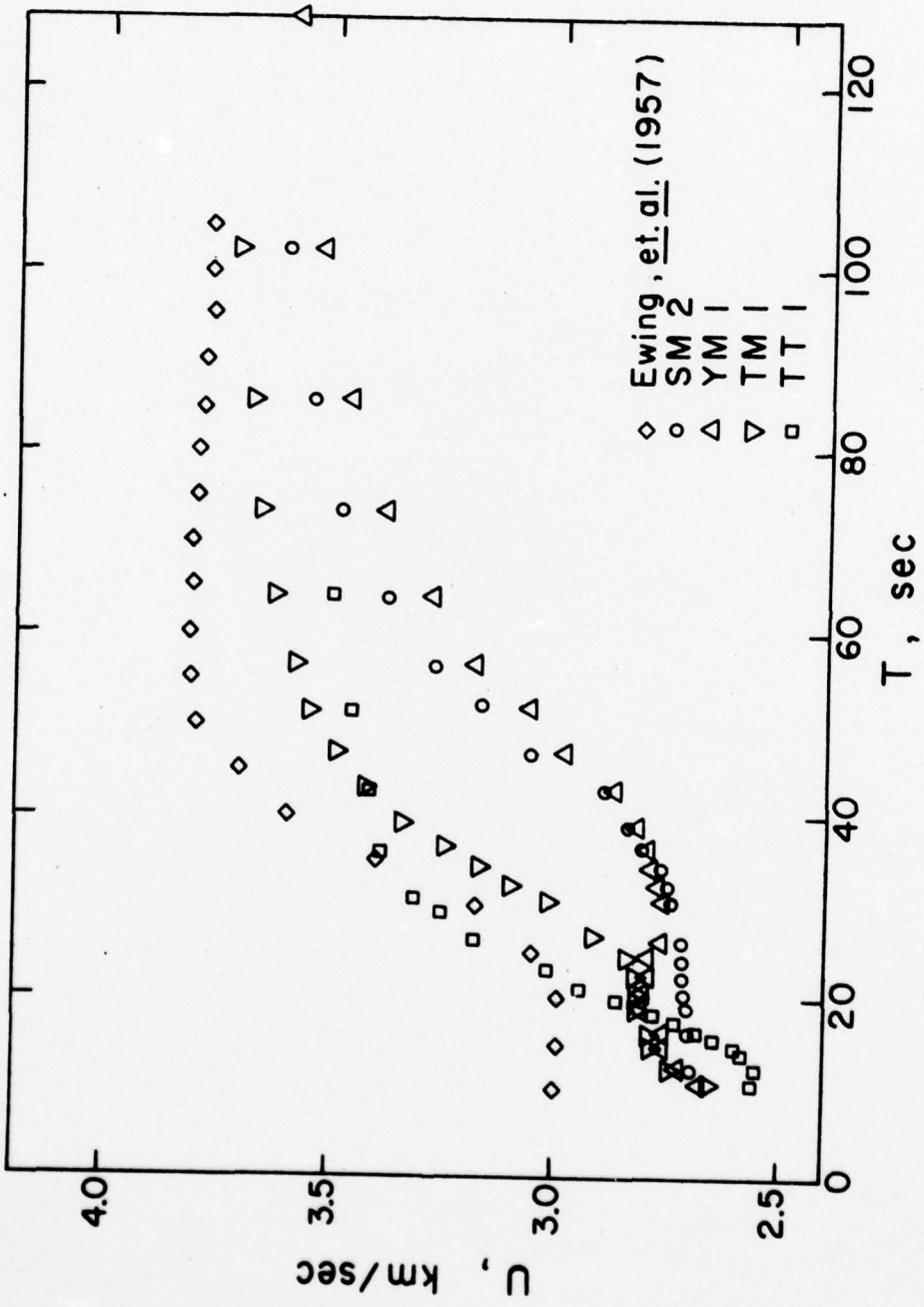
Ewing, et. al. (1957)
SM 2
YM 1
TM 1
TT 1
U, km/sec
T, sec
4.0
3.5
3.0
2.5
0
20
40
60
80
100
120

Group velocities across the Tibetan plateau are the lowest of all the regions of China. For the fundamental mode, Rayleigh wave group velocities ranged between 3.60 km/sec to 2.60 km/sec. Steep slopes for both paths across the Tibetan plateau occur between 40 to 60 seconds, where change in the group velocity can range as high as 0.6 km/sec. Love waves were not used in the inversion because of the absence of amplitude maxima in the dispersion curves between 30 to 60 seconds. Various studies have been made (Thatcher and Brune, 1979, Boore, 1969, James, 1971) that discussed the problem of interference of Love waves crossing inhomogeneous media. Tung (1974) attributed this problem in the Tibetan plateau to Love waves following a non-least time path. A possible structural implication is that there exist structures along the path corresponding to wave lengths of the Love waves causing the wave energy to travel a non-least time path with slower velocities.

Starting and final shear wave velocity models with standard deviation bars for the path Szechwan to Mashad are presented in Figures (28 and 29). In Tables (10-13) the initial and final model parameters and the resolution matrix for each model are presented. The resolution matrix for the eight layer model is listed in Table (11). From the width of the resolving kernels it is possible to resolve layers of 15 km in the upper crust, 15-20 km in the middle crust, and 25-30 km in the lower crust.

FIGURE 28: Resulting shear wave velocity model for SM1

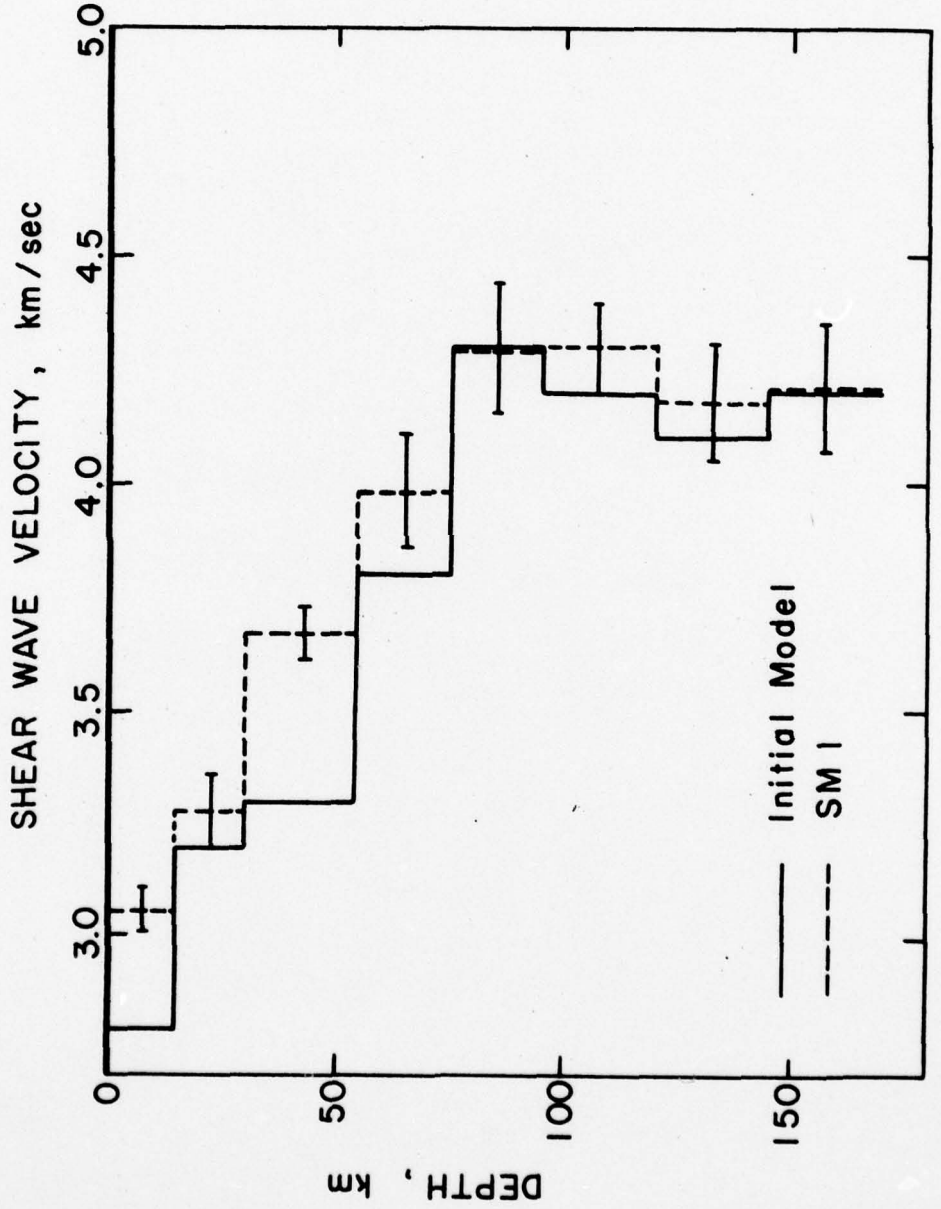
SHEAR WAVE VELOCITY, km/sec
3.0
3.5
4.0
4.5
5.0
DEPTH, km
0
50
100
150
Initial Model
SM I

FIGURE 29: Resulting shear velocity model for SM2

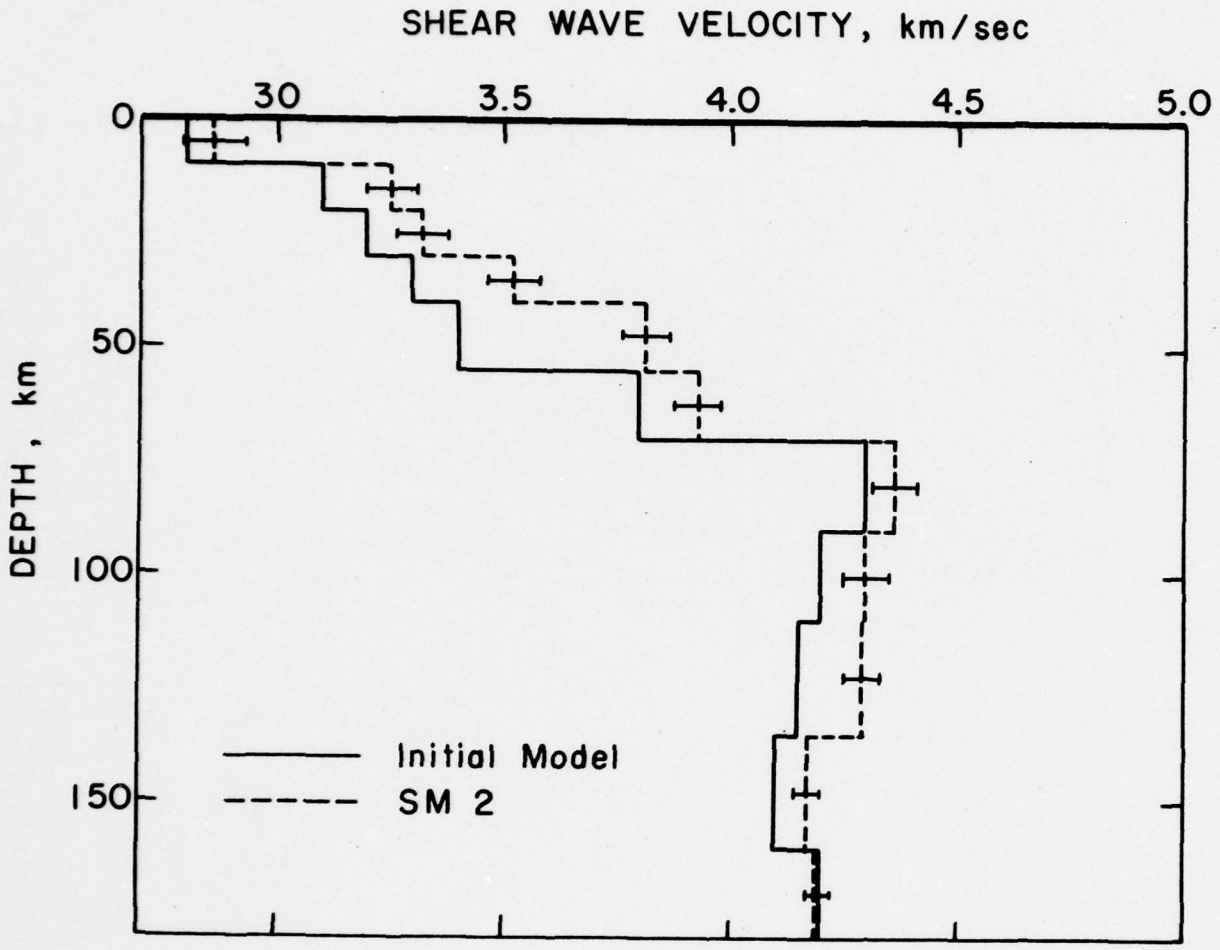
SHEAR WAVE VELOCITY, km/sec
3.0
3.5
4.0
4.5
5.0
0
50
100
150
DEPTH, km
Initial Model
SM 2

TABLE 9

Definition of Model Abbreviations

SM1: Szechwan-Mashad, 8 layer model

SM2: Szechwan-Mashad, 11 layer model

YM1: Yunnan-Mashad

TM1: Tangshan-Mashad

TT1: Tangshan-Taipei

TABLE 10: Model Fit for Path Szechwan-Mashad (8 Layers)

	Initial Model				Final Model	
Layer	H(km)	α(km/sec)	β(km/sec)	ρ(gr/cm)	β(km/sec)	SDX_o	SDX
1	15	5.55	2.80	2.70	3.06	0.189	0.046
2	15	5.60	3.20	2.90	3.28	0.189	0.070
3	25	6.40	3.30	3.00	3.67	0.147	0.063
4	20	6.60	3.80	3.10	3.98	0.164	0.114
5	25	7.50	4.45	3.30	4.39	0.164	0.140
6	25	7.20	4.20	3.35	4.31	0.147	0.128
7	25	7.20	4.10	3.36	4.18	0.147	0.137
8	25	7.20	4.20	3.37	4.21	0.147	0.143

TABLE 11: Resolution Matrix for Path Szechwan-Mashad (8 Layers)

Layer	1	2	3	4	5	6	7	8
1	0.989	0.0007	0.007	0.001	0	0	0	0
2	0.007	0.951	0.029	-0.042	0.004	0.005	-0.001	0
3	-0.013	0.049	0.918	0.054	-0.084	-0.018	0.003	-0.004
4	0.001	-0.056	0.043	0.769	0.158	-0.055	-0.054	0.035
5	-0.008	0.006	0.067	0.158	0.456	0.250	0.021	-0.071
6	-0.004	0.008	-0.018	-0.069	0.313	0.435	0.255	0.063
7	-0.004	-0.002	0.004	-0.068	0.026	0.255	0.310	0.206

TABLE 12: Model Fit for Path Szechwan-Mashad (11 Layers)

		Initial Model			Final Model		
Layer	H(km)	α(km/sec)	β(km/sec)	ρ(gr/cm)	β(km/sec)	SDX_o	SDX
1	10	5.50	2.80	2.70	2.87	0.222	0.034
2	10	5.60	3.10	2.90	3.25	0.222	0.124
3	10	5.65	3.20	2.92	3.32	0.222	0.131
4	10	6.25	3.30	3.00	3.52	0.222	0.147
5	15	6.45	3.40	3.05	3.81	0.181	0.108
6	15	6.60	3.80	3.10	3.93	0.181	0.129
7	20	7.45	4.45	3.30	4.36	0.156	0.133
8	20	7.20	4.20	3.34	4.30	0.156	0.138
9	25	7.20	4.15	3.35	4.29	0.140	0.129
10	25	7.20	4.10	3.36	4.17	0.140	0.135
11	25	7.20	4.20	3.37	4.19	0.140	0.138

TABLE 13: Resolution Matrix for Path Szechwan-Mashad (11 Layers)

Layer	1	2	3	4	5	6	7	8	9	10	11
1	0.736	0.273	-0.012	0.021	0.039	0.016	0.018	0.004	-0.003	-0.003	0.004
2	0.274	0.686	0.196	-0.077	-0.031	-0.026	-0.006	-0.001	0.002	0.001	0
3	0.126	0.195	0.652	0.231	-0.031	-0.014	-0.001	0.004	0.004	-0.005	-0.005
4	0.021	-0.046	0.231	0.498	0.222	-0.060	-0.092	0.007	0.002	-0.004	-0.004
5	0.059	-0.046	-0.045	0.338	0.494	0.223	-0.009	-0.004	-0.032	0.023	0.010
6	0.025	-0.039	-0.024	-0.091	0.221	0.472	0.182	0.033	-0.021	-0.036	-0.034

Starting and final shear wave velocity models with standard deviation bars for the path Yunnan-Mashad are presented in Figure (3). Tables (14) and (15) illustrate the initial and final model parameters and the resolution matrix. From the width of the resolving kernels (Table 13) it is possible to resolve a 10-15 km layer at the top of the crust, 15-20 km layer in the middle of the crust, and a 20-25 km layer at the base of the crust.

Resolution in the mantle is poor for both paths. The standard deviations were less than .10 km/sec for all models presented. Increasing the resolution in the crust and mantle by adjusting the trade-off parameter δ, leads to both large standard deviations and instabilities in the shear wave velocity model. An increase in the resolution for both paths across the Tibetan plateau can be achieved from the addition of Love waves and higher period (greater than 120 seconds) data.

A measure of the amount of new information obtained from the data is given by comparing the magnitudes of the apriori (SDX_o) to the postpriori (SDX) standard deviations given in Tables (8, 10, 12). In the upper mantle there is only a small amount of new information being obtained from the data, and the final model is being most effected by the starting model. As a result, a low velocity layer can only be inferred from the small amount of new information being obtained. The addition of data

FIGURE 30: Resulting shear wave velocity model for YM1

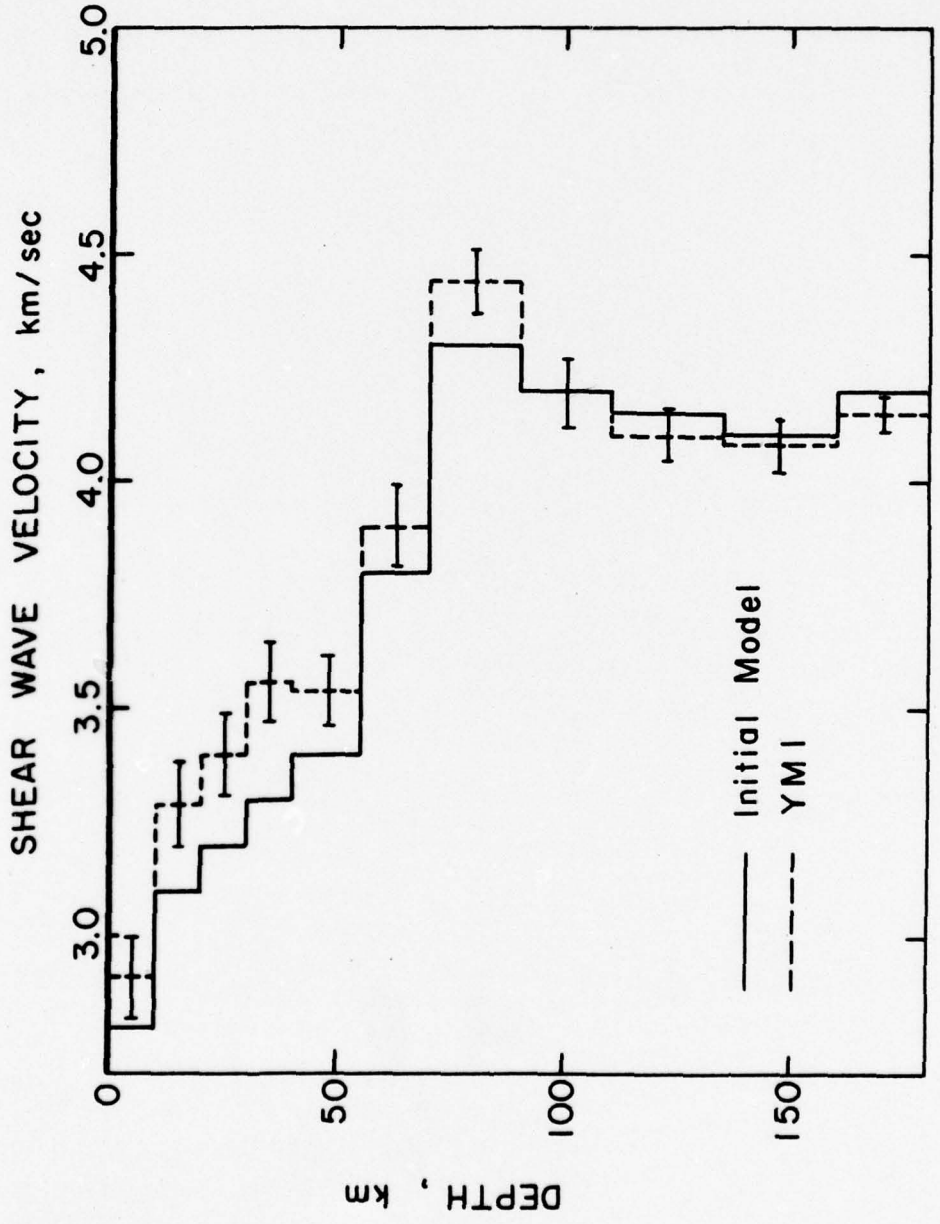
SHEAR WAVE VELOCITY, km/sec
3.0
3.5
4.0
4.5
5.0
0
50
100
150
DEPTH, km
Initial Model
YM1

TABLE 14: Model Fit for Path Yunnan-Mashad

		Initial Model			Final Model		
Layer	H(km)	α(km/sec)	β(km/sec)	ρ(gr/cm)	β(km/sec)	SDX_o	SDX
1	10	5.50	2.80	2.70	2.91	0.347	0.144
2	10	5.60	3.10	2.90	3.29	0.347	0.157
3	10	5.65	3.20	2.92	3.40	0.347	0.208
4	10	6.25	3.30	3.00	3.56	0.347	0.242
5	15	6.45	3.40	3.05	3.54	0.283	0.180
6	15	6.60	3.80	3.10	3.90	0.283	0.201
7	20	7.45	4.45	3.30	4.44	0.245	0.200
8	20	7.20	4.20	3.34	4.19	0.245	0.208
9	25	7.20	4.15	3.35	4.10	0,219	0.190
10	25	7.20	4.15	3.36	4.10	0.219	0.205
11	25	7.20	4.20	3.37	4.15	0.219	0.213

TABLE 15: Resolution Matrix for Path Yunnan-Mashad

Layer	1	2	3	4	5	6	7	8	9	10	11
1	0.926	0.163	-0.132	0.028	0.028	-0.001	0.002	0.003	0	0	0
2	0.163	0.839	0.194	-0.076	-0.021	-0.010	-0.008	-0.005	0.005	-0.004	-0.002
3	0.132	0.192	0.640	0.238	-0.011	0.020	0.001	-0.024	-0.016	-0.007	-0.003
4	0.028	-0.076	0.238	0.471	0.235	-0.072	-0.029	-0.001	-0.007	-0.010	-0.007
5	0.039	-0.031	-0.017	0.353	0.548	0.202	-0.003	-0.035	-0.029	-0.019	-0.012
6	-0.001	-0.015	0.030	-0.018	0.202	0.494	0.202	0.002	-0.057	-0.057	-0.033
7	0.004	-0.017	0.001	-0.058	-0.004	0.269	0.323	0.207	0.037	-0.047	-0.005
8	0.006	-0.011	-0.047	-0.003	-0.047	-0.003	0.207	0.282	0.161	0.044	-0.015

for periods longer than 120 seconds and good Love wave data would significantly increase the amount of new information.

The shear wave velocity structure for both paths crossing the Tibetan plateau is similar. The crust is approximately 70 km thick and may be broken into four layers. The first layer shear velocities range between 2.87 to 3.06 km/sec suggesting a layer approximately 15 km thick of sedimentary origin. Tung (1974) and Mu, et al. (1974) discussed the existence of thick sedimentary layers in the Mount Jolmo Lungma (known in the West as Mount Everest) region of the Himalayas. Both Birch (1963) and Simmons (1964) report shear velocities for sedimentary rocks at 10 to 15 km of approximately 3.00 to 3.08 km/sec. A second layer with shear wave velocities ranging from 3.20 to 3.40 km/sec, approximately 15 km thick suggests a layer partly of granitic composition. A third layer with shear velocities between 3.40 to 3.70 km/sec, approximately 15 to 20 km thick, suggests a granitic layer. Birch and Bancroft (1958), Birch (1961, 1963) and Simmons (1964) report shear wave velocities for granite under 3 to 5 kilobars of pressure of 3.45 - 3.70 km/sec. Simmons (1964) reported that granite with a shear wave velocity of 3.56 km/sec at 1 kilobar pressure, has a shear wave velocity of 3.79 km/sec at a pressure of 10 kilobars. Since depths of 50 to 70 km correspond to pressures of approximately 20 kilobars, a 25 to 30 km thick layer with an average

shear wave velocity of 3.90 km/sec is reasonable.

The shear wave velocity profile for the Tibetan plateau is in agreement with those values presented by Tung (1974) and Bird and Toksoz (1977). Inverting Rayleigh and Love wave group velocities by a trail and error method of inversion, Chun and Yoshii (1977) presented an average shear velocity structure across the Tibetan plateau. A crustal thickness of 70 km and a velocity reversal in the middle crust were reported but standard deviations for the shear velocities and their resolution were not discussed. Owing to a 15 to 20 km resolution in the middle crust it is doubtful a velocity reversal could be observed for data over the two paths presented.

As a result of the small amount of information (apriori vs. postpriori standard deviations) derived from just inverting Rayleigh waves, conclusions about the upper mantle structure of the Tibetan plateau are tentative. The upper mantle shear velocities are lower than either the Gutenburg earth model of Tacheuchi, et al. (1964) or the Brune and Dorman (1963) model for the Canadian Shield (Figure 31). The velocity at the top of the mantle is approximately 4.4 km/sec with indications of a low velocity layer at 90 km. Since the low velocity layer can only be inferred the significance of the extremely low velocities at 4.10 km/sec is tentative. Low shear velocities in the upper mantle of Tibet have been reported by Tung (1974)

FIGURE 31: Comparison of the Canadian Shield model (Burne and Dorman, 1963) and the Gutenburg Earth model (Tacheuchi et al., 1964) with models SM2 and YM1

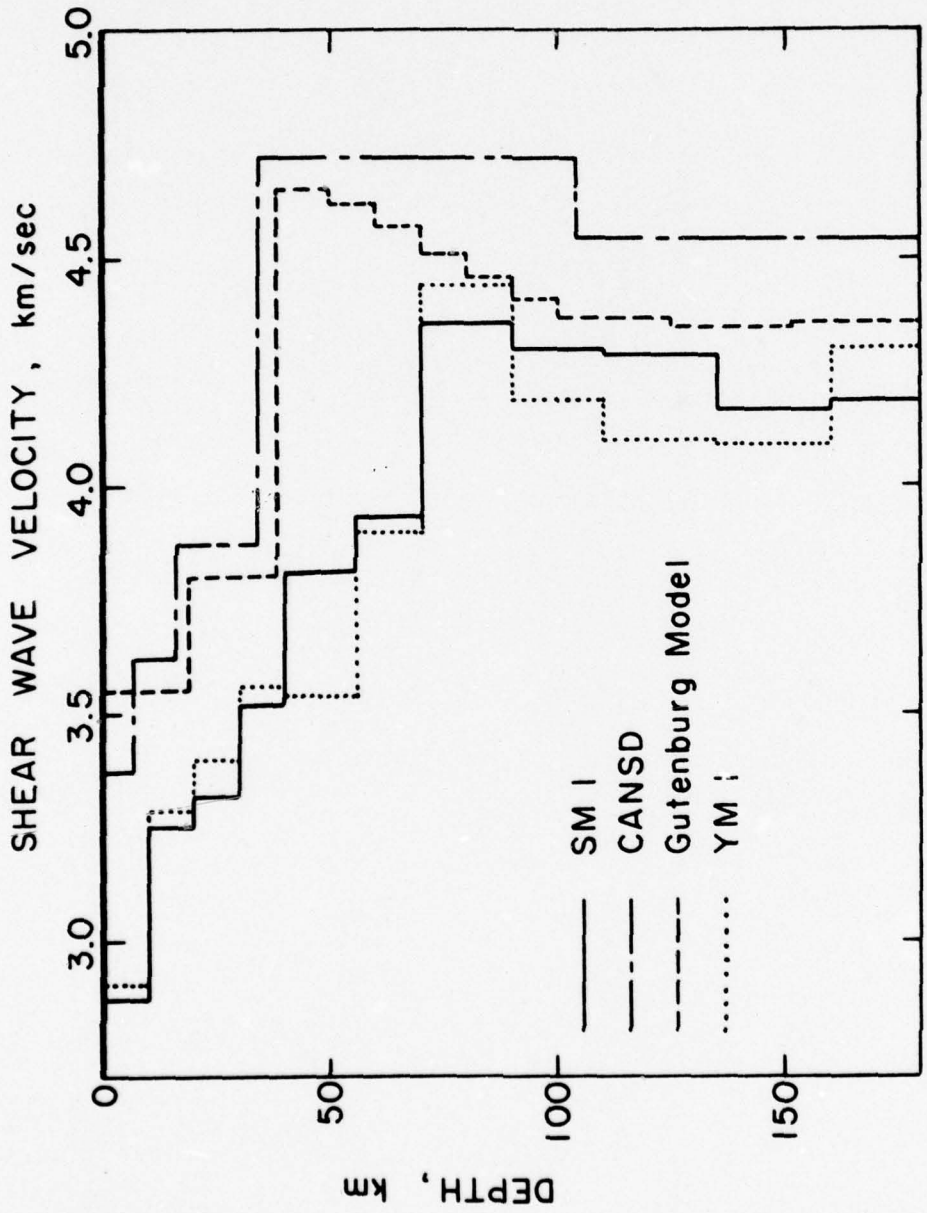
SHEAR WAVE VELOCITY, km/sec
3.0
3.5
4.0
4.5
5.0
DEPTH, km
0
50
100
150
SM I
CANSD
Gutenburg Model
YM I

which suggests a high degree of partial melting and a reduction of resistance to movement (Anderson, 1972).

Tangshan to Mashad

The path between Tangshan and Mashad, Iran (Figure 9) crosses Northeast China, North Central China, and the Tien Shan mountain range within Northwestern China. This path crosses two subplates, the North China subplate and Tien Shan fold belt unit, according to Sun and Teng (1977). Tung (1974) found crustal thicknesses of 30, 40, and 45 km for Northeast, Central and Northwestern China respectively. Crustal thicknesses in the Tien Shan and Pamir mountains have been reported as high as 65 km (Arkhangel' skaya, 1964).

A list of the earthquakes and surface wave trains used over the path Tangshan to Mashad are listed in Table (16). The fit of the theoretical model to the observed group velocities for the Rayleigh and Love waves is given in Figure (32). The theoretical Rayleigh wave group velocity is lower than the average continental Rayleigh wave dispersion (Ewing et al., 1957). Starting and final shear wave velocity models with standard deviation bars are presented in Figure (33). Tables (17) and (18) present the starting and final model parameters and the resolution matrix. From the width of the resolving kernals presented in Table (18) it is possible to resolve a 10 km layer at the top of the crust, 10 to 15 km layer in the middle of

TABLE 16

Seismogram Components Used for the

Path Tangshan to Mashad

Earthquake	Recording Station	Component	Wave Type	Distance (km)
July 29, 1976	MAIO	Vertical	Rayleigh	5119
July 29, 1976	MAIO	North-South	Love	5119
July 30, 1976	MAIO	North-South	Love	5072
Aug. 2, 1976	MAIO	Vertical	Rayleigh	5053
Aug. 8, 1976	MAIO	Vertical	Rayleigh	5100
Aug. 8, 1976	MAIO	Vertical	Rayleigh	5118
Aug. 8, 1976	MAIO	North-South	Love	5100
Aug. 14, 1976	MAIO	Vertical	Rayleigh	5103
Aug. 14, 1976	MAIO	North-South	Love	5103

FIGURE 32: Theoretical and observed group velocities for TM1

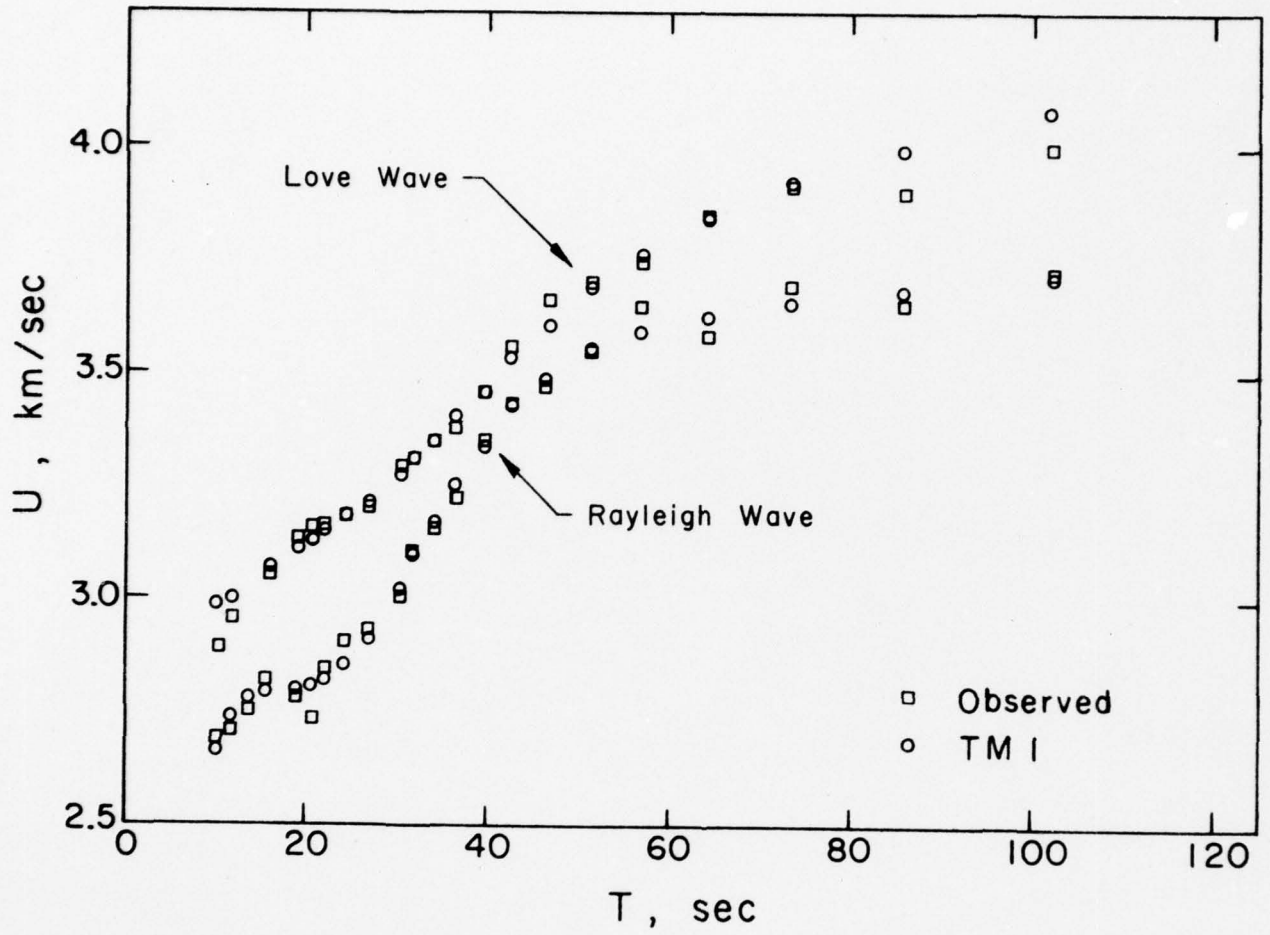
Love Wave
Rayleigh Wave
Observed
TM I
U , km/sec
T , sec
4.0
3.5
3.0
2.5
0
20
40
60
80
100
120

FIGURE 33: Resulting shear wave velocity model for TM1

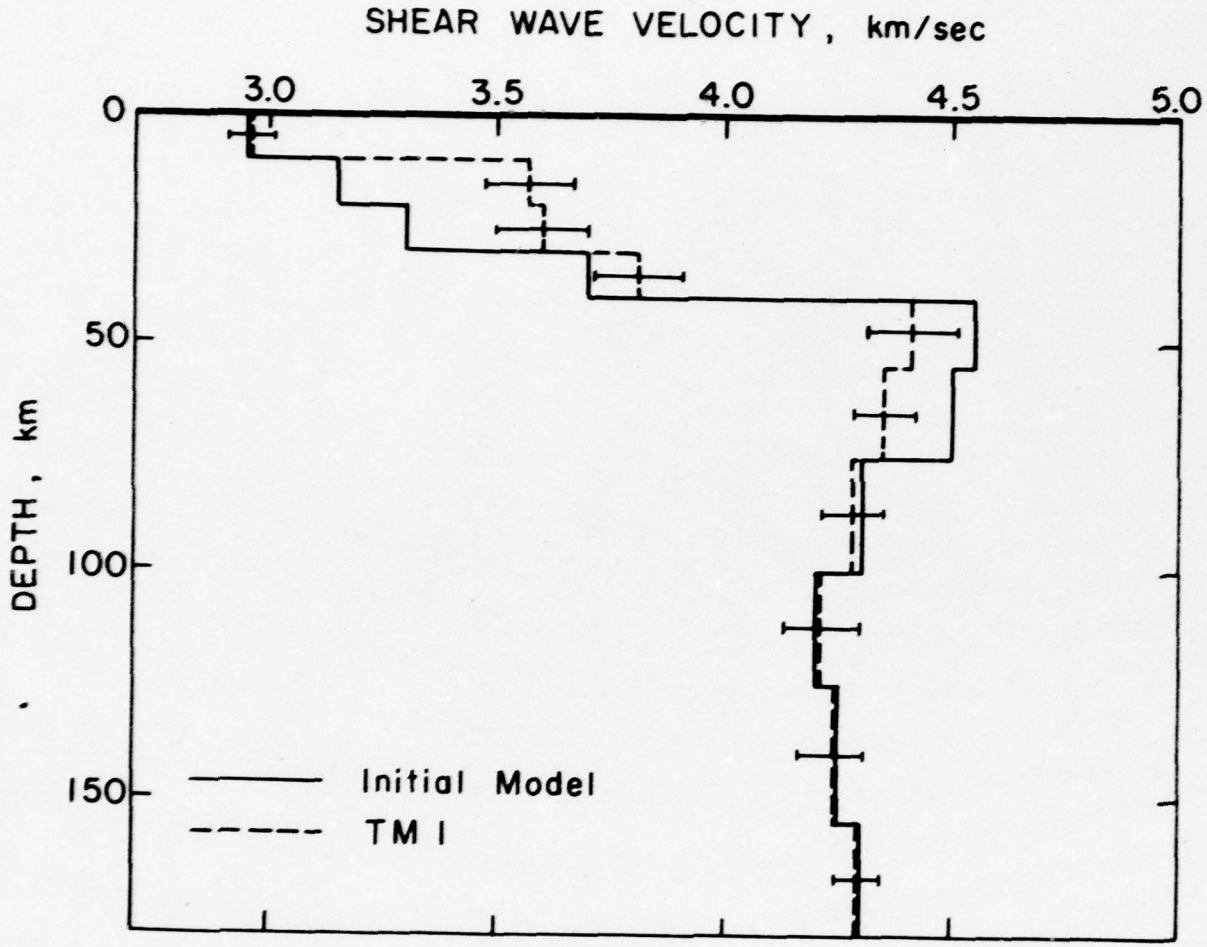
SHEAR WAVE VELOCITY, km/sec
3.0
3.5
4.0
4.5
5.0
0
50
100
150
DEPTH, km
Initial Model
TM I

TABLE 17: Model Fit for Path Tangshan-Mashad

Layer	H(km)	α(km/sec)	β(km/sec)	ρ(gr/cm)	β(km/sec)	SDX_o	SDX
1	10	5.40	2.95	2.80	2.96	0.427	0.059
2	10	6.40	3.15	2.95	3.57	0.427	0.149
3	10	6.45	3.30	3.05	3.60	0.427	0.212
4	10	6.60	3.70	3.12	3.61	0.427	0.280
5	15	7.70	4.55	3.30	4.41	0.349	0.234
6	20	7.50	4.50	3.33	4.35	0.302	0.209
7	25	7.40	4.30	3.35	4.28	0.270	0.201
8	25	7.30	4.20	3.36	4.21	0.270	0.223
9	30	7.30	4.25	3.38	4.24	0.246	0.219
10	30	7.35	4.30	3.39	4.29	0.246	0.235

TABLE 18: Resolution Matrix for Path Tangshan-Mashad

Layer	1	2	3	4	5	6	7	8	9	10
1	0.980	0.039	-0.037	0.016	-0.004	0	-0.001	0	0.001	0
2	0.039	0.877	0.127	-0.063	0.006	0.008	0	-0.007	-0.008	-0.006
3	-0.037	0.128	0.752	0.218	-0.056	-0.030	0.025	0.015	-0.002	-0.009
4	0.016	-0.063	0.218	0.569	0.220	-0.019	-0.054	-0.013	0	-0.001
5	-0.007	0.009	-0.084	0.330	0.546	0.208	-0.008	-0.024	-0.007	-0.009
6	0	0.016	-0.061	-0.038	0.277	0.519	0.253	-0.009	-0.078	-0.059
7	-0.004	0	0.064	0.013	0.014	0.317	0.445	0.251	0.040	-0.053
8	0	-0.019	0.039	-0.033	-0.040	-0.010	0.251	0.317	0.181	0.039

the crust, and a 20 km layer at the base of the crust.

When Rayleigh and Love waves are inverted simultaneously a considerable amount of new information may be derived from the data. Observing the magnitude of the apriori (SDX_o) vs. the postpriori (SDX) standard deviations, considerable new information is obtained at depths of 100 km (seventh layer). Below this depth the new information obtained from the data is less and the final model is most effected by the starting model.

The average crustal thickness over the path from Tangshan to Mashad is approximately 45 km, and in as much as this path is not a pure path, only average shear velocities are presented (Figure 33). A three layer crust is an adequate model for this path. The first layer approximately 10 km thick has an average shear velocity of approximately 3.00 km/sec suggesting a partly sedimentary layer (Birch, 1963 and Simmons, 1964). The second layer, 15 to 20 km thick, has an average shear wave velocity of 3.55 km/sec. The layer at the base of the crust, 20 to 25 km thick, has an average shear wave velocity of approximately 3.80 km/sec suggesting a layer of granitic origin (Birch, 1963 and Simmons, 1964). The average shear wave velocity at the top of the mantle is 4.40 to 4.45 km/sec, and the low velocity layer begins at depths of approximately 80 km. Using a three layer earth model proposed by Dorman (1959), Schechkov (1961, 1964) and Schechkov

and Saverensky (1961) were able to fit mixed path dispersion data for Northwest China to a theoretical three layer model:

		Thickness
layer 1	β_1 = 3.40 km/sec	.20 km
layer 2	β_2 = 3.83 km/sec	.30 km
layer 3	β_3 = 4.50 km/sec	∞

with the average crustal thickness, 50 km. Tung (1974), applying the concept of regionalization to paths crossing Northwest China, presented a three layer crust of 45 km thickness. Tung (1974) calculated that shear velocities throughout the crust and upper mantle are lower than the mixed-path average shear velocities presented. The low velocity zone presented is not as prominent as Tung (1974) reported and can only be inferred from the information obtained from the data.

A comparison of the Candian Shield model (Brune and Dorman, 1963) and the Gutenburg earth model (Tacheuchi et al., 1964), with the average shear velocity model for Tangshan to Mashad is presented in Figure (34). Both models have higher shear velocities in the crust and at the top of the upper mantle than the theoretical model presented for the path Tangshan-Mashad. The tectonics over the path between Tangshan and Mashad provide a possible cause of the lower velocity at the top of the

FIGURE 34: Comparison of the Canadian Shield model (Brune and Dorman, 1963) and the Gutenburg Earth model (Tacheuchi et al., 1964) with model TM1

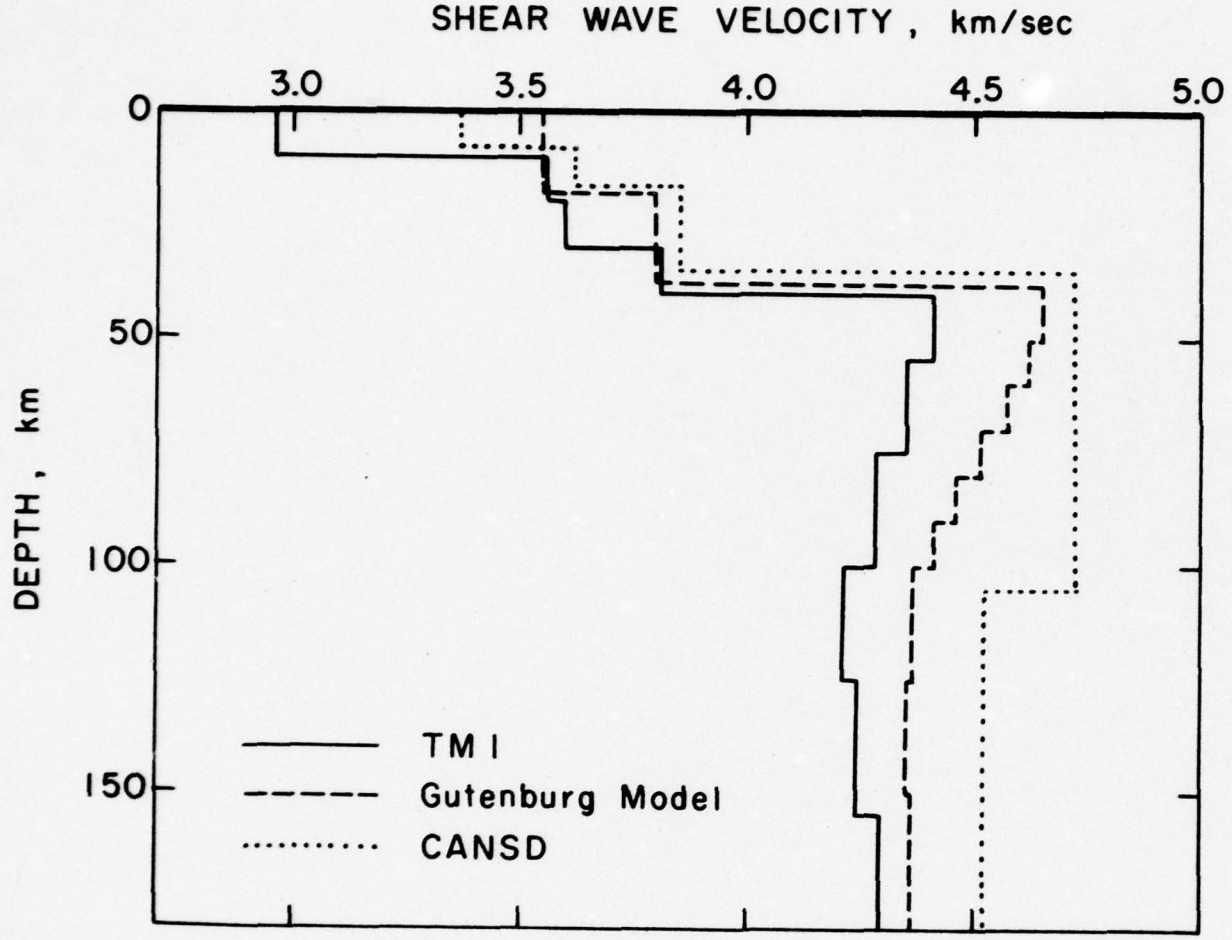
SHEAR WAVE VELOCITY, km/sec
3.0
3.5
4.0
4.5
5.0
0
50
100
150
DEPTH, km
TM I
Gutenburg Model
CANSD

mantle. The catalog of historical earthquakes presented by the Chinese Institute of Geophysics, Academia Sinica (Lee et al., 1976) shows a considerable seismic activity throughout the region traversed by the surface waves. Successive stages of subduction of the Indian plate below the Eurasian plate which are assoicated with areas as far north as Tarim basin and Mongolia (Chang and Zeng, 1973, and Zonenshain, 1973) are consistent with a thicker crust, lower group velocities and lower shear velocities in the upper mantle. These results suggest a theory of origin of the Tien-Shan fold belt attributable to the collision of the Eurasian and Indian subplates from the evidence of crustal thickening.

Tangshan-Taipei

For most of the path between Tangshan and Taipei (Figure 9) the surface waves are parallel to the east coast of China. According to the tectonic map of the Institute of Geology of the Chinese Academy of Sciences (Figure 5) the crustal thickness along most of the path is about 30 km. A starting model for the inversion was chosen to reflect the 30 km crustal thickness.

A list of the earthquakes and surface wave trains used is given in Table (19). The fit of the theoretical to the observed Rayleigh and Love wave group velocities is presented in Figure (35). A comparison of the theoretical Rayleigh wave group to the average continental Ray-

TABLE 19

Seismogram Components Used for the Path Tangshan-Taipei

Earthquake	Recording Station	Component	Wave Type	Distance (km)
July 28, 1976	TATO	Vertical	Rayleigh	1661
July 28, 1976	TATO	Radial	Rayleigh	1661
July 28, 1976	TATO	North-South	Love	1661
July 30, 1976	TATO	Vertical	Rayleigh	1670
July 30, 1976	TATO	Radial	Rayleigh	1670
July 30, 1976	TATO	North-South	Love	1670
Aug. 1, 1976	TATO	Vertical	Rayleigh	1656
Aug. 1, 1976	TATO	Radial	Rayleigh	1656
Aug. 1, 1976	TATO	North-South	Love	1656
Sept. 6, 1976	TATO	Vertical	Rayleigh	1672

FIGURE 35: Theoretical and observed group velocities for model TT1

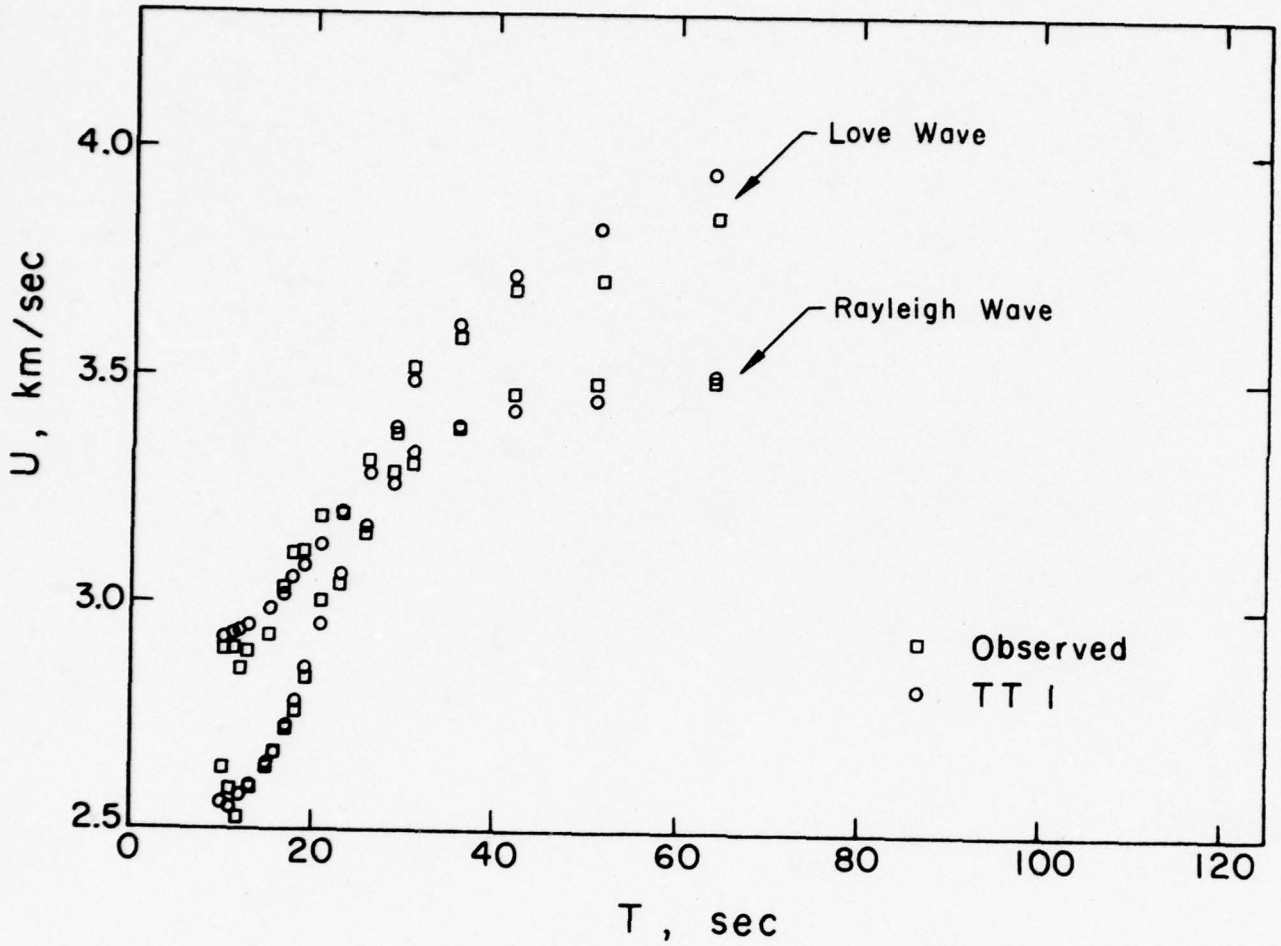
Love Wave
Rayleigh Wave
Observed
TT I
U, km/sec
T, sec
4.0
3.5
3.0
2.5
0
20
40
60
80
100
120

leigh wave group velocities (Ewing et al., 1957) shows lower group velocities at both short and intermediate periods.

The starting and final shear wave velocity models with standard deviation bars are presented in Figure (36). The shear wave velocity parameters and the resolution matrix are presented in Tables (20 and 21). From the width of the kernels of the resolution matrix (Table 21) it is possible to resolve a 5 to 7 km layer at the top of the crust, a 10 km layer in the middle of the crust, and a 15 to 20 km layer at the base of the crust. Examination of the apriori (SDX_o) and postpriori (SDX) standard deviations (Table 20) indicate a small amount of information exists in the data below the fifth layer. Thus long period data is necessary for increased information in the mantle. Since the path length from Tangshan to Taipei is approximately 1700 km, periods greater than 64 seconds do not have proper mode separation. As a result it is unlikely that for this path, new information below the top of the mantle may be obtained, and the shear wave velocity structure is most affected by the starting model.

A crust with a thickness of 30 km, composed of three layers is an adequate model for the structure over the path. The first layer approximately 5 to 7 km thick suggests a sedimentary layer with shear wave velocity of approximately 2.95 km/sec. A second layer approximately

FIGURE 36: Resulting shear wave velocity model for TT1

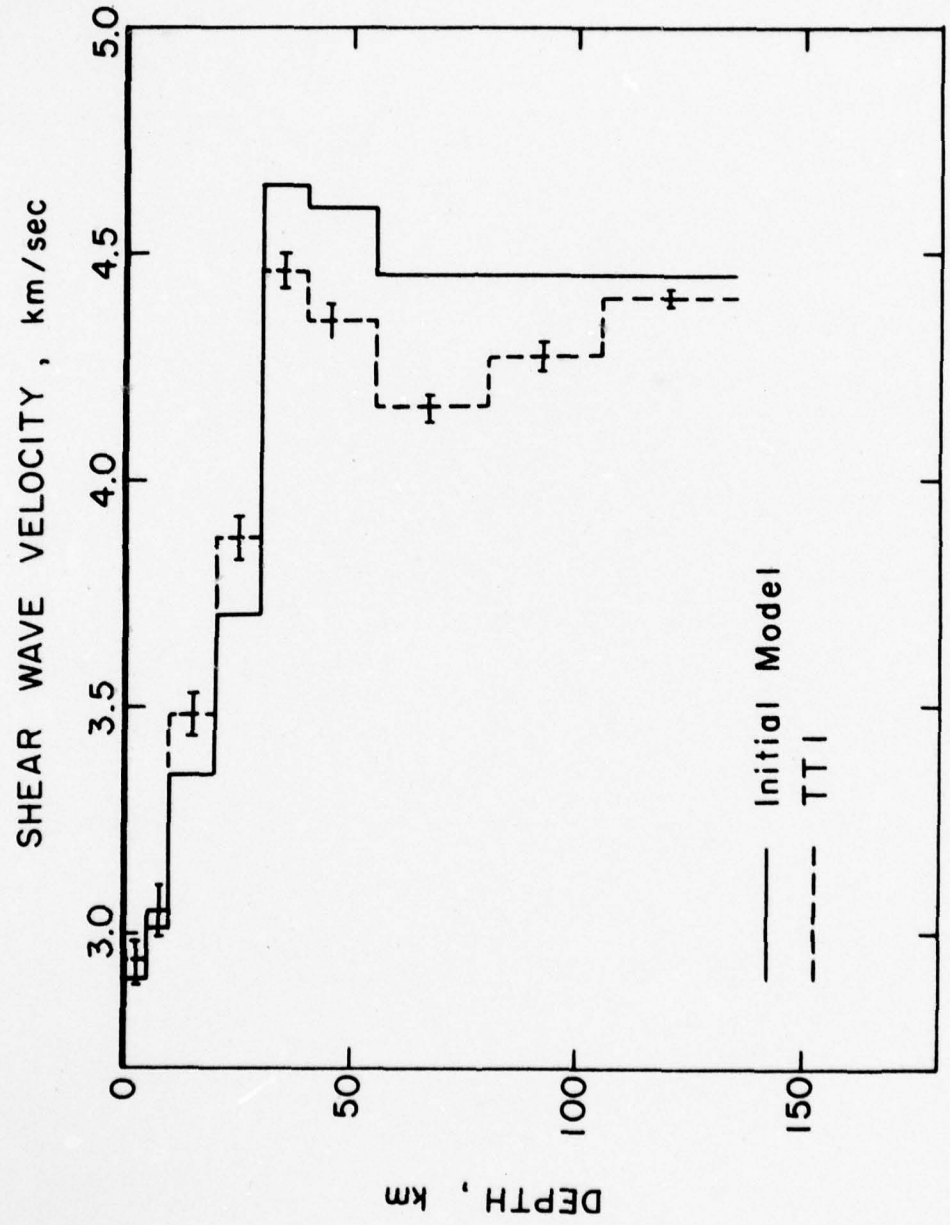
SHEAR WAVE VELOCITY , km/sec
3.0
3.5
4.0
4.5
5.0
0
50
100
150
DEPTH , km
Initial Model
TT I

TABLE 20: Model Fit for Path Tangshan-Taipei

		Initial Model				Final Model	
Layer	H(km)	α(km/sec)	β(km/sec)	ρ(gr/cm)	β(gr/cm)	SDX_o	SDX
1	5	4.80	2.90	2.70	2.94	0.185	0.087
2	5	5.25	3.05	2.90	3.01	0.185	0.125
3	10	5.55	3.35	2.96	3.48	0.131	0.073
4	10	6.00	3.70	3.05	3.87	0.131	0.083
5	10	8.10	4.65	3.25	4.46	0.131	0.101
6	15	8.10	4.60	3.30	4.35	0.107	0.091
7	25	8.05	4.45	3.33	4.16	0.083	0.069
8	25	8.00	4.45	3.35	4.27	0.083	0.078
9	25	8.00	4.45	3.36	4.40	0.083	0.081

TABLE 21: Resolution Matrix for Path Tangshan-Taipei

Layer	1	2	3	4	5	6	7	8	9
1	0.779	0.261	-0.025	0.012	0.009	0.002	-0.008	-0.002	0
2	0.261	0.545	0.148	-0.079	-0.015	0.015	0.009	-0.002	-0.003
3	-0.051	0.297	0.686	0.217	-0.053	-0.074	-0.006	-0.006	0.001
4	0.025	-0.158	0.217	0.492	0.246	0.034	-0.056	-0.032	-0.013
5	0.018	-0.031	-0.053	0.246	0.281	0.159	0.001	-0.034	-0.022
6	0.007	0.047	-0.011	0.051	0.239	0.274	0.122	-0.003	-0.030
7	-0.041	0.047	-0.015	-0.014	0.004	0.203	0.295	0.134	0.010

10 km thick has shear wave velocity of approximately 3.50 km/sec. The third layer, approximately 15 to 20 km thick corresponds to shear wave velocity of approximately 3.85 km/sec. In the mantle a low velocity layer can only be inferred owing to the lack of new information from the data. A comparison of the Candian Shield Model (Burne and Dorman, 1963) and the Gutenburg earth model (Tacheuchi et al., 1964) with the shear wave velocity profile for the path Tangshan to Taipei (Figure 37) shows higher velocities in the mantle and base of the crust.

The shear wave velocity at the top of the mantle, 4.46 km/sec is lower than the shear velocity of the Canadian Shield Model (4.65 km/sec). Tung (1974), for a path crossing Northeast China and recorded in Hong Kong, calculated a mantle shear wave velocity of 4.42 km/sec at the top of the mantle. A consideration of the tectonics over the path from Tangshan to Taipei explains the lower velocities in the mantle.

The region traversed is considered an "intra plate" region although a considerable seismic history is evident from the catalog of historical earthquakes compiled by the Chinese Institute of Geophysics, Academia Sinica (Lee et al., 1976). For example, in the northeastern portion of the South China subplate (Figure 3) is the Tanlu fault. The Tanlu fault may be traced from LANDSAT photographs (Lee et al., 1976) north across the border of

FIGURE 37: Comparison of the Canadian Shield model and the Gutenburg Earth model (Tacheuchi et al., 1964) with model TT1

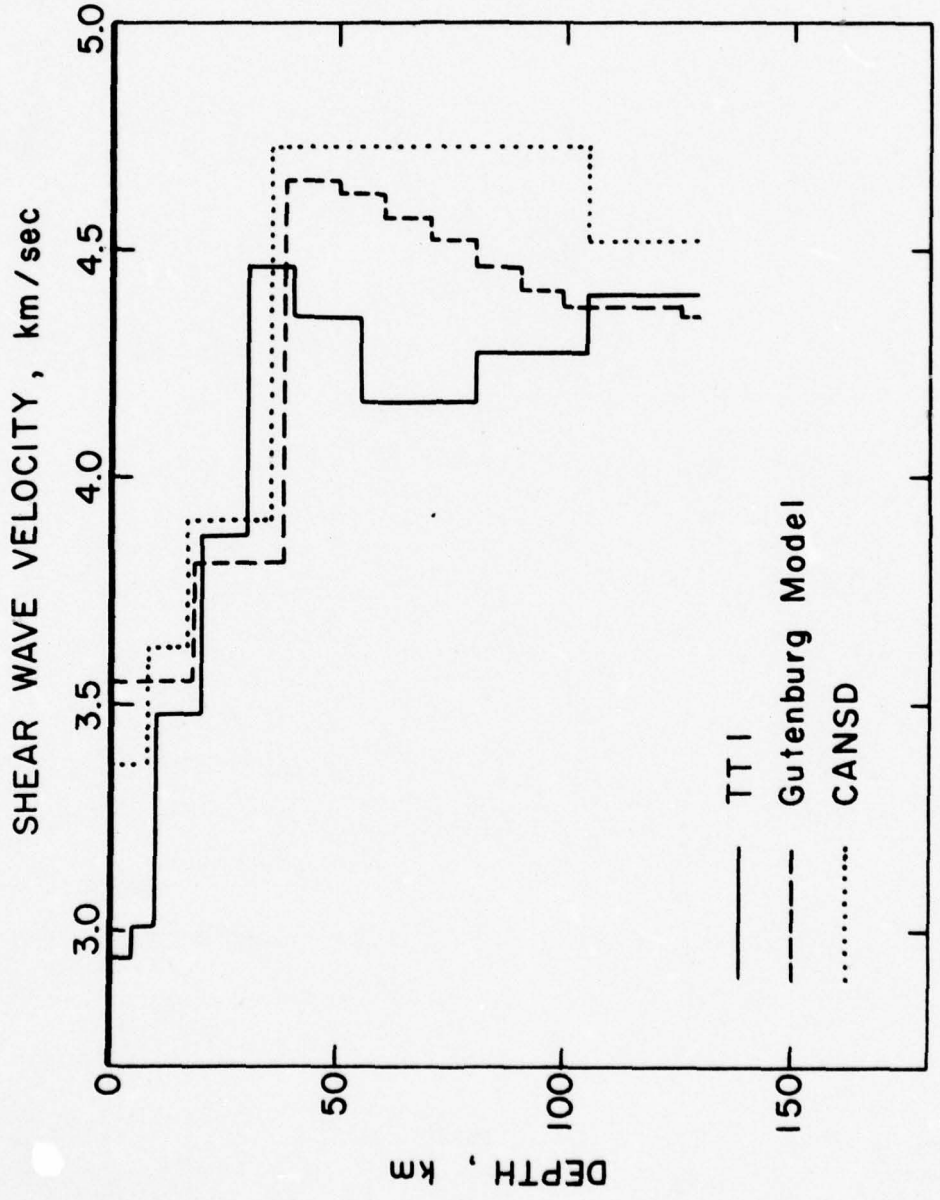
SHEAR WAVE VELOCITY, km/sec
3.0
3.5
4.0
4.5
5.0
0
50
100
150
DEPTH, km
TT I
Gutenburg Model
CANSD

the North China subplate through Shantung Province, Pohai (Gulf of Chihli) and into Liaoning Province (near Tangshan earthquake (July, 1976) and the Haichang earthquake (February, 1975) indicate the northern portion of the path from Tangshan to Taipei passes through a tectonically active region.

The southern portion of the path Tangshan-Taipei traverses a region affected by the Philippine Sea plate being subducted beneath the Eurasian plate. The tectonics of this region have been discussed by Sun and Teng (1977). Considerable seismic activity exists throughout Northern Taiwan and a major north-south trending fault parallels the east coast of Taiwan. Sun and Teng (1977) discuss the importance of this fault to a subduction zone of Mesozoic or Cenozoic age. The eastern provinces of Fuchien, Kiangus, Chiekiang, Kwantung, Anhwai, and Kiangsi are covered by large-scale volcanic intrusions which are of Mesozoic age (Figure 38). These volcanic intrusions are attributed to a magma source which was a consequence of the melting from the subduction of the Pacific plate. Finally, higher than normal heat flow (three to four heat flow units) has been observed north of Taiwan, which is associated with areas over plate subduction (Yasuii et al., 1970). All these factors would contribute to a shear wave velocity profile lower than normal in the upper mantle.

FIGURE 38: Map of provinces of China

(Lee et al., 1976)

Provinces of China. Modified from Hsieh (1973, p. 260).

CONCLUSIONS

By using a multiple-filter technique, group velocities for various regions of China were obtained from earthquakes recorded at SRO stations in Mashad and Taipei. A nonlinear least square technique was used to invert the surface wave group velocity for shear wave velocity structures. The major findings concerning the nature of the crust and mantle are:

1. Group velocities obtained for the pure path across the Tibetan plateau are unusually low when compared to the average continental dispersion. Results of the inversion indicate a 4 layer total, 70 km thick crust is an adequate model for the Tibetan plateau. Crustal shear velocities are in agreement with previously reported values.

2. Group velocities for the mixed path between Tangshan-Mashad, Iran are lower than the average continental dispersion. Results of the inversion indicate that a 3 layer total, 45 km thick crust is an adequate model. A low velocity zone is inferred from the data at depths of approximately 80-90 km.

3. Group velocities for the path between Tangshan-Taipei, Taiwan are closest of the three regions (at higher periods) to the average continental dispersion. Results of the inversion indicate that a 3 layer total, 30 km

crust is an adequate model.

For all three models presented the structure of the upper mantle from information provided by the data is only tentative. In comparing the apriori (SDX_o) to the post-priori (SDX) standard deviation in the mantle it was observed that the final model was influenced by the starting model more than by the data. Attempts to increase the information obtained from the data and the resolution presented one with either unacceptably large standard deviations or unstable shear velocity models. Only in the data for the path Tangshan-Mashad, in which inversions were performed simultaneously for long period Rayleigh and Love waves, was new information obtained about the upper mantle.

In previous surface wave studies of Mainland China a trial-and-error inversion approach was applied to obtain a shear wave velocity model from Rayleigh wave group velocity data. Proper consideration has not been given to either the information obtained from the data or the resolution. In all these studies the influence of the starting model upon the final model was not discussed and the validity of the upper mantle shear velocities presented is therefore somewhat questionable.

In conclusion, in the surface wave inversion for a crust and upper mantle model, both long period Rayleigh and Love waves should be inverted simultaneously to obtain

more information from the data. Further, the dispersion curves must not be contaminated by surface waves traveling non-least time path or by complex structure along the path. This often presents a problem in tectonically active regions, resulting in the inability to obtain a good Love wave dispersion curve from the data. Finally, the problems due to epicentral distance must be considered. If the epicentral distance crosses more than one geological province the dispersion curves and shear velocity models represent an average crustal and upper mantle structure over a wide region. If the epicentral distance is too short, proper surface wave mode separation will not be achieved. Only after these factors are considered can one arrive at a better shear wave velocity structure by means of surface wave inversion for a specific geological province.

REFERENCES

Anderson, D.L., Sammis, C. and Jordan, T., 1972, Composition of the mantle and core, the nature of the solid Earth: Edited by E.L. Robertson, McGraw Hill, 1972, p. 677.

Arkhangel'skaya, V.M., 1964, A study of short period surface Seismic Rayleigh waves II: Izvestiya Acad. Sci. USSR Geophys. Ser., pp. 807-821, English Translation.

Backus, G. and Gilbert, F., 1967, Numerical Application of a formalism for geophysical inverse problems: Geophys. J. 13, pp. 247-276.

_____, 1968, The resolving power of gross Earth data: Geophys. J. 16, pp. 169-205.

_____, 1970, Uniqueness in the inversion of inaccurate gross Earth data: Phil. Trans. Roy. Soc. (London), Ser. A266, pp. 123-192.

Birch, F., 1963, Some geophysical applications of high pressure research in solids under pressure: edited by W. Paul and D.M. Warschauer; McGraw-Hill Book Company, New York, 1963.

_____ and Bancroft, D., 1938, The effect of pressure on the rigidity of rocks: J. Geol., 46, pp. 59-83 113-141.

Bird, P. and Toksoz, M.N., 1977, Strong attenuation of Rayleigh waves in Tibet: Nature, V266, pp. 163-165.

Bloch, S., Hlaes, A.L. and Landisman, M., 1969, Velocities in the crust and upper mantle of Southern Africa from multi-mode surface-wave dispersion: Bull. Seism. Soc. Am. v. 59, pp. 1599-1630.

Boore, D.M., 1969, Effect of higher mode contamination on measure Love wave phase velocities: J. Geophys. Res. 74, pp. 6612-6616.

Braile, L.W. and Keller G.R., 1975, Fine structure of the crust inferred from linear inversion of Rayleigh wave dispersion: Bull. Seism. Soc. Am. v. 65, pp. 71-82.

Brune, J.N. and Dorman, J., 1963, Seismic waves and Earth structure in the Canadian Shield: Bull. Seism. Soc. Am. v. 52, pp. 167-210.

Burrett, C., 1974, Plate tectonics and fusion of Asia: Earth and Planet. Sci. Letters; v. 21, pp. 181-189.

Cardwell, R.K. and Isacks, B.L., 1976, Investigation of the 1966 earthquake series in Northern China using the method of joint epicenter determination: Bull. Seism. Soc. Am. v. 66, pp. 1965-1982.

Chang, C.F. and Zeng, S.L., 1973, Tectonic features of the Mount Jolmo Lungma region in Southern Tibet, China: Scientia Geologica Sinicia; no. 1, pp. 1-12.

Chinese Academy of Sciences, 1974, A preliminary note on the basic tectonic features and their developments in China: Scientia Geologica Sinica; no. 1, pp. 1-17.

Chun, K.Y. and Yoshii, 1977, Crustal structure of the Tibetan plateau: A surface wave study by a moving window analysis: Bull. Seism. Soc. Am., v. 67, pp. 735-750.

Cooley, J.W. and Tukey, J.W., 1965, An algorithm for the machine calculation of complex Fourier series: Mathematics of Computation, v. 19, pp. 297-301.

Crossen, R.S., 1976, Crustal structure modeling of earthquake data 1, simultaneous least squares estimation of hypocenter: J. Geophys. Res. 81, pp. 3030-3046.

Der, Z., Masse, R. and Landisman, M., 1970, Effects of observational errors on the resolution of surface waves at intermediate distances: J. Geophys. Res. 75, pp. 3399-3409.

_____ and Landisman, M., 1972, Theory for errors, resolution, and separation of unknown variables in inverse problems, with application to the mantle and crust in Southern Africa and Scandinavia: Geophys. J. 27, pp. 137-179.

Dewey, J.F. and Bird, J.M., 1970a, Mountain belts and the new global geotectonics: J. Geophys. Res. 73, p. 2625.

_____, 1970b, Plate tectonics and geosynclines: Tectonophysics 10, p. 265.

_____ and Burke, K.C.A., 1973, Tibetan, Variscan and Precambrian basement reactivation: Products of continental collisions: J. Geol. 81, p. 683.

Dorman, J., 1959, Numerical solution for Love wave dispersion on a half space with a double surface layer: Geophysics 24, pp. 12-19.

Dziewonski, A. and Hales, A.L., 1972, Numerical analysis of dispersed seismic waves: Method in computational physics, v. II, Academic Press, p. 306.

Ewing, W.M., Jardetzky, W.S. and Press, F., 1957, Elastic waves in layered media: McGraw-Hill Book Co., p. 380.

Franklin, J.N., 1970, Well-posed stochastic extensions of ill-posed linear problems: J. Math. Anal. 31, pp. 682-716.

Gupta, H.K. and Narain, H., 1967, Crustal structure in the Himalayan and Tibetan plateau region from surface wave dispersion: Bull. Seism. Soc. Am., v. 57, no. 2, pp. 235-248.

Hamilton, W., 1970, The Uralides and motion of the Russian and Siberian platforms: Geol. Soc. Am. Bull. 81, p. 2553.

Hermann, R.B., 1973, Some aspects of band-pass filtering of surface waves: Bull. Seism. Soc. Am., v. 63, pp. 663-671.

Jackson, D.D., 1972, Interpretation of inaccurate, insufficient, and inconsistent data: Geophys. J. Roy. Astron. Soc. 28, pp. 97-109.

_____ and Burkhard, N.R., 1976, Density and surface wave inversions: Geophys. Res. Let. v. 3, no. 11, pp. 637-638.

James, D.E., 1971, Anomalous Love wave phase velocities: J. Geophys. Res. 76, pp. 2077-2083.

Jell, P.A., 1973, Middle Cambrian geography deduced from an analysis of Trilobite distributions: Nature 240, p. 288.

Katsumata, M. and Sykes, L.R., 1969, Seismicity and tectonics of the Western Pacific: Izu-Mariana-Cardine and Ryukyu-Taiwan regions: J. Geophys. Res. 74, pp. 5923-5948.

Kobayashi, T., 1967, The Cambrian of Eastern Asia: J. Fac. Sci. Univ. Tokyo 16, p. 1131.

Kosminskaya, I.P., Mikhota, G.G. and Tulina, Y.V., 1958, Crustal structure of the Pamir-Altai zone from seismic depth sounding data: Izvestiya Acad. Soc. USSR, Geophys. Ser., pp. 673-683, English translation.

Kovach, R.L., 1959, Surface wave dispersion for an Asio-African and an Eurasian path: J. Geophys. Res. 64, pp. 805-813.

Langzos, C., 1961, Linear differential operators: D. Van Nostrand Co., London.

Lee, W.H.K., Wu, F.T. and Jacobsen, C., 1976, A catalog of historical earthquakes in China compiled from recent Chinese publications: Bull. Seism. Soc. Am., v. 66, pp. 2003-2016.

McElhinny, M.W., 1973, Plaeomagnetism and plate tectonics of Eastern Asia, in The Western Pacific, ed. by P. J. Coleman, Univ. West. Austr. Press, p. 407.

Molnar, P.T., Fitch, J. and Wu, F.T., 1973, Fault plane solutions of shallow earthquakes and contemporary tectonics in Asia: Earth and Planet. Sci. Letters 19, pp. 101-112.

Molnar, P.T. and Tapponier, P., 1975, Cenozoic tectonics of Asia: Effects of a continental collision: Science 189, pp. 419-426.

_____, 1977, The collision between India and Eurasia: Sci. Am., v. 236, no. 4, pp. 30-41.

Masaru, K., 1974, Gravity anomalies in East Nepal and their implication to the crustal structure of the Himalayas: Geophys. J. Roy. Astr. Soc. 39, pp. 283-299.

Mu, E.Z., Vin, J.X., Wen, S.X., Wang, Y.G. and Zhang, G.G., 1973, Stratigraphy of the Mount Jolmo Lunga region in Southern Tibet: Chinese Scientia Geologica Sinica, no. 1, pp. 13-25.

Negi, J.G. and Singh, V.P., 1973,Love wave dispersion analysis for crustal structure of laterally inhomogeneous Himalayas: Bull. Seism. Soc. Am., v. 63, no. 3, pp. 1163-1172.

Negume, T., 1956, On the travel time of and dispersion of surface waves: Geophys. Mag. 27, pp. 93-194.

Peterson, J., Butler, H.M., Holcomb, L.G. and Hutt, C.R., 1976, The Seismic Research Observatory: Bull. Seism. Soc. Am. 66, pp. 2049-2074.

Rastogi, B.K., Singh, J. and Verma, B.K., 1973, Earthquake mechanism and tectonics in Assam Burma region: Tectonophysics 18, pp. 355-366.

Rezova, E., 1936, Construction of travel-time curves and determination of the fundamental seismic elements for Central Asia: Acad. Sci. USSR Inst. Seismic., Publ. 72, p. 28, Leningrad.

Riznichenko, Y.V., 1958, Seismische teiten sandierung zur untersuchungder erdkrusle: Studia Geophys. et Geodoetz, p. 133-140.

Rosenthal, R. and Teng, T., 1977, Crustal and upper mantle velocity and Q structure of Mainland China: University of Southern California Geophysical Laboratory, Tech. Report 77-5.

Saha, B.P., 1965, M_2 or first shear mode continental Rayleigh waves from Russian nuclear explosion of 30 October 1961: Ind. J. Met. Geophys. 16, pp. 270-280.

Savarensky E.F. and Shechkov, B.N., 1961, The structure of the Earth's crust in Siberia in the Far East from Love wave and Rayleigh wave dispersion: Izvestiya Acad. Sci. USSR Geophys. Ser., p. 454-456, English translation.

Shechkov, B.N., 1961, Structure of the Earth's crust in Eurasia from dispersion of the surface waves: Izvestiya Acad. Sci. USSR Geophys. Ser., pp. 450-453, English translation.

_____, 1964, Seismic surface dispersion and Eurasian crustal structure: Izvestiya Acad. Sci. USSR Geophys. Ser., p. 183-187, English translation.

Shi, Z.L., Huan, W.L., Wu, H.R. and Lao, X.L., 1973, On the intensive seismic activity in China and its relation to plate tectonics: Scientia Geologica Sinica, no. 4, pp. 293-305.

Simmons, G., 1964, Velocity of shear waves in rocks to 10 kilobars: J. Geophys. Res. 69, no. 6, p. 1123.

Steinhart and Meyer, 1961, Explosion studies of continental structure: Carnegie Inst. Wash. Publ. 622, p. 409.

Stonely, R., 1955, Rayleigh waves in a medium with two surface layers: Mon. Nat. Roy. Astron. Soc. Geophys. Supp. 7, pp. 71-75.

Sun, N.C. and Teng, T., 1977, Tectonic plates of China: University of Southern California, Geophysical Laboratory, Tech. Report, 77-4.

Tandon, A.N., 1954, Study of the great Assam earthquake of August 1950 and its aftershocks: Ind. J. Met. Geophys. 5, pp. 95-137.

Tandon, A.N., and Chandhury, H.M., 1963, Seismic waves from high yield atmospheric explosions: Ind. J. Met. Geophys. 14, pp. 283-301.

Tacheuchi H., Dorman, J. and Saito, M., 1964, Partial derivatives of surface wave phase velocity with respect to physical parameter changes within the Earth: Geophys. Res. 69, p. 3429.

Thatcher, W. and Bruen, J.N., 1969, Higher mode interference and observed anomalous apparent Love wave velocities: J. Geophys Res. 74, pp. 6603-6611.

Toksoz, M.N. and Anderson, D.L., 1966, Phase velocities of long period surface waves and structure of the upper mantle: J. Geophys. Res. 71, p. 1649.

Tseng, J.S. and Sung, Z.A., 1963, Phase velocity of Rayleigh waves in China: Acta Geophysica Sinica 12, no. 2, pp. 148-165.

Tung, J.P., 1974, The surface wave study of crustal and upper mantle structure of Mainland China: Ph.D. dissertation, University of Southern California, 248 pp.

U.S. Air Force (compiled), A Bouguer anomaly map of Asia, 1971.

Whittington, H.B. and Hughes, C.P., 1972, Ordovician geography and faunal provinces: Phil. Trans. Roy. Soc. London 263, p. 235.

Wiggins, R.A., 1972, The general linear inverse problems: Implications of surface waves and free oscillations for Earth structure: Rev. Geophys. Space Phys. 10, pp. 251-285.

Yasuii, M., Epp, D., Nagasaka, K., Kishii, T., 1970, Terrestrial heat flow in the seas around Nansei Shoto (Ryukyu Islands): Tectonophysics 10, pp. 225-235.

York, J.E., Cardwell, R. and Ni, J., 1976, Seismicity and Quaternary faulting in China: Bull. Seism. Soc. Am., v. 66, pp. 1983-2001.

Zonenshain, L.P., 1973, The evolution of Central Asiatic geosynclines through sea-floor spreading: Tectonophysics 19, pp. 213-232.

Zverev, Z.N., 1962, Deep seismic soundings of the Earth's crust in the USSR: Collection of papers, Gostoptek hizdat, Leningrad.

APPENDIX I

FIGURE 39: Unrotated seismogram for the path

Yunnan-Mashad, July 3, 1976

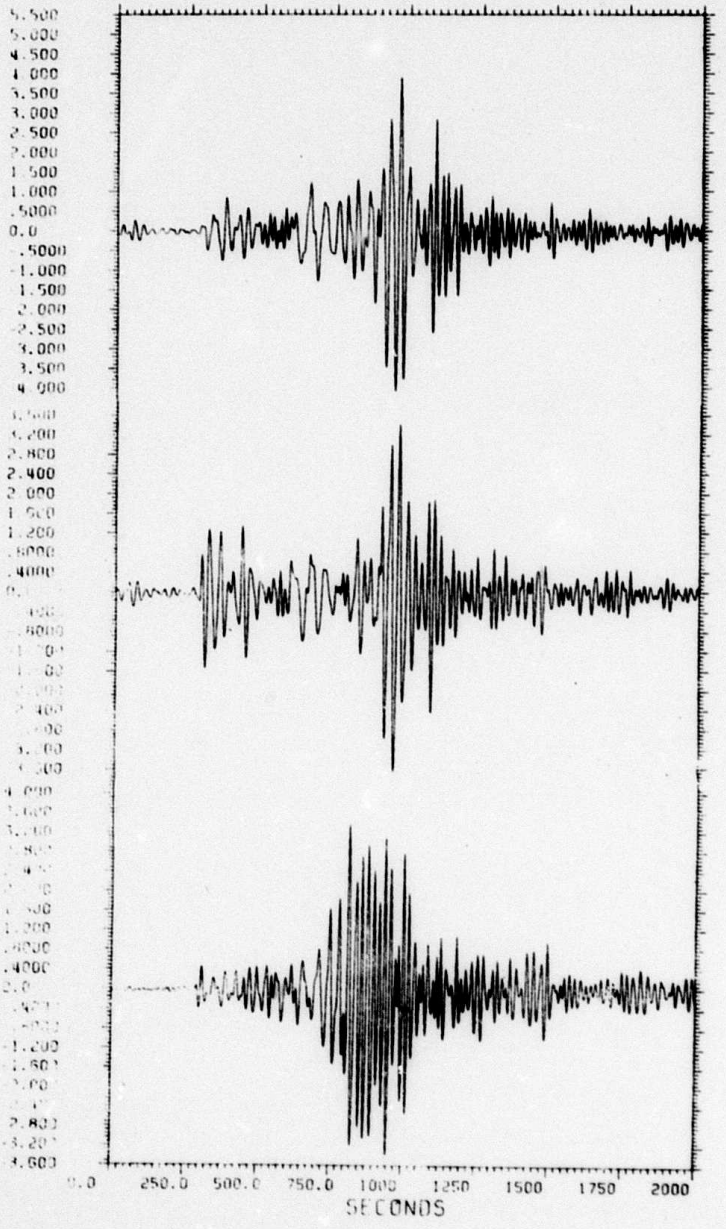
5.500
5.000
4.500
4.000
3.500
3.000
2.500
2.000
1.500
1.000
.5000
0.0
-.5000
-1.000
1.500
2.000
-2.500
3.000
3.500
4.000
2.800
2.400
2.000
1.200
.4000
-1.200
0.0
250.0
500.0
750.0
1000
1250
1500
1750
2000
SECONDS

FIGURE 40: Rotated seismogram for the path Yunnan-Mashad, July 3, 1976

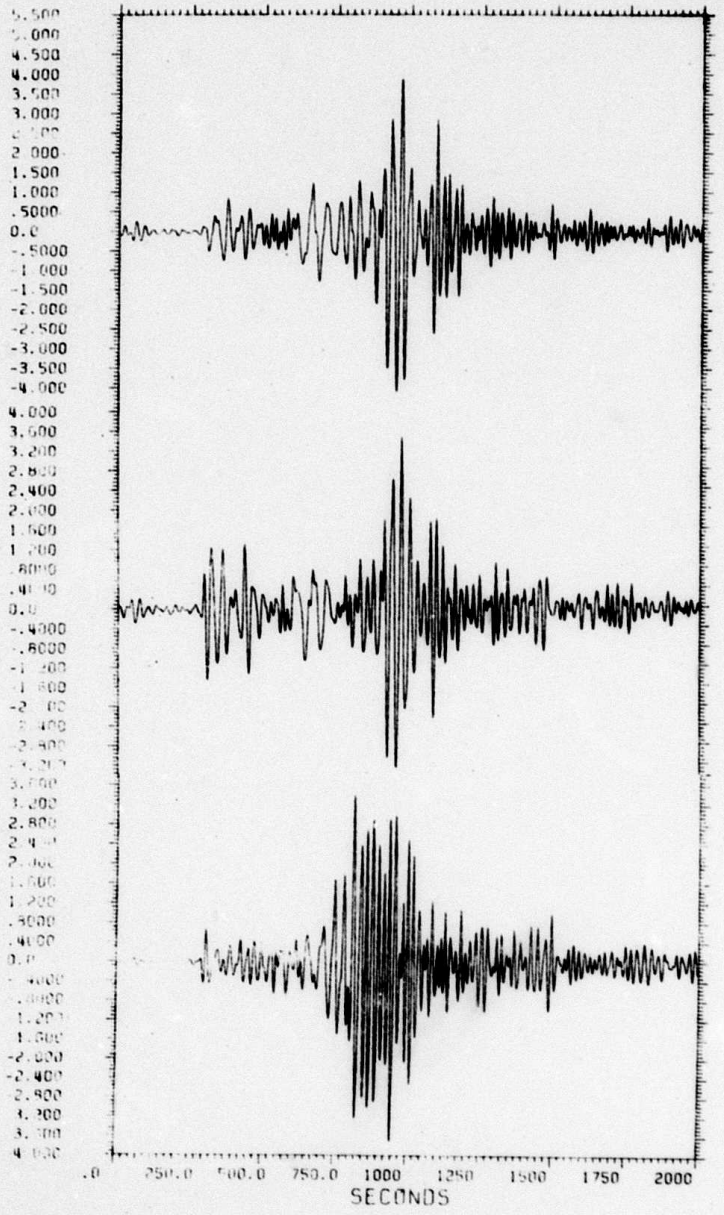
4.500
4.000
3.500
3.000
2.000
1.500
1.000
.5000
0.0
-.5000
-1.000
-1.500
-2.000
-2.500
-3.000
-3.500
-4.000
4.000
3.600
3.200
2.400
.4000
0.0
-.4000
-.8000
.0
250.0
500.0
750.0
1000
1250
1500
1750
2000
SECONDS

FIGURE 41: Unrotated seismogram for the path Szechwan-Mashad, August 16, 1976

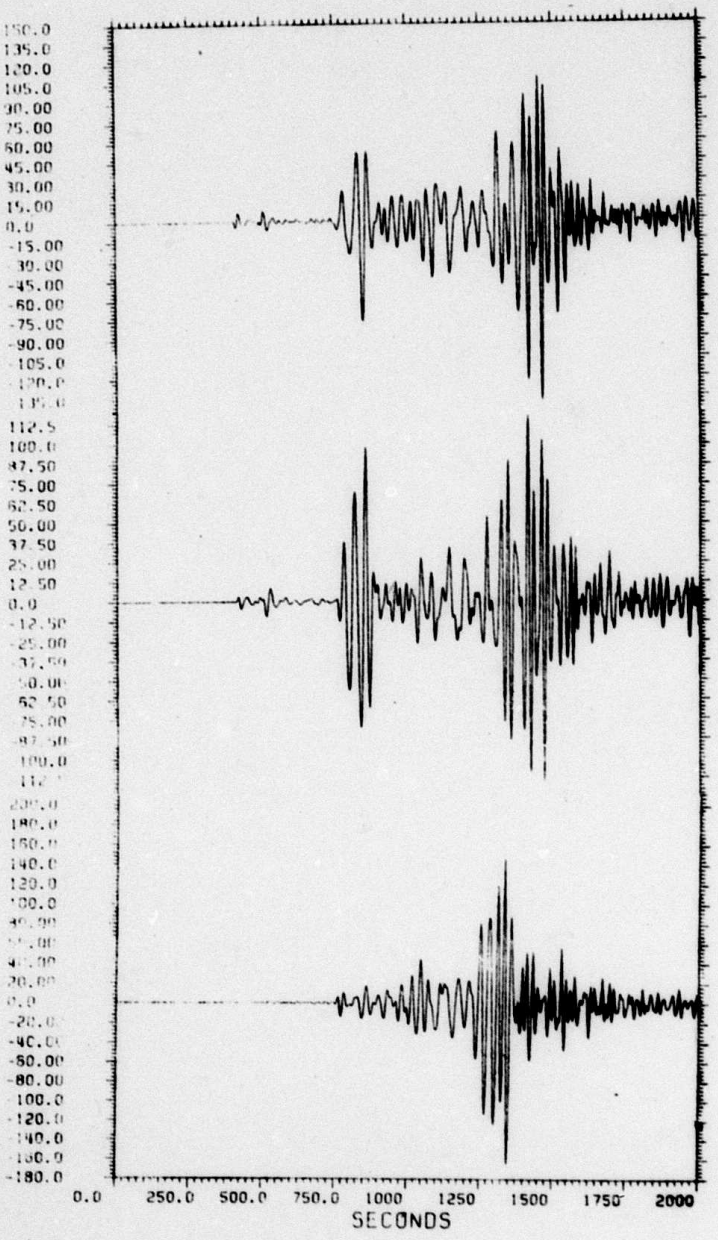
150.0
135.0
120.0
105.0
90.00
75.00
60.00
45.00
30.00
15.00
0.0
-15.00
-30.00
-45.00
-60.00
-75.00
-90.00
-105.0
-120.0
112.5
100.0
87.50
75.00
62.50
50.00
37.50
25.00
12.50
0.0
-12.50
-25.00
-37.50
-50.00
-62.50
-75.00
-87.50
-100.0
-112.5
200.0
180.0
160.0
140.0
120.0
100.0
80.00
60.00
40.00
20.00
0.0
-20.00
-40.00
-60.00
-80.00
-100.0
-120.0
-140.0
-160.0
-180.0
0.0
250.0
500.0
750.0
1000
1250
1500
1750
2000
SECONDS

FIGURE 42: Rotated seismogram for the path Szechwan-Mashad, August 16, 1976

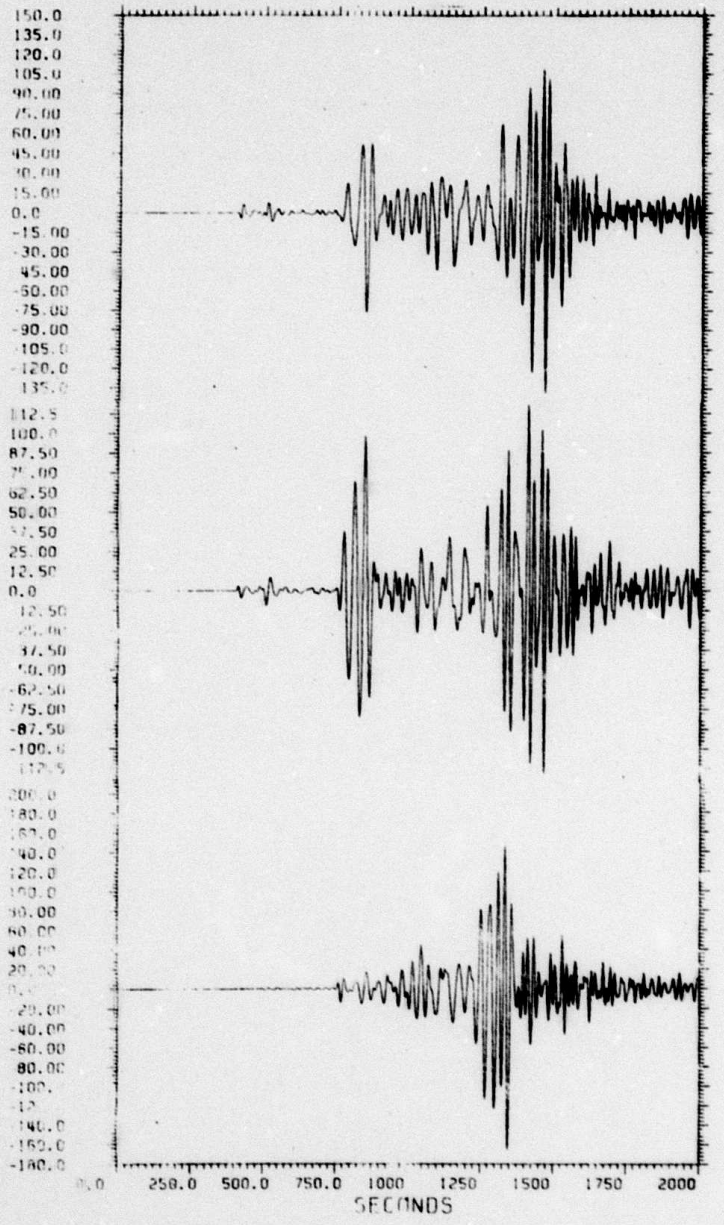
150.0
135.0
120.0
105.0
90.00
75.00
60.00
45.00
30.00
15.00
0.0
-15.00
-30.00
-45.00
-60.00
-75.00
-90.00
-105.0
-120.0
-135.0
112.5
100.0
87.50
75.00
62.50
50.00
37.50
25.00
12.50
0.0
-12.50
-25.00
-37.50
-50.00
-62.50
-75.00
-87.50
-100.0
-112.5
200.0
180.0
160.0
140.0
120.0
100.0
80.00
60.00
40.00
20.00
0.0
-20.00
-40.00
-60.00
-80.00
-100.
-12
-140.0
-160.0
-180.0
0.0
250.0
500.0
750.0
1000
1250
1500
1750
2000
SECONDS

FIGURE 43: Unrotated seismogram for the path

Tangshan-Taipei, July 30, 1976

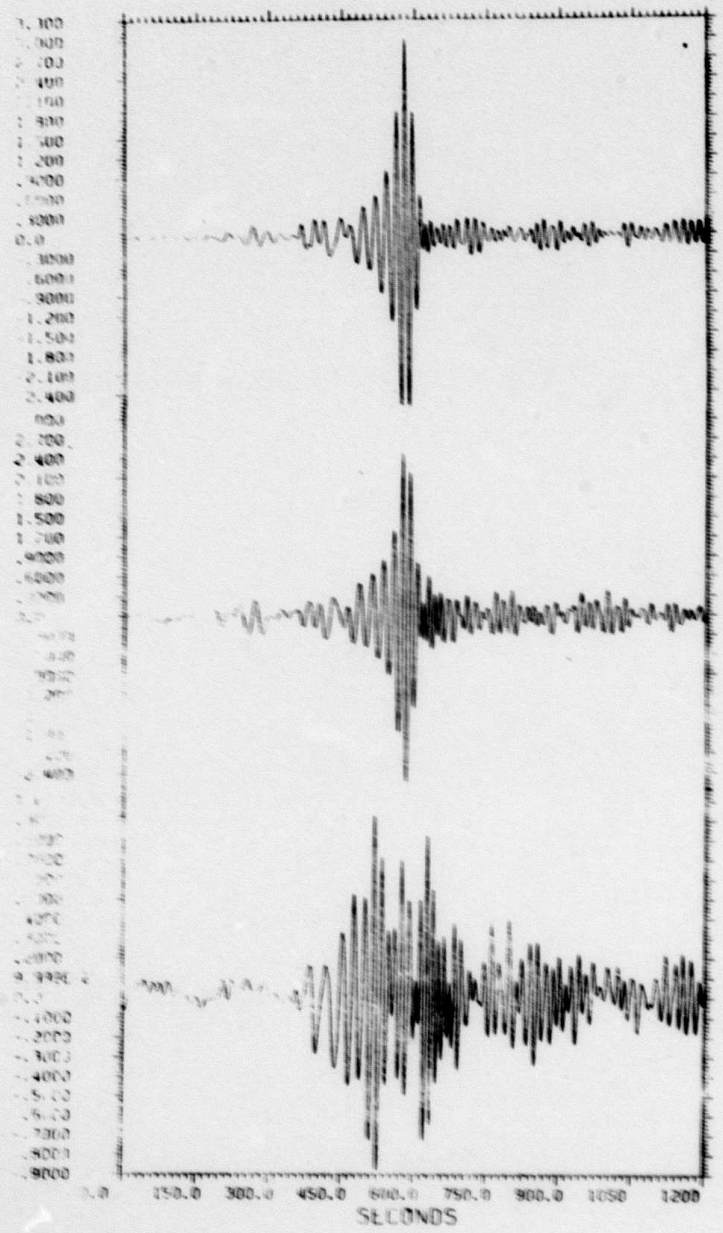
150.0
300.0
450.0
600.0
750.0
900.0
1050
1200
SECONDS

FIGURE 44: Rotated seismogram for the path Tangshan-Taipei, July 30, 1976

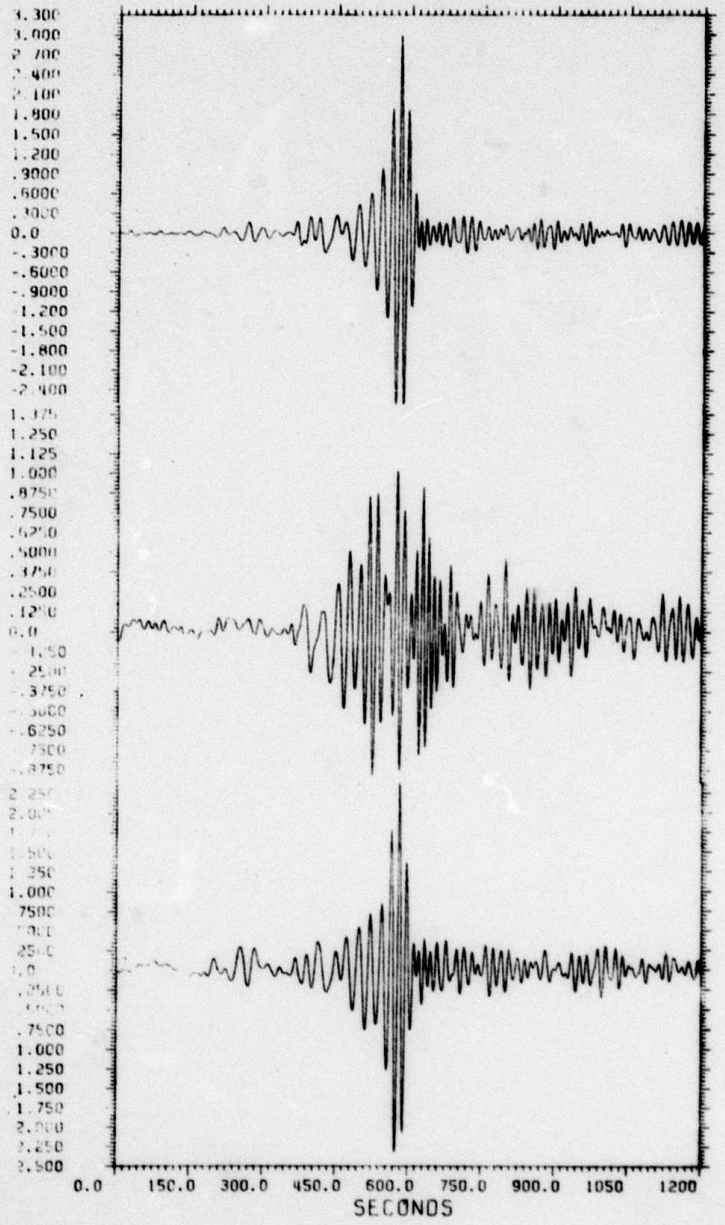
0.0
150.0
300.0
450.0
600.0
750.0
900.0
1050
1200
SECONDS

APPENDIX II

FIGURE 45: Results of multiple filtering of radial Rayleigh component, Yunnan-Mashad, May 31, 1976

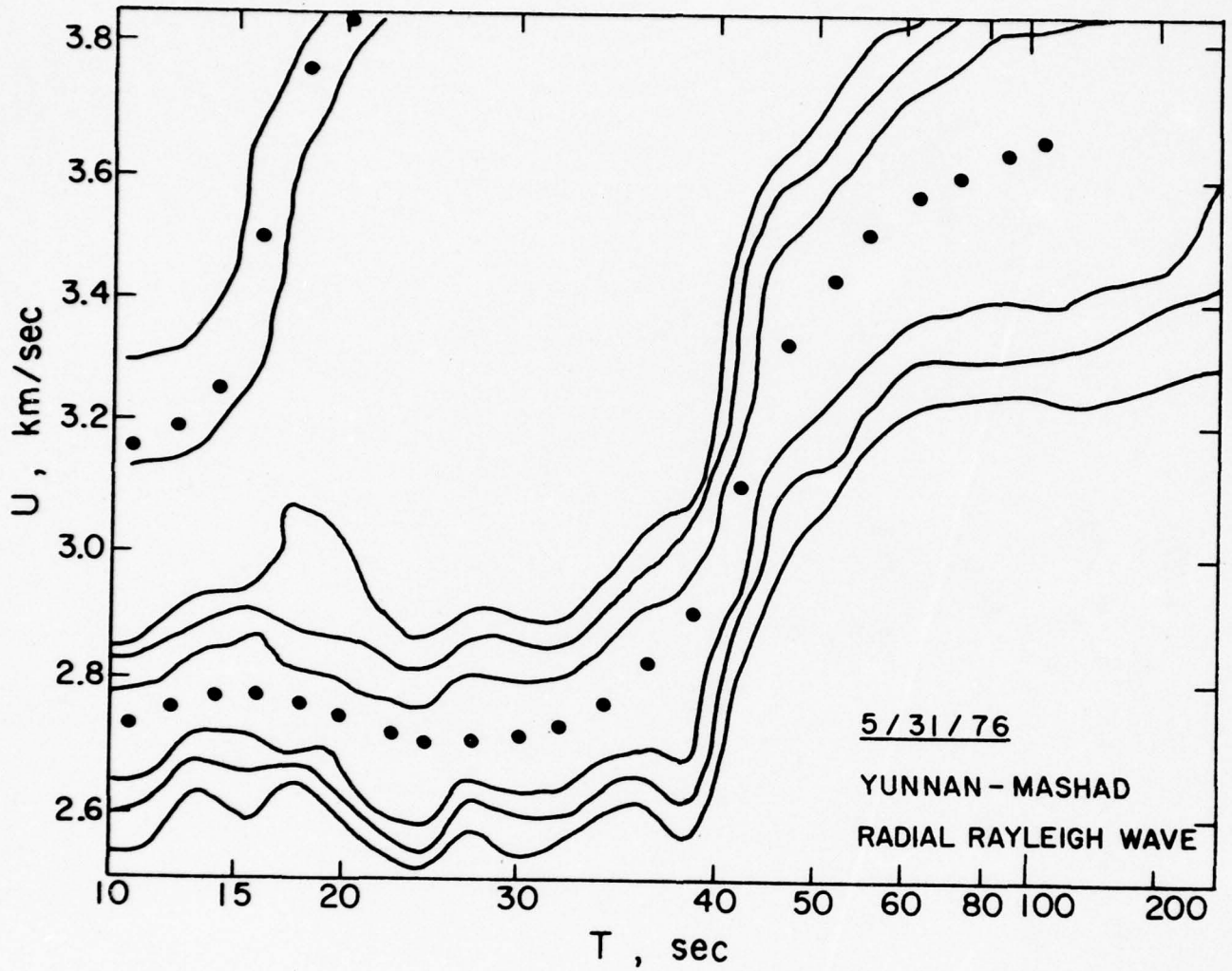
3.8
3.6
3.4
3.2
3.0
2.8
2.6
U , km/sec
10
15
20
30
40
50
60
80
100
200
T , sec
5/31/76
YUNNAN - MASHAD
RADIAL RAYLEIGH WAVE

FIGURE 46: Results of multiple filtering of Rayleigh component, Yunnan-Mashad, July 31, 1976

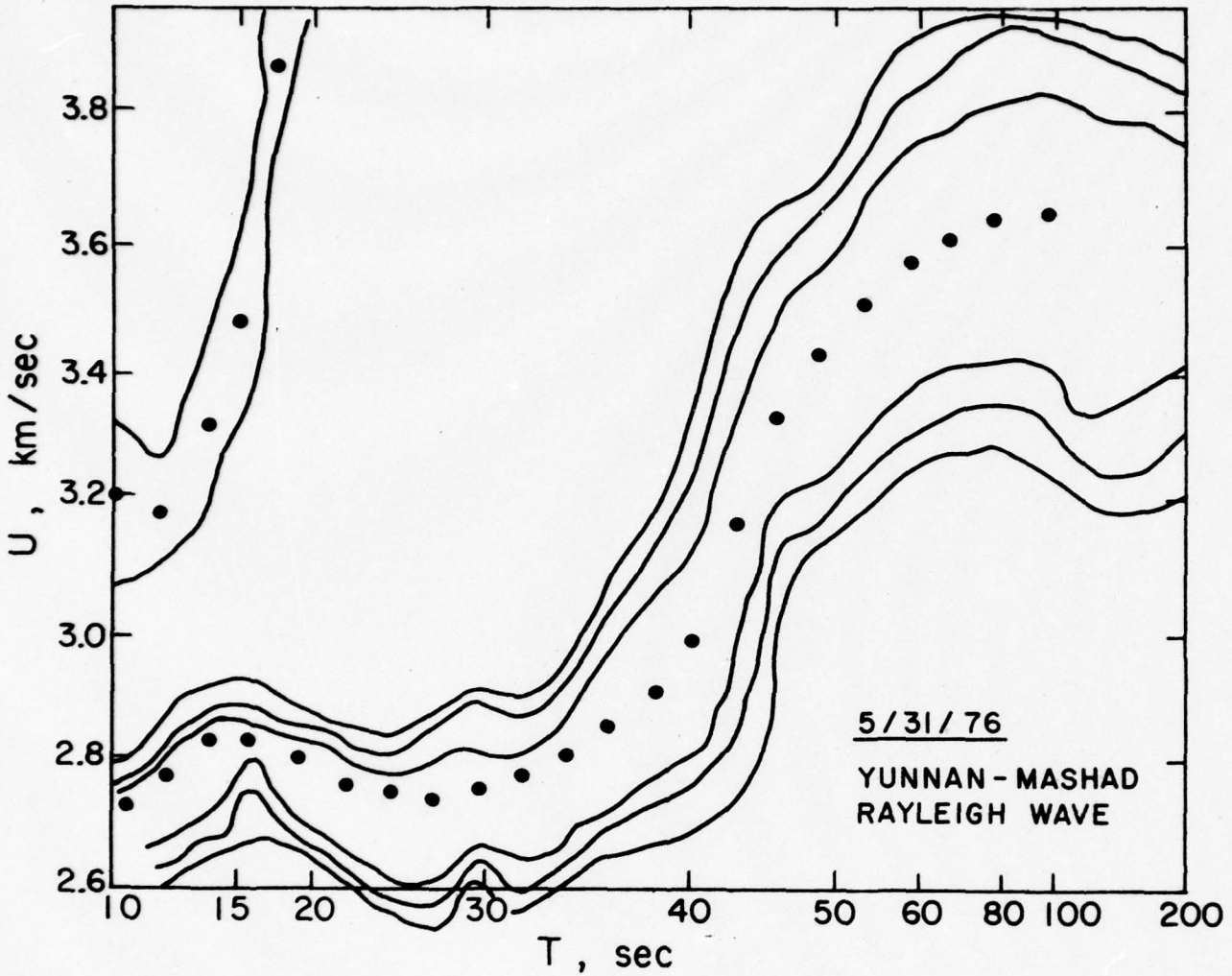
3.8
3.6
3.4
3.2
3.0
2.8
2.6
U , km/sec
10
15
20
30
40
50
60
80
100
200
T , sec
5/31/76
YUNNAN - MASHAD
RAYLEIGH WAVE

FIGURE 47: Results of multiple filtering of radial Rayleigh component, Szechwan-Mashad, August 16, 1976

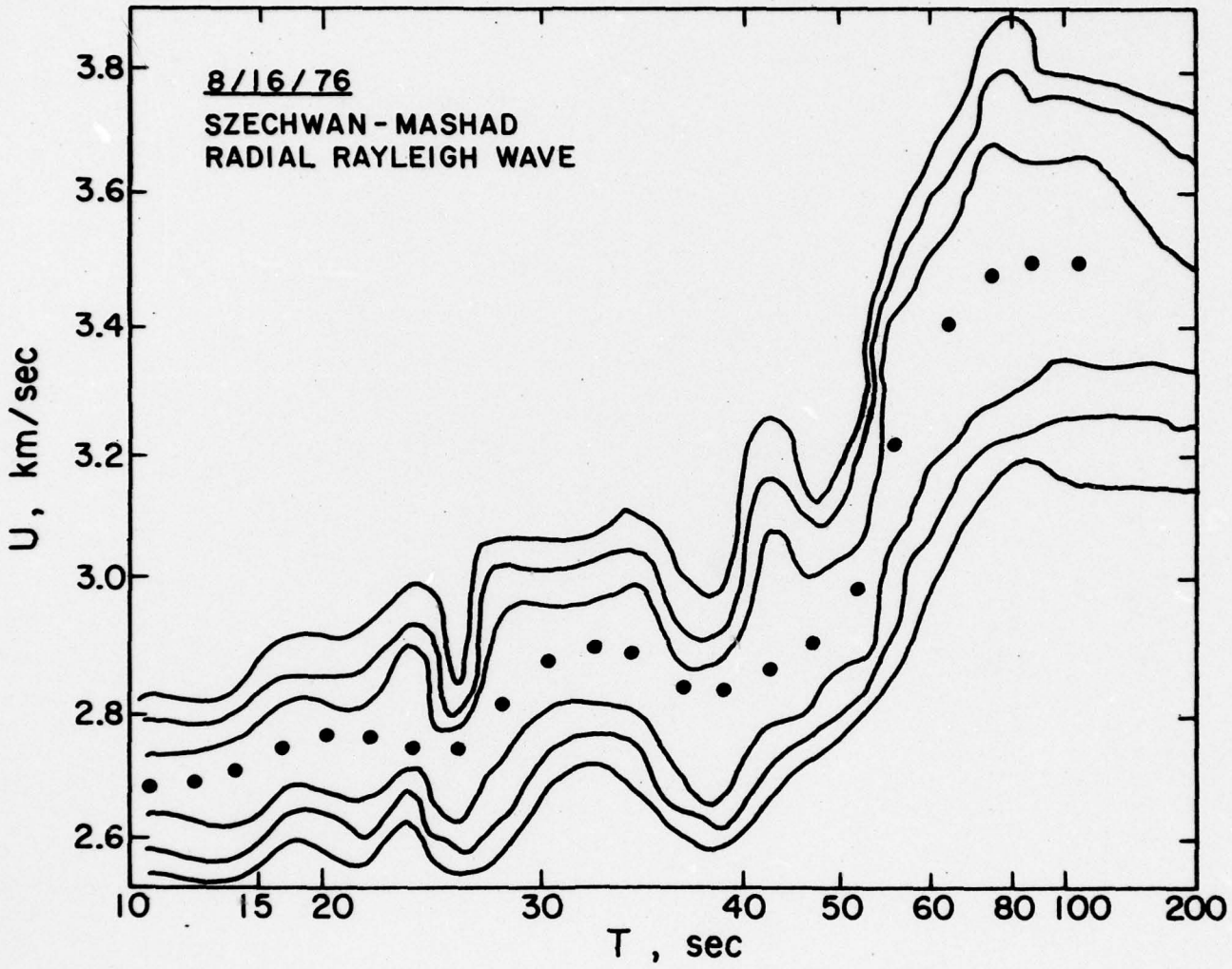
8/16/76
SZECHWAN - MASHAD
RADIAL RAYLEIGH WAVE
U, km/sec
3.8
3.6
3.4
3.2
3.0
2.8
2.6
10
15
20
30
40
50
60
80
100
200
T, sec

FIGURE 48: Results of multiple filtering of the Rayleigh component, Szechwan-Mashad, August 16, 1976

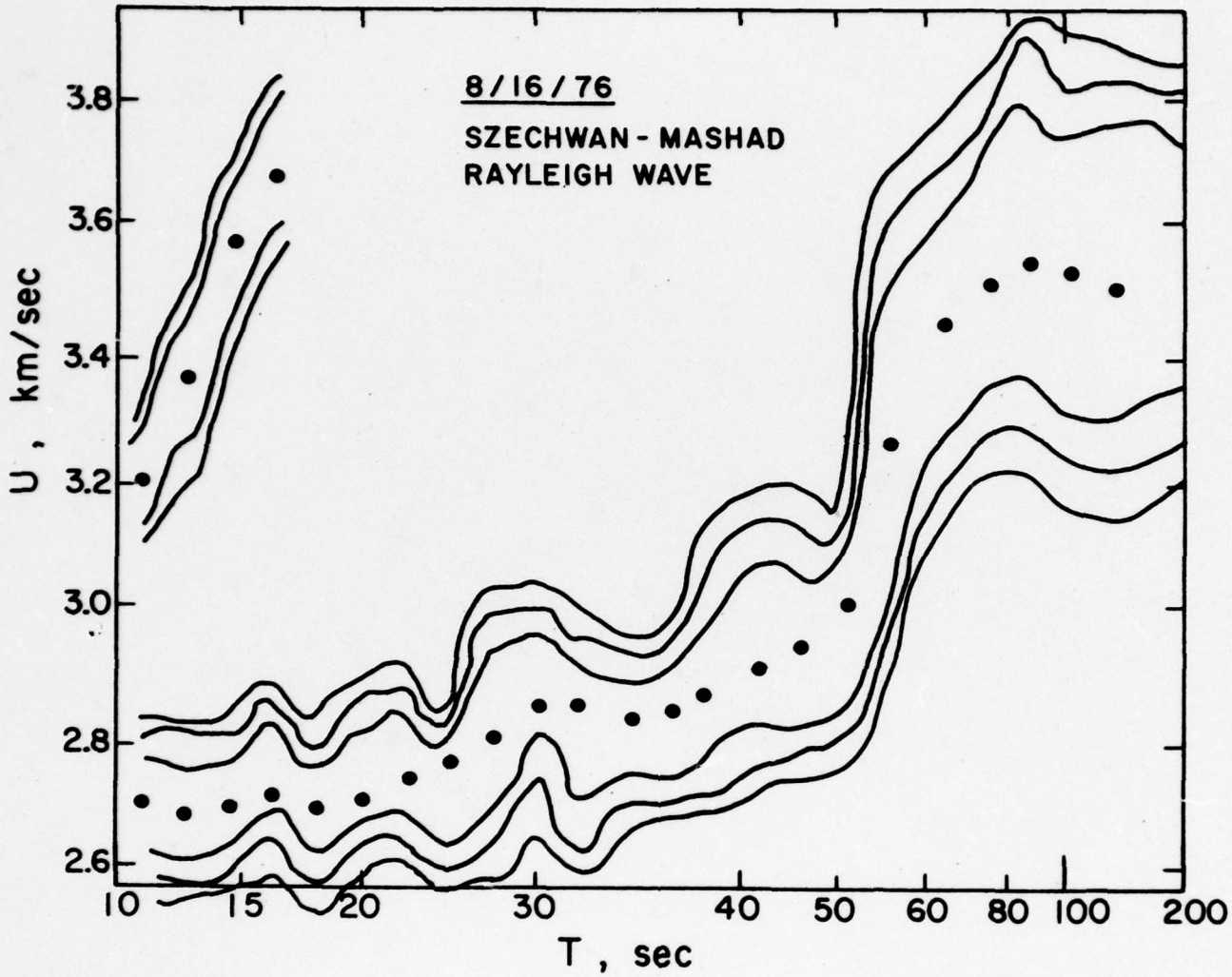
8/16/76
SZECHWAN - MASHAD
RAYLEIGH WAVE
U , km/sec
3.8
3.6
3.4
3.2
3.0
2.8
2.6
10
15
20
30
40
50
60
80
100
200
T , sec

FIGURE 49: Results of multiple filtering of radial Rayleigh component, Tangshan-Mashad, August 8, 1976

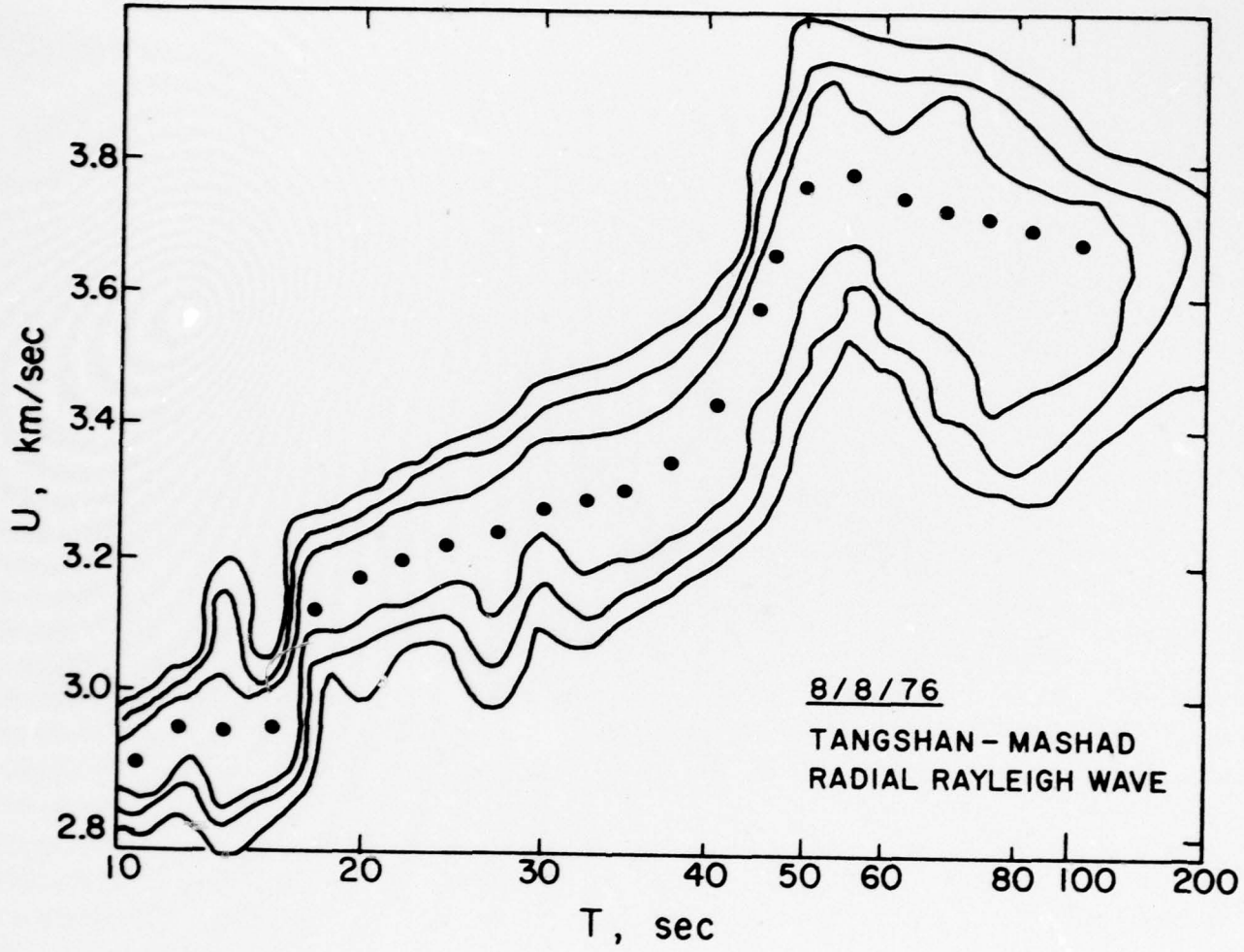
3.8
3.6
3.4
3.2
3.0
2.8
U, km/sec
10
20
30
40
50
60
80
100
200
T, sec
8/8/76
TANGSHAN - MASHAD
RADIAL RAYLEIGH WAVE

FIGURE 50: Results of multiple filtering for Rayleigh component, Tangshan-Mashad, August 8, 1976

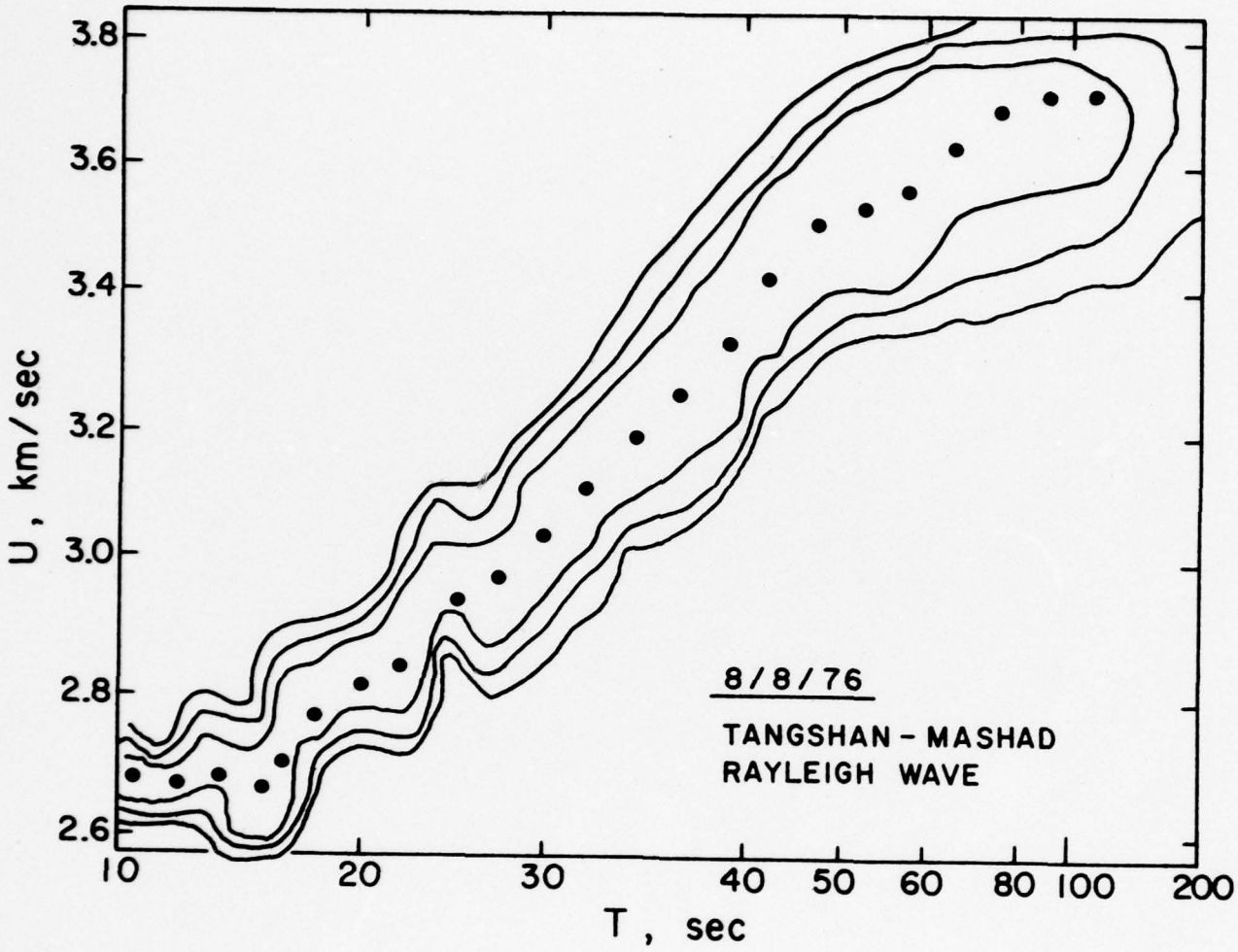
3.8
3.6
3.4
3.2
3.0
2.8
2.6
U, km/sec
10
20
30
40
50
60
80
100
200
T, sec
8/8/76
TANGSHAN - MASHAD
RAYLEIGH WAVE

FIGURE 51: Results of multiple filtering for radial Rayleigh component, Tangshan-Taipei, July 30, 1976

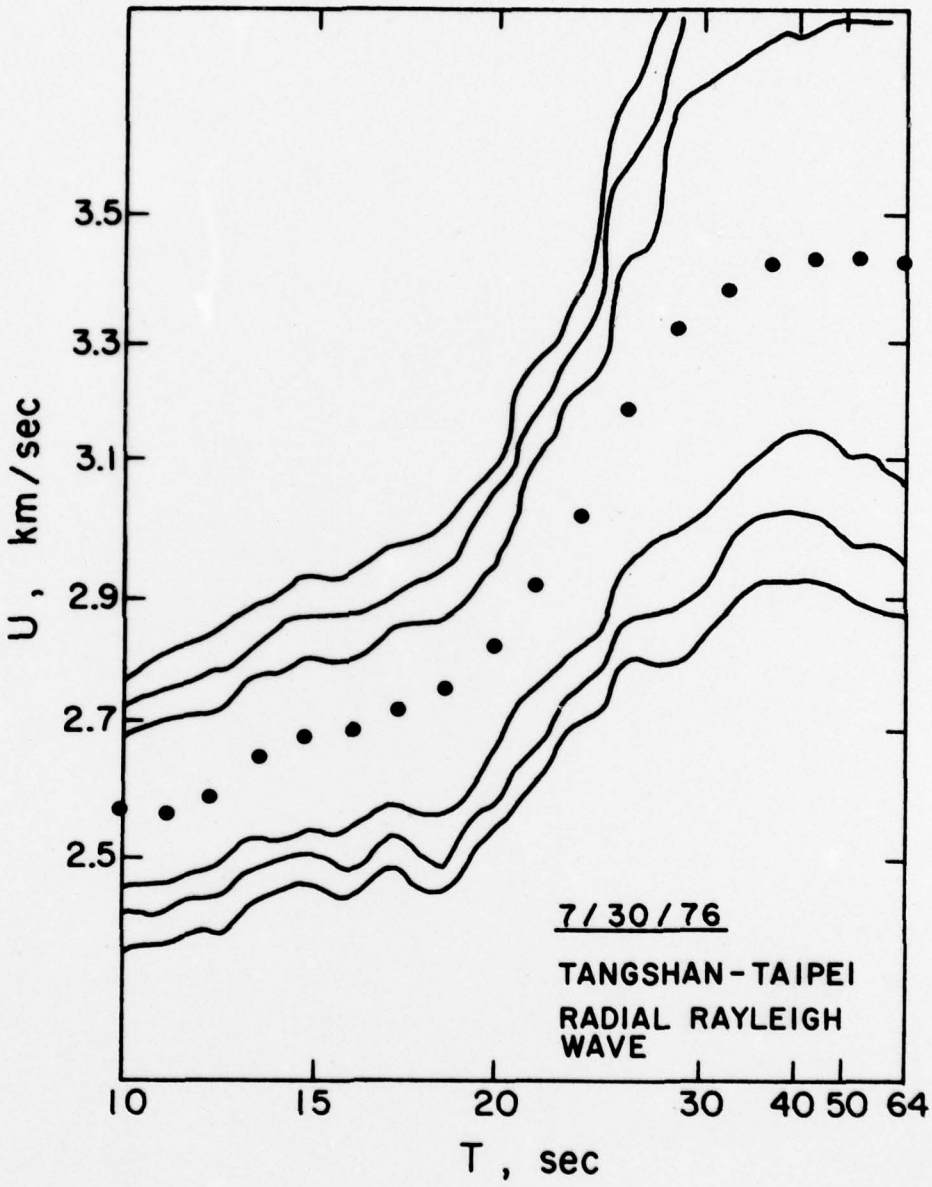
3.5
3.3
3.1
2.9
2.7
2.5
U , km/sec
10
15
20
30
40
50
64
T , sec
7/30/76
TANGSHAN-TAIPEI
RADIAL RAYLEIGH
WAVE

FIGURE 52: Results of multiple filtering for Rayleigh component, Tangshan-Taipei, July 30, 1976

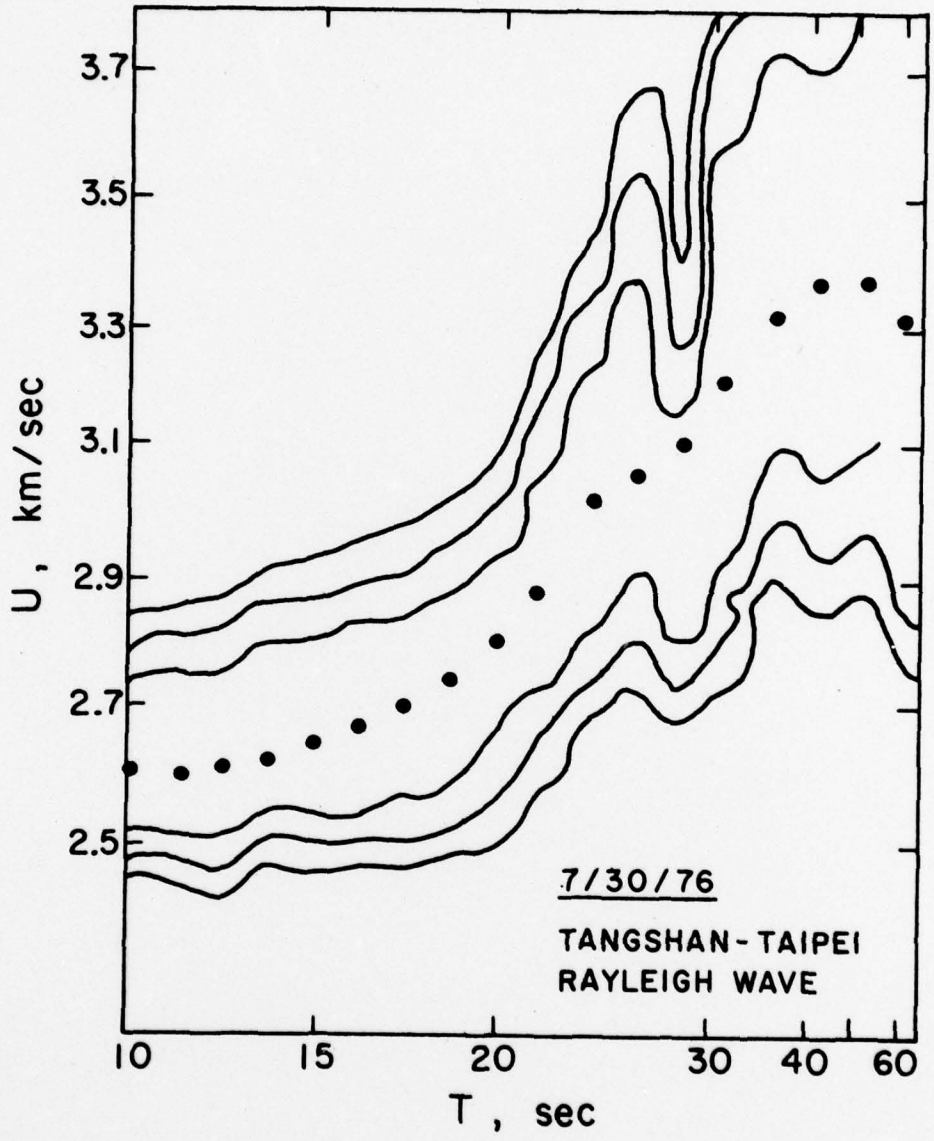
3.7
3.5
3.3
3.1
2.9
2.7
2.5
U, km/sec
10
15
20
30
40
60
T, sec
7/30/76
TANGSHAN - TAIPEI
RAYLEIGH WAVE

FIGURE 53: Results of multiple filtering for Love component, Tangshan-Taipei, July 30, 1976

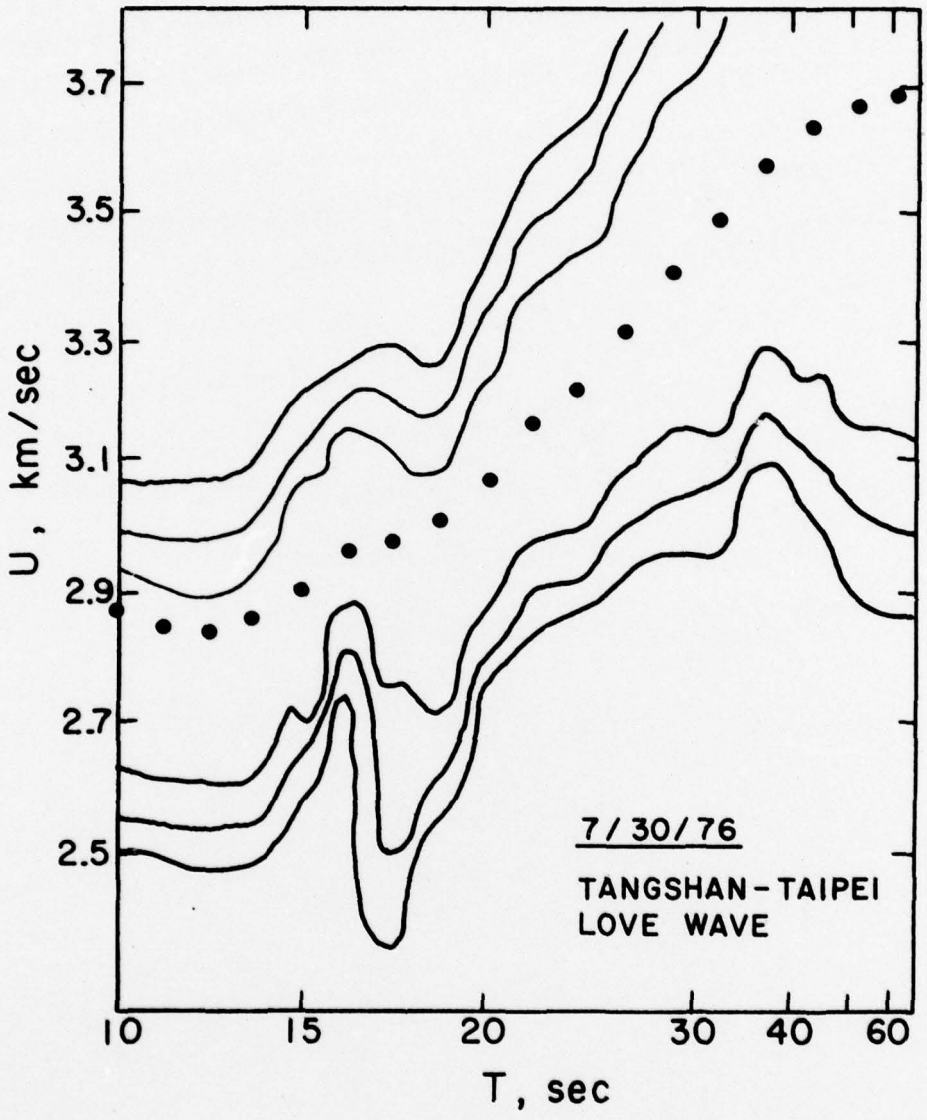
3.7
3.5
3.3
3.1
2.9
2.7
2.5
U, km/sec
10
15
20
30
40
60
T, sec
7/30/76
TANGSHAN-TAIPEI
LOVE WAVE

SECURITY CLASSIFICATION OF THIS PAGE (When Data Entered)

REPORT DOCUMENTATION PAGE

READ INSTRUCTIONS BEFORE COMPLETING FORM

1. REPORT NUMBER: AFOSR-TR-78-0761	2. GOVT ACCESSION NO.
3. RECIPIENT'S CATALOG NUMBER	
4. TITLE (and Subtitle): CRUSTAL AND UPPER MANTLE VELOCITY AND Q STRUCTURES OF MAINLAND CHINA.	5. TYPE OF REPORT & PERIOD COVERED: INTERIM rept.
6. PERFORMING ORG. REPORT NUMBER	
7. AUTHOR(s): Ta-liang/Teng Iva/Pines	8. CONTRACT OR GRANT NUMBER(s): F49620-76-C-0010, ARPA Order 3291
9. PERFORMING ORGANIZATION NAME AND ADDRESS: Geophysical Laboratory, University of Southern California, Los Angeles, CA 90007	10. PROGRAM ELEMENT, PROJECT, TASK AREA & WORK UNIT NUMBERS: 62701E TF10 A.O.3291
11. CONTROLLING OFFICE NAME AND ADDRESS: ARPA/NMR, 1400 Wilson Boulevard, Arlington, VA 22209	12. REPORT DATE: 11 Nov 1977
	13. NUMBER OF PAGES: 172 (12) 173 p.
14. MONITORING AGENCY NAME & ADDRESS (if different from Controlling Office): AFOSR/NP, BOLLING AFB, BLDG.#410, WASHINGTON DC 20332	15. SECURITY CLASS. (of this report): Unclassified
	15a. DECLASSIFICATION/DOWNGRADING SCHEDULE

16. DISTRIBUTION STATEMENT (of this Report)

Approved for public release; distribution unlimited.

DDC RECEIVED MAY 17 1978 B

17. DISTRIBUTION STATEMENT (of the abstract entered in Block 20, if different from Report)

18. SUPPLEMENTARY NOTES

19. KEY WORDS (Continue on reverse side if necessary and identify by block number)

20. ABSTRACT (Continue on reverse side if necessary and identify by block number)

New data from the Seismological Research Observatory (SRO) is used in conjunction with a non-linear least squares technique to invert surface wave group velocity data for the shear wave velocity structure for paths crossing the Chinghai-Tibet, North China and South China subplates. A number of earthquakes are used over a single path in order to deduce a measure of the observational uncertainty. Group velocity standard deviations range from 0.04 km/sec to 0.20 km/sec for Rayleigh waves and 0.04 km/sec to 0.20 km/sec for Love waves over the period range 10-128 seconds. The results of the

DD FORM 1 JAN 73 1473 EDITION OF 1 NOV 65 IS OBSOLETE UNCLASSIFIED

SECURITY CLASSIFICATION OF THIS PAGE (When Data Entered)

408 456

inversion indicate a 4 layer total, 70 km thick crust is an adequate model for the Tibetan plateau. Group velocities obtained for the path crossing the Tibetan plateau are unusually low. Group velocities for the mixed path beteen Tangshan-Mashad, Iran are lower than the average continental dispersion. Results of the inversion indicate a 3 layer total, 45 km thick crust is an adequate model. Group velocities for the path between Tangshan-Taipei, Taiwan are closest of the three regions (at higher periods) to the average continental dispersion. Results of the inversion indicate that a 3 layer total, 30 km crust is an adequate model. Shear velocities derived from the inversion of group velocity data are presented for the crust and upper mantle for each path.